

# UC Davis

## UC Davis Electronic Theses and Dissertations

### Title

Consequences of kelp loss: using restoration as a tool to inform ecology

### Permalink

<https://escholarship.org/uc/item/51f7192k>

### Author

Elsmore, Kristen

### Publication Date

2021

Peer reviewed|Thesis/dissertation

Consequences of kelp loss: using restoration as a tool to inform ecology

By

KRISTEN ELSMORE  
DISSERTATION

Submitted in partial satisfaction of the requirements for the degree of

DOCTOR OF PHILOSOPHY

in

Ecology

in the

OFFICE OF GRADUATE STUDIES

of the

UNIVERSITY OF CALIFORNIA

DAVIS

Approved:

---

Brian Gaylord, Chair

---

Kerry J. Nickols

---

Tessa M. Hill

Committee in Charge

2021

## **ACKNOWLEDGEMENTS**

I am forever grateful for my advisor, Dr. Brian Gaylord, who provided a nurturing and supportive environment for me to explore research questions and develop as a scientist. He took the time to work with me to fine tune and shape my questions, ideas, presentations, and writing, making sure to retain my voice throughout. No matter how nervous or stuck I felt going into a meeting with him, I would walk away feeling better every time, with clear next steps or the confidence to carry on. Brian's interdisciplinary approach to science is an inspiration to me, showing how different facets of science and disciplines more broadly can be integrated and leveraged to better understand the world around us. Recognizing that no single person can provide the support one needs for graduate school, Brian supported and encouraged the various partnerships and collaborations I developed throughout pursuit of my degree. I deeply appreciate that he allowed me the freedom to foster those relationships and to flail (a bit, but not too much) through the various projects so I could learn by doing. He also fostered the best team of lab mates I could have asked for. Above all, Brian is kind. This is an invaluable trait in a mentor, and I am so fortunate to have had an advisor who had my best interest as a scientist, and as a person, in mind every step of the way. I feel so fortunate to have been mentored by Brian and been a member in his lab.

I would also like to thank Dr. Tessa Hill and Dr. Kerry Nickols, my committee members, for providing invaluable feedback on various stages and forms of my research. Beyond direct support of my research, Tessa provided advice on navigating different collaborations and contributing to the Bodega Marine Lab and Coastal Marine Sciences Institute communities. I am

especially appreciative of Tessa's scientific communications workshop, as I continue to use what I have learned to share research findings and build new relationships with scientists, stakeholders, and the public. Kerry has guided and encouraged me long before I started graduate school. I will never forget our long chats about science, kelp, and life, floating on the boat outside the Hopkins kelp forest during the wee hours of the night. Or being harassed by a sea lion underwater while trying to find an ADCP that went for a bit of a wild ride. Kerry exposed me to the exciting questions that can be explored with an interdisciplinary approach and continuously helps me navigate the sometimes-isolating feeling of conducting research straddled between physical oceanography and ecology. I deeply appreciate Kerry welcoming me in her lab, where I have had the pleasure of meeting and collaborating with so many wonderful people.

The BML community was a constant source of logistical and moral support, as well as friendship and adventure. I would especially like to thank Kristin Aquilino, Sam Bashevkin, Connor Dibble, Katie DuBois, Ellie Fairbain, Carina Fish, Marcella Heineke, Kate Hewett, Jordan Hollarsmith, Emily Hubbard, Helen Killeen, Kat Magana, Sarah Merolla, Jeff Miller, Hannah Palmer, Aurora Ricart, Matteo Robbins, Robbin Roettger, Erin Satterthwaite, Priya Shukla, Sadie Small, Melissa Ward, and Matt Whalen, each of whom contributed significantly to my graduate experience over the years, and I deeply appreciate their friendship, passion for science, and love of nature and silliness. I would also like to thank Jason Herum, James Fitzgerald, Mike Anghera, and Dan Abbott for supporting my field efforts throughout the state.

My graduate experience would not have been the same without my lab mates. They have been a constant source of support and friendship and I have learned so much from each of them. Brittany Jellison had invaluable advice on stats, experimental design, scientific communication,

and maintaining work-life balance. Counting seemingly endless bouts of snails in the dark and getting sufficiently covered in the forever-stickiness of Tanglefoot will be forever ingrained in my memory (and my field clothes). I always enjoyed the long conversations about stats, delicious food, and scuba diving with Gabriel Ng. Aaron Ninokawa provided a great sense of balance, perspective, and laughs – I undoubtedly missed many subtle jokes and science puns through the years. I appreciate the many conversations with Alisha Saley about stats, research, and life and I am also grateful for her organizational skills and our underwater adventures. Ashley Smart was a wonderful source of creativity in experimental design and scientific communication and provided a great example in interpersonal communication and advocacy. Laura Jurgens, Kristina Barklay, Scott Gabara, and Tallulah Winquist were a lovely source of scientific discussion as well as field and lab support and friendship through the years. I would also like to thank the members of the Nickols lab, especially Deme Panos and Brian Cohn, who made long field days fun and rewarding.

The Bay Foundation has been an invaluable support system throughout my graduate degree, providing perspective and countless underwater hours swimming (oh so much swimming!) and counting kelp. I would especially like to thank Tom Ford, Heather Burdick, Armand Barilotti, Parker House, Ben Grime, Karina Johnson, and Ariadne Reynolds. I am also very appreciative of Gary Thompson and Terry Herzik for their contributions to the fieldwork for my first two chapters.

The team at Reef Check California, Tristin McHugh, Dr. Jan Freiwald, Morgan Murphy-Cannella, and Ian Norton, as well as the fishermen working on the bull kelp restoration project, helped facilitate sample collections for my third chapter. I am deeply grateful of this team as well

as to Victoria Hickman, Kelsi Hope, and Francheska Torres, who assisted with dissections and measurements of countless urchins! I am also thankful for the many discussions about urchin jaws with Dr. Maya deVries and Sam Stein.

I have been fortunate to be supported by multiple funding sources and am extremely thankful for their financial support throughout my degree. I would like to thank the National Science Foundation for awarding me the Graduate Research Fellowship that provided the freedom and time for me to explore my research ideas. I would also like to thank the California State Coastal Conservancy, University of Southern California, Sea Grant, California Sea Grant, the Bilinski Foundation, the Society of Environmental Toxicology and Chemistry Northern California Chapter, and the University of California Institute for Mexico and the United States Small Grants Program for also funding field and lab components of my research.

My family has been so supportive of my passion for marine science and pursuit of this degree, and they have played a critical role in getting me to this stage in one piece. I want to thank my parents, Diane and Tim, for supporting my dreams and always fostering my sense of curiosity, even when it meant me coming home smelling of fish guts and seal poop or missing the occasional holiday. I want to thank my brothers, Geoffrey and Nicky, for not only putting up with my persistent fascination with the ocean throughout the years, but for providing couches to sleep on, driveways upon which to rinse stinky sensors, and soldering skills for sensor assembly. I also want to thank my husband, Ian, who has supported me in this journey in so many ways. In this last year especially, he has kept me sane, well fed, and very loved.

## DISSERTATION ABSTRACT

Canopy-forming kelp forests are found all over the world and operate as marine foundation species, creating underwater forests that provide structural habitat, shelter, and food for numerous other taxa (North 1971; Dayton 1972; Miller et al. 2018). In California's coastal waters, these forests tend to be dominated by one of two species: *Macrocystis pyrifera*, the giant kelp, or *Nereocystis luetkeana*, the bull kelp, occupying southern and northern California regions, respectively. Both species form forests that extend throughout the water column and form thick surface canopies (Springer et al. 2010; Schiel and Foster 2015). Supporting a myriad of other species for seaweed gatherers and indigenous harvesters, as well as for local commercial and recreational fisheries (e.g., rockfish, red urchin, and abalone), these forests hold cultural and economic significance to coastal communities as well as California more broadly (Carr 1989; Turner 2001).

Kelp forests face a number of environmental stressors which can operate independently or synergistically to cause localized kelp declines and, in some cases, widespread deforestation. For example, in southern California, hotspots of kelp loss have historically been driven by poor water quality attributed to increased coastal development (e.g., sedimentation, sewage discharge, contamination), as well as increased grazing pressure by purple sea urchins (*Strongylocentrotus purpuratus*). However, extreme storm events such as those associated with El Niño conditions can cause deforestation across much larger spatial scales (Wilson and Togstad 1983; Tegner and Dayton 1987). For example, storm waves from the 1982-1983 El Niño facilitated a loss of over 90% of the giant kelp canopy along Palos Verdes Peninsula, one of the largest *M. pyrifera* stands

in California (Wilson and Togstad 1983). Shifts in urchin abundances that preceded the storm, in addition to dislodgement and redistribution of those urchins into deeper waters during the storm contributed to further weakening of the kelp and inhibited recovery in some areas (Wilson and Togstad 1983). While improvements to water quality resulted in the recovery of kelp in some areas, urchin grazing pressures continue to inhibit kelp growth and recovery back to the region's historic coverage (Schiel and Foster 2015).

In recent years, northern California's *N. luetkeana* forests were hit with what scientists have called the "perfect storm" of conditions, resulting in catastrophic loss of this canopy-forming species (Rogers-Bennet and Catton 2019). While not completely understood, the suite of conditions that aligned to facilitate a loss of 90% of California's bull kelp forests were three-fold: 1) elevated seawater temperatures, which weaken bull kelp individuals 2) sea star wasting disease, which led to the decimation of the sunflower sea star (*Pycnopodia helianthoides*), an important predator in the kelp forest system, and 3) most relevant here, an explosion of purple urchins (*Strongylocentrotus purpuratus*), which notoriously overgraze kelp forests when in high numbers (Rogers-Bennett and Catton 2019). What was once extensive bull kelp forests has now become desolate seascapes of bare rock, caked with purple urchins and red urchins (*Mesocentrotus franciscanus*). Deforestation is a challenge faced by nearshore kelp communities around the globe, and though each system has a unique suite of triggering conditions, the consequences are the same – profound loss of biogenic habitat and dramatically altered community structure and functioning.

Restoration has emerged as a mechanism by which to facilitate kelp recovery around the world (Eger et al. 2020). In California, recent kelp restoration efforts have focused on reducing

the urchin grazing pressure exerted on the remaining kelp adults and new recruits (Williams et al. 2021; Ray et al. in review). In partnership with local commercial urchin divers, nongovernmental organizations The Bay Foundation and Reef Check are working to reduce purple urchin densities along the Palos Verdes Peninsula and Mendocino coastline, respectively. Subsequent recovery of kelp, in response to urchin density reductions (Williams et al. 2021; Reef Check unpublished data), provides a unique experimental framework by which to explore physical and biological consequences of kelp loss, recovery, and the role kelp forests play in modulating their physical environment.

Loss and regrowth of kelp forests can each have profound impacts on their surrounding environment. Here I explore the consequences of *Macrocystis pyrifera* forests' disappearance and regrowth on the local surface gravity waves and alongshore current velocities as well as the consequences of *Nereocystis luetkeana* forest disappearance on jaw-test allometry of two important species of sea urchin (*Strongylocentrotus purpuratus* and *Mesocentrotus franciscanus*).

Chapter one leverages the before-after experimental framework of an ongoing *M. pyrifera* restoration project along the Palos Verdes Peninsula to quantitatively distinguish energy dissipation of surface gravity waves due to the presence of a kelp forest from that due to frictional processes at the seabed. I found that the kelp forest had a detectable but modest capacity to damp wave energy. Interactions with the seabed alone reduced wave energy flux, on average, by 12% over 180 meters of travel, with an additional 7% reduction arising when an established forest was present. Kelp-associated decreases in wave energy flux were slightly greater for waves of longer periods and smaller wave heights than waves with shorter periods

and larger wave heights. These findings suggest that *Macrocystis pyrifera* forests have a limited but non-trivial capacity to enhance shoreline protection from nearshore waves.

Chapter two builds on the same before-after experimental framework of the *M. pyrifera* restoration project along Palos Verdes Peninsula and quantifies alongshore current velocities outside and within a temperate rocky reef environment that twice underwent a transition from a barren state to one in which a thick surface canopy was present. Findings suggest there is a threshold density during forest emergence at which much of the attenuation of alongshore depth-averaged velocity occurs – three stipes per square meter with a surface canopy present. Incremental increases in damping occur as the forest matures, highlighting that relatively young, thin forests can induce substantially reduced flows. Additionally, the presence of a young forest's subsurface canopy and its subsequent increase in height create a seasonally changing profile of reduced velocities through the water column. These results indicate greater complexity in how canopy-forming kelp influence nearshore flow properties than has often been recognized. Importantly, emerging forests can alter the nearshore environment through modulation of current speeds shortly following initial recruitment, with consequences for transport of larvae, nutrients, and sediment throughout the forest and adjacent habitats.

Chapter three explores relationships among gonad production, size (i.e., test diameter), and jaw morphology (i.e., length, width, shape, weight) between *Strongylocentrotus purpuratus* and *Mesocentrotus franciscanus*, two dominant urchin species of California's temperate rocky reefs. Within this chapter, I also characterize the extent to which those allometric relationships change across differing habitat conditions, classified as bull kelp (*Nereocystis luetkeana*) forest, reef with understory algae-only (no surface kelp canopy), and urchin barren, to better understand

the role of habitat context on species-specific gonad, test, and jaw allometry. Both species of urchin exhibited greater production of gonad material in the kelp and understory habitats than the barren habitat, highlighting the stark differences in food availability across the habitats. The relationship between jaw length and test diameter did not differ between habitat conditions, in contrast to what has been documented in other kelp-barren systems (e.g., *M. pyrifera* forests and barrens of Monterey Bay, CA) and with other urchin species around the world (e.g., *Heliocidaris erythrogramma*). Further, *M. franciscanus* exhibited relatively wider jaws than *S. purpuratus* in the kelp habitat, however, such species-specific differences disappeared in the barren habitat, challenging the use of jaw shape to distinguish species within fossil records in lieu of habitat context. However, because *M. franciscanus* had relatively heavier jaws than *S. purpuratus* across all habitats, the relationship between jaw weight and test diameter could be leveraged to parse out distinct species from urchin remains. These results indicate greater complexity in the allometric relationships of urchin tests and their jaws, specifically when comparing between species and across differing or unknown habitat conditions. Habitat context should be considered when building growth models using jaw-test relationships for fisheries management, specifically for *S. purpuratus*, and when inferring species from midden and fossil records for reconstruction of human harvesting patterns across space and through time.

### **Literature Cited**

Carr, M.H. 1989. Effects of macroalgal assemblages on the recruitment of temperate zone reef fishes. *J. Exp. Mar. Biol. and Ecol.* 126:59-76.

Dayton, P.K. 1972. Toward an understanding of community resilience and the potential effects of enrichments to the benthos at McMurdo Sound, Antarctica. *Proceedings of the Colloquium on Conservation Problems in Antarctica*, B.C. Parker (Ed.) Allen Press, 81-96.

Eger, A.M., E. Marzinelli, P. Gribben, C.R. Johnson, C. Layton, P.D. Steinberg, G. Wood, B.R. Silliman, and A. Vergés. 2020. Playing to the positives: Using synergies to enhance kelp forest restoration. *Frontiers in Marine Science*. 7:544. doi: 10.3389/fmars.2020.00544

Foster, M.S. and D.R. Schiel. 2010. Loss of predators and the collapse of southern California kelp forests (?): Alternatives, explanations, and generalizations. *Journal of Experimental Marine Biology and Ecology*. 393:59-70.

Schiel, D.R., and M.S. Foster. 2015. *The Biology and Ecology of Giant Kelp Forests*. University of California Press Books, doi:0.1525/9780520961098.

Miller, R.J., K.D. Lafferty, T. Lamy, L. Kui, A. Rassweiler, and D.C. Reed. 2018. Giant kelp, *Macrocystis pyrifera*, increases faunal diversity through physical engineering. *Proceedings of the Royal Society B: Biological Sciences* 285: 20172571, doi:10.1098/rspb.2017.2571.

North, W.J. 1971. The biology of giant kelp beds (*Macrocystis*) in California. *Nova Hedwigia* 32: 1-600.

Ray, J., T.A. McHugh, M.W. Esgro, K.E. Elsmore, J. Freiwald. In Review. Exploring pathways to recovery: a northern California bull kelp restoration case study. *Global Kelp Restoration Guidebook*. The Nature Conservancy.

Rogers-Bennett, L. and C.A. Catton. 2019. Marine heat wave and multiple stressors tip bull kelp forest to sea urchin barrens. *Scientific Reports*. 9:1–9.

Springer, Y.P., C.G. Hays, M.H. Carr, and M.R. Mackey. 2010. Toward ecosystem-based management of marine Macroalgae—The bull kelp, *Nereocystis luetkeana*. *Oceanography and Marine Biology: An Annual Review*, 48, 1-42.

Tegner, M.J. and P.K. Dayton. 1987. El Nino effects on southern California kelp forest communities. *Advances In Ecological Research*. 17:243-279.

Turner, N.J. 2001. "Coastal peoples and marine plants on the northwest coast", <https://hdl.handle.net/1912/2545>.

Williams, J.P., J.T. Claisse, D.J. Pondella II, C.M. Williams, M.J. Robart, Z. Scholz, E.M. Jaco, T. Ford, H. Burdick, and D. Witting. 2021. Sea urchin mass mortality rapidly restores kelp forest communities. *Marine Ecology Progress Series*. 664:117-131.

Wilson, K.C. and H. Togstad. 1983. Storm caused changes in the Palos Verdes kelp forests. In: The effects of waste disposal on kelp communities. Institute of Marine Resources, University of California, pp. 301-307.

## TABLE OF CONTENTS

Acknowledgements .....	ii
Dissertation Abstract .....	vi
<b>Chapter 1</b>	
<i>Wave damping by giant kelp, Macrocystis pyrifera</i> .....	1
Abstract .....	2
Introduction .....	3
Methods .....	6
<i>Study site</i> .....	6
<i>Kelp surveys</i> .....	7
<i>Wave theory</i> .....	7
<i>Wave measurements and analyses</i> .....	12
<i>Influence of kelp on wave attenuation</i> .....	15
Results .....	16
<i>Kelp densities</i> .....	16
<i>Wave conditions</i> .....	17
<i>Wave damping by kelp</i> .....	19
Discussion .....	20
<i>Factors governing damping potential</i> .....	20
<i>Wave versus current damping</i> .....	22
<i>Limitations of the study</i> .....	23

Conclusion .....	23
Acknowledgements .....	24
Literature Cited .....	24
Tables .....	31
Figures .....	33
Appendices .....	39

## **Chapter 2**

<i>Macrocystis pyrifera</i> forest development shapes the physical environment through current velocity reduction .....	41
Abstract .....	42
Introduction .....	43
Methods .....	46
<i>Study site</i> .....	46
<i>Kelp forest dynamics</i> .....	47
<i>Alongshore current velocity measurements</i> .....	48
<i>Influence of kelp on depth-averaged currents</i> .....	48
<i>Influence of subsurface canopy on alongshore currents</i> .....	50
Results .....	50
<i>Kelp forest dynamics</i> .....	50
<i>Influence of kelp on depth-averaged alongshore currents</i> .....	52
<i>Influence of subsurface canopy on alongshore currents</i> .....	54
Discussion .....	55

<i>Forest structure</i> .....	55
<i>Subsurface canopy</i> .....	57
<i>Residence time</i> .....	58
<i>Transport of particulates and detritus</i> .....	59
Conclusion .....	61
Acknowledgments .....	61
Literature Cited .....	62
Tables .....	68
Figures .....	69
<b>Chapter 3</b>	
<i>Jaw-test allometry of two temperate urchin species across habitat conditions</i> .....	76
Abstract .....	77
Introduction .....	79
Methods .....	84
<i>Urchin collections</i> .....	84
<i>Morphological measurements</i> .....	85
<i>Statistical analysis</i> .....	86
Results .....	87
<i>Urchin test morphology</i> .....	87
<i>Gonad production</i> .....	87
<i>Jaw morphology</i> .....	88
Discussion .....	89

<i>Species-specific differences</i> .....	90
<i>Habitat-specific differences</i> .....	92
<i>Implications for management</i> .....	96
Acknowledgments .....	99
Literature Cited .....	99
Tables .....	104
Figures .....	106
Appendices .....	114

## **CHAPTER 1**

Wave damping by giant kelp, *Macrocystis pyrifera*\*

---

\*Co-authors: Kerry J. Nickols, Luke P. Miller, Tom Ford, Mark W. Denny, Brian Gaylord

## ABSTRACT

A range of aquatic vegetation types provide shoreline protection by damping coastal ocean waves. Canopy-forming kelps, including giant kelp (*Macrocystis pyrifera*), have been thought to provide this service. However, supporting data are limited. Previous in situ efforts relied mostly on comparisons between nominally similar sites possessing kelp or not. Because other factors – especially seafloor bathymetry and topographic features – often differ across sites, efforts to isolate effects of kelp on waves confront challenges. In particular, it can be difficult to distinguish energy dissipation due to kelp from frictional processes at the seabed that often covary with kelp presence. To eliminate such confounds, we measured waves within and outside of rocky reef habitat, both in the absence and presence of giant kelp, at Marguerite Reef, Palos Verdes, CA, USA. Nested within a broader kelp restoration project, this site transitioned from a bare state to one supporting a fully formed forest (density of 8 stipes per meter squared). We quantified the change in wave energy flux due to the presence of kelp, as waves propagated from outside and into reef habitat. Our results demonstrate that the kelp forest had a detectable but modest capacity to damp wave energy. Interactions with the seabed alone reduced wave energy flux, on average, by 12% over 180 meters of travel, with an additional 7% reduction arising when an established forest was present. Kelp-associated decreases in wave energy flux were slightly greater for waves of longer periods and smaller wave heights than waves with shorter periods and larger wave heights. These findings suggest that *Macrocystis pyrifera* forests have a limited but non-trivial capacity to enhance shoreline protection from nearshore waves.

## INTRODUCTION

Canopy-forming macroalgae create underwater forests and habitat for over 800 other species (North 1971; Dayton 1972; Schiel and Foster 2015; Miller et al. 2018), in part through alteration of abiotic factors. For instance, giant kelp, *Macrocystis pyrifera*, the largest seaweed in the world, produces a dense network of floating surface blades that reduces light levels while simultaneously influencing seawater chemistry (Reed and Foster 1984; Hirsh et al. 2020). The blades and accompanying fronds that extend through the water column additionally slow current speeds and modify patterns of vertical mixing (Jackson and Winant 1983; Gaylord et al. 2004, 2007, 2012; Rosman et al. 2007, 2010).

*Macrocystis* and other forest-forming kelps also have a close relationship with ocean waves. Large waves generated by storms dominate the dynamics of abundance and primary production in giant kelp (Reed et al. 2011), and interactions between waves and kelps have long inspired interest in the possibility that kelp forests might attenuate wave energy. Indeed, even Charles Darwin, during his 1831-1836 voyage on the Beagle (Darwin 1839), mused about *Macrocystis*' potential value in this regard:

“The beds of this sea-weed, even when of not great breadth, make excellent natural floating breakwaters. It is quite curious to see, in an exposed harbour, how soon the waves from the open sea, as they travel through the straggling stems, sink in height, and pass into smooth water.”

Despite Darwin's observations and those made by others, the extent to which canopy-forming kelps might damp waves remains less than fully clear. The "smooth water" shoreward of kelp beds is most readily explained by the removal of capillary waves – small, centimeter-scale ripples whose physics are governed by water's surface tension. The bigger waves that characterize seas and swell, and which dislodge kelps and instigate shoreline erosion, are fundamentally different. Their behavior is controlled by the restoring action of gravity, and they can be orders of magnitude larger and more powerful (Denny 1988).

Quantitative assessments of wave attenuation by kelp and other seaweeds have been pursued in a number of studies. Early work employed mathematical or laboratory approaches that modeled kelp forests as arrays of rigid cylinders or tethered floats (Seymour and Hanes 1979; Dalrymple et al. 1984; Kobayashi et al. 1993). This research, much of which was applied to *Macrocystis pyrifera*, suggested as much as 20-94% reductions in transmitted wave energy by kelp mimics. Related theoretical, laboratory, and field experiments targeting much smaller seaweeds (i.e., ones without a surface canopy) found wave energy reductions up to 85% (Dubi and Torum 1996; Mork 1996). Likewise, wave damping in seagrasses and saltmarshes has been shown to reach 40% and 80%, respectively, depending on species (e.g., Mendez and Losada 2004; Riffe et al. 2011; Paul et al. 2012; Houser et al. 2015; Luhar et al. 2017). Although the latter ecosystems differ from canopy-forming seaweeds in key ways, the sum total of this work has reinforced the idea that kelp forests might reduce levels of coastal wave action and thereby combat shoreline erosion (e.g., Arkema et al. 2017).

Other lines of research, however, imply a substantially lower potential benefit of kelp forests for dissipating wave energy. This complementary axis of study emphasizes the structural and biomechanical traits of organisms. In particular, it highlights the capacity for canopy-

forming kelps to sway back and forth with waves (Koehl 1984). Numerical models that account for such flexible movement of seaweeds indicate strong dynamical effects, a portion of which could influence rates of wave energy loss (Denny et al. 1998). This finding applies especially to large canopy-forming species (Denny et al. 1997), although there is relevance also to fully submerged taxa that do not interact with the water's surface (Gaylord and Denny 1997; Gaylord et al. 2001). Laboratory measurements using scaled kelp mimics (Rosman et al. 2013), as well as field recordings (Gaylord et al. 2008; Mullarney and Pilditch 2017) support the applicability of such models for understanding flow-organism interactions. In cases where levels of expected wave damping were computed explicitly, they appear constrained (Gaylord et al. 2003; Henderson 2019). Wave dissipation by a subsurface species of kelp, *Ecklonia radiata*, also appears undetectable under most wave conditions (Morris et al. 2020). Thus, ambiguity has persisted regarding the capacity of various forms of kelp to damp wave energy.

In the case of *Macrocystis pyrifera*, the most widespread canopy-forming kelp along the U.S. west coast, field experiments are limited, but tend to comport with prior dynamical models in suggesting small to negligible effects on transmitted wave energy (Elwany et al. 1995; Rosman et al. 2007). Elwany et al. (1995) relied on comparisons of wave energy at paired sites of similar bathymetry, where one site had kelp and the other did not. In this case, differences in energy between sites were insufficiently large to emerge from the statistical noise. Rosman et al. (2007) quantified wave energy at stations both outside and inside a forest, but this study was not designed to distinguish between effects of waves propagating into shallower depths, versus dissipative effects of kelp. Difficulties in establishing adequate no-kelp controls, against which kelp treatments could be directly matched, is characteristic of all prior studies and has

contributed to the challenge of making strong inferences about levels of wave damping by kelp forests (Tinoco et al. 2020).

In the present study, we exploited a kelp forest restoration project in Palos Verdes, California, to explicitly disentangle effects of giant kelp on wave attenuation from other factors. In the locality of this project, areas that were once overgrazed by the purple urchin, *Strongylocentrotus purpuratus*, and devoid of kelp (termed ‘urchin barrens’) returned to a kelp forest state after urchin densities were reduced through culling. The resulting transition from an urchin barren to a healthy kelp forest presented a unique opportunity to measure wave conditions before, during, and after forest regeneration. In particular, it made possible a before-after design whereby wave measurements could be collected both in the absence and presence of kelp, with bathymetry and other factors held constant. In this regard, this study was able to test unambiguously the physical effects of a canopy-forming kelp on waves.

## **METHODS**

### *Study site*

Marguerite Reef (33.75712, -118.41842), along the Palos Verdes Peninsula of Southern California, USA, operated as the focal site for this study (Fig. 1). Bedrock and large boulders, common substrate for *M. pyrifera*, were interspersed with sand patches. Unlike habitats with substrate dominated by fine sediments, which can shift through time, the bottom topography of this rocky reef remained static. Prior to the study, Marguerite Reef was blanketed by an urchin barren and devoid of a kelp forest. Urchins were subsequently removed, as a part of a large-scale restoration of *M. pyrifera* that began in Fall of 2016 and continued into January 2017.

### *Kelp surveys*

Kelp forest regrowth, following the restoration activities, was characterized monthly between November 2016 and November 2017 along eight evenly spaced transects (30 m x 4 m, 30 m apart) oriented along-isobath, spanning the cross-shore extent of the rocky reef. Along each transect, *M. pyrifera* individuals and stipes were counted to estimate the density of giant kelp. Only individuals with heights greater than 1 m were included in these counts. The kelp forest density time series was then partitioned into categories describing the overall kelp conditions (i.e., No Kelp, Transition, and Kelp), to allow for categorical assignment for statistical analyses outlined below. Time periods characterized as “No Kelp” spanned from the start of the study in November 2016 to the first sightings of the singled-bladed sporophytes on the sea floor, in April 2017. The “Kelp” period began once stipes reached the surface and most kelp individuals had four stipes (a commonly used criterion for classifying individuals as adults; Dayton et al. 1992), which occurred late in July 2017. The Kelp period ended in late October 2017; we terminated the study then to exclude subsequent sharp reductions in kelp density due to seasonal senescence characteristic of Southern California kelp forests (Rodriguez et al. 2013). The “Transition” period extended between the No Kelp and Kelp time periods, characterized by new forest growth and rapid change in kelp density.

### *Wave theory*

Surface gravity waves, which comprise the seas and swell that interact most strongly with kelp and are of concern for coastal erosion, propagate as physical disturbances of the sea surface.

They can be characterized by their height,  $H$ ; their wavelength,  $L$ ; and frequency,  $f$ . The former is the difference in sea surface displacement between peak and trough, the wavelength spans the distance between successive peaks, and the frequency is the inverse of wave period,  $T$ , which is the time elapsed between the passage of one peak until the next arrives. As is detailed elsewhere (e.g., Kinsman 1965; Denny 1988), any such wave has kinetic and potential energy components that sum to yield a total energy per unit area of ocean surface,  $E$ :

$$E = \frac{1}{8}\rho g H^2 \quad (1)$$

where  $\rho$  is the density of seawater and  $g$  is the acceleration due to gravity.

The rate at which a given wave's energy is propagated across space is the product of  $E$  and the so-called group velocity,  $C_g$ , which is the speed traveled by packets of waves of similar physical characteristics, where:

$$C_g = \frac{c}{2} \left( 1 + \frac{2kd}{\sinh(2kd)} \right) \quad (2)$$

Eqn. 2 contains several parameters, including the wavenumber,  $k$  ( $=2\pi/L$ ) and water depth,  $d$ . Sinh is the hyperbolic sine, where  $\sinh(x) = 0.5(e^x - e^{-x})$ . The quantity  $C$  is the wave celerity, the speed of transit of an individual wave, which is always at least as fast as its corresponding wave packet;  $C$  is defined by the wave dispersion relation (Kinsman 1965):

$$C = \left[ \frac{g}{k} \tanh(kd) \right]^{1/2} \quad (3)$$

where  $\tanh$  is the hyperbolic tangent,  $\tanh(x) = (e^x - e^{-x}) / (e^x + e^{-x})$ .

The rate of transmission of wave energy per unit width of wave crest for a given wave, also called the wave energy flux (or wave power), is conserved in the absence of friction or dissipation. As alluded to above, this quantity,  $P$ , is given by:

$$P = C_g E \quad (4)$$

Because  $C_g$  declines with decreasing water depth (Eqn. 2), waves tend to shoal (increase in height) as they approach the shore in order to meet the demand for conservation of wave energy flux.

The relationships of equations 1-4 are most readily visualized in terms of an individually propagating wave. However, natural sea states include waves of many heights, wavelengths, and frequencies, most of differing phase, which superpose on one another to yield a “random sea.” The summed wave energy flux from all of these constituents must be considered when evaluating any putative effects of kelp on wave attenuation. In practice, this task is accomplished using tools of spectral analysis to isolate from simple time series of sea surface displacement the

contributions of waves of differing frequency. In particular, a time record of surface displacement,  $\eta(t)$ , can be represented in terms of a Fourier series:

$$\eta(t) = \sum_{i=1}^N a_i \cos(2\pi t i f_f - \phi_i) \quad (5)$$

where  $N$  is the number of waveforms of different frequency or period that sum to produce the overall record of surface displacement (note that these are harmonics of the fundamental frequency,  $f_f$ , which is the inverse of the total duration of the time series),  $a_i$  is the amplitude ( $a_i = H/2$ ) of a given waveform ( $i$ ),  $t$  is time, and  $\phi_i$  is the phase shift appropriate to the waveform. By means of trigonometric identities this expression can also be rewritten:

$$\eta(t) = \sum_{i=1}^N (\alpha_i \cos 2\pi t i f_f + \beta_i \sin 2\pi t i f_f) \quad (6)$$

With this notation (taking note also that  $a_i \neq \alpha_i$ ), the height of the waveform corresponding to frequency  $i$  is given by:

$$H_i = 2\sqrt{\alpha_i^2 + \beta_i^2} \quad (7)$$

where  $\alpha$  and  $\beta$  are the so-called Fourier coefficients of Eqn. 6. The total wave energy flux,  $Q$ , accounting for the full complement of waves underlying the random sea, and combining equations 1 and 7, is then computed as the sum of the energy fluxes from each underlying wave frequency component:

$$Q = \sum_{i=1}^N C_{g,i} E_i \quad (8)$$

where now the group velocities and energy fluxes associated with waves of differing frequency or period are explicitly tracked.

Relationships among the total wave energy flux,  $Q$ , outside and inside the reef, in the absence and presence of kelp, can be used to isolate dissipative losses due to kelp from other agents of energy loss. In the present experiment,  $Q$  was quantified both at the station outside of the kelp forest ( $Q_{outside}$ ), and within the bed near its inshore edge ( $Q_{inside}$ ). Time records of sea surface displacement, measured at each station, were employed to compute the elements of  $Q$  (i.e.,  $C_g$  and  $E$ ), using the equations outlined above. The difference between  $Q_{outside}$  and  $Q_{inside}$  then quantifies the loss of wave energy flux as waves propagate from outside to inside the reef habitat. If no energy loss occurs, the  $Q$ 's would be equal. However, energy losses always arise, and in the absence of kelp, such losses are dominated by the effects of bottom friction. This baseline difference can then be compared to that arising in the presence of kelp, with any additional offset between  $Q_{outside}$  and  $Q_{inside}$  indicating the effects of kelp. We note that although refraction (waves “bending” in shallow water until they propagate perpendicular to isobaths) can influence values of  $Q$  at a given location, satellite imagery of our site indicates that wave crests

have already refracted before reaching the study site and approach mostly normal to shore by the outside station (Planet Team 2020; Fig. S1). More importantly, the key comparison of the above analysis is not between values of  $Q$  at the two stations, but rather how the quantity ( $Q_{outside} - Q_{inside}$ ) changes between times of kelp and no kelp. Although effects of refraction on the latter are formally possible, scenarios of appreciable modification are implausible, given the perpendicular approach of waves to Marguerite Reef, and the reef's positioning on a relatively straight segment of the shoreline with roughly parallel depth contours. Likewise, while interactions between shoreward and reflected waves could influence values of  $Q$  through constructive and/or destructive wave interference, the rugose topography of the beach and its modest slope make substantial reflection unlikely.

#### *Wave measurements and analyses*

In undertaking the calculations of  $Q_{outside}$  and  $Q_{inside}$ , bottom-mounted pressure sensors (SBE-26 Seagauge Wave & Tide Recorder [Sea-Bird Scientific, Bellevue WA, USA]), were deployed inside and outside the kelp forest habitat at mean depths of 6 m and 17 m, respectively. Both sensors were positioned outside of the surf zone, such that there should be negligible losses due to turbulent dissipation. Pressure measurements were taken throughout the duration of the project in both the absence and presence of kelp over a suite of incident sea state conditions. Seven instrument deployments were conducted, during which the SBE-26s recorded pressure at the seafloor at 4 Hz, over 17 min bursts, four times a day, for a duration of 21 days per deployment.

Because pressure signals of wave-driven surface displacements attenuate exponentially with depth, sea surface time series were reconstituted per accepted methods by back-correcting the depth-attenuated records acquired by the sensors. The back-correction is frequency dependent, given that higher frequency waves attenuate faster with depth. Such higher frequency waves also have shorter wavelengths in a given water depth. For a specified wave frequency (or wavelength), the attenuation factor is (Denny 1988):

$$K = \cosh(kz)/\cosh(kd) \tag{9}$$

where  $z$  is the distance above the seafloor and  $\cosh$  is the hyperbolic cosine, where  $\cosh(x) = 0.5(e^x + e^{-x})$ . The surface displacement associated with a wave of given frequency or period is therefore determined by dividing its at-depth pressure by the appropriate  $K$  to re-expand the attenuated waveform.

Because any noise in the pressure record could also get re-expanded (yielding spurious estimates of surface displacement), the resolution of the sensors was also quantified by deploying them immediately below a Datawell Waverider MkIII buoy (CDIP buoy 158) that records sea surface heights directly, without any attenuation. This was done in water of the same depth as the outside station (17 m). Using this procedure, it was possible to verify that the bottom-mounted sensors and the de-attenuation protocol accurately estimated surface displacements associated with waves with periods longer than 3.7 sec. Shorter period waves were vulnerable to noise re-expansion. In all subsequent analyses only waves with periods in excess of this cutoff were used.

Statistical summary parameters also were computed at the outside station to characterize the incident sea state, prior to any potential physical interactions with kelp. In particular, significant wave height,  $H_s$ , and the dominant (or peak) wave period,  $T_p$ , were determined from the wave data, burst-by-burst, as:

$$H_s = 4\sigma \quad (10)$$

$$T_p = \frac{1}{f(\max(S))} \quad (11)$$

where  $\sigma$  is the standard deviation of the sea surface displacement and  $f(\max(S))$  is the wave period at which the power spectrum of sea surface displacement,  $S$ , exhibits its maximum.

Ultimately, as discussed previously, the key quantity of interest is how the difference in wave energy flux between the outside ( $Q_{outside}$ ) and inner edge of the forest ( $Q_{inside}$ ) depends on the absence or presence of kelp. Because incident wave conditions also vary through time (as indexed by changes in  $Q_{outside}$  across bursts), the spatial differences in wave energy flux from outside to inside the forest can be normalized:

$$\Delta Q_{norm} = \frac{Q_{outside} - Q_{inside}}{Q_{outside}} = 1 - \frac{Q_{inside}}{Q_{outside}} \quad (12)$$

where  $\Delta Q_{norm}$  is the change in energy flux from outside to inside, normalized by the incident energy flux,  $Q_{outside}$ . This quantity is therefore the proportional change in wave energy flux between the outside and inside stations, with positive values representing energy loss.

### *Influence of kelp on wave attenuation*

$\Delta Q_{norm}$  represents the wave energy flux lost due to wave-benthos interactions *plus* any due to wave-kelp interactions. If *M. pyrifera* has no effect on wave conditions, given that the bottom terrain did not change between time periods in the absence and presence of kelp, the proportional change in wave energy flux would remain invariant.

To test for differences in  $\Delta Q_{norm}$  in the absence and presence of kelp, a linear regression was constructed with proportional change in wave energy flux from outside to inside as the response variable, and kelp condition (i.e., No Kelp and Kelp) as a predictor. This analysis yields a basic understanding of how the presence of kelp influences wave energy flux. However, kelp forests may attenuate waves of different height or period differently. To evaluate this possibility, the linear regression model was structured to include not only kelp condition (i.e., No Kelp and Kelp), but also the dominant wave period ( $T_p$ ) and significant wave height ( $H_s$ ) at the outside station, as well as their associated interactions, as additional predictors for the proportional change in wave energy flux from outside to inside. Finally, to check if the latter model was overfitted, a backward step-wise model selection was conducted to determine the best fitting model. Associated AIC scores and models tested are shown in Table 1. The residuals in the model were tested for normality using a Shapiro test and assessed for heteroscedasticity visually. Residuals appear homoscedastic, but do not fall within a normal distribution (Shapiro test,

p=0.002). Given the large sample size and the fact that a violation of non-normality would not change the point estimates, the model appears appropriate for describing the dataset, although the confidence intervals could be slightly inflated. Pairwise comparisons of the effect of kelp, between  $H_s$  and  $T_p$ , were conducted using a Tukey correction. All statistical tests were accomplished in R version 3.6.1 (R Core Team, 2019) and pairwise comparisons were conducted using the package *emmeans* (Length 2020).

## RESULTS

### *Kelp densities*

The benthos was devoid of all vegetation throughout the No Kelp period. Single-bladed kelp recruits appeared at Marguerite Reef in April 2017 and grew to the surface throughout the following seven months (Fig. 2). The overall stipe density of *Macrocystis pyrifera* increased rapidly throughout the Transition period (April through July 2017), reaching densities typical of mature *M. pyrifera* populations found in California (1.9-15 stipes m<sup>-2</sup>, North 1971) by the Kelp period (Fig. 2A), which encompassed late July through October 2017. At the onset of the Transition period, the new kelp forest was composed of many small individuals, each consisting of one or two stipes per individual (Fig. 2B). Over time, the young individuals began to support more stipes per plant, such that most entered the adult classification (four or more stipes) early in the Kelp period. There was little to no presence of an understory algal community throughout the experimental time period, with the extremely rare sighting of understory species that often occupy Southern California's rocky reefs, including *Sargassum horneri*, *Sargassum muticum*,

*Pterygophora californica*, *Eisenia arborea*, and *Egregia menziesii*, even following re-establishment of the giant kelp canopy.

### *Wave conditions*

Coastal wave conditions varied appreciably throughout the study. Incident significant wave heights ( $H_s$ ), as recorded at the outside measurement station and computed burst-by-burst, ranged from 0.34 – 4.3 meters. Dominant wave periods ( $T_p$ ) spanned 4.17 – 19.6 seconds. The modal incident significant wave height was 0.6 meters, and the modal dominant wave period was 15 seconds. Conditions also encompassed both narrow-banded sea states dominated by single wave periods, as well as broader-banded sea states where waves of a variety of periods arrived at the site. Time series of sea surface displacement displayed a strong signature of waves both at the outside station and at the station located on the inshore edge of the forest domain (Fig. 3). However, this trend held regardless of whether kelp was present or not. Note if kelp had a dramatic damping effect, the amplitudes of the surface elevation record, in the presence of kelp, would have been greatly depressed, resulting in reduced deviations from the zero line. However, such a pattern did not manifest in our dataset, preventing simple comparisons of time series across the outside and inside stations from providing insight into potential levels of wave attenuation by *Macrocystis*. This pattern was not surprising given that as waves move shoreward, they both increase in height through shoaling, while simultaneously experiencing bottom friction that tends to decrease their height. Due to these contrasting processes, rudimentary comparisons of outside versus inside records of sea surface displacement intrinsically provide a poor way to assess effects of kelp on wave energy attenuation (Fig. 3).

Spectral analyses could in theory provide a more effective tool for evaluating wave damping potential. As noted in the Methods, such approaches enable time series of sea surface displacement to be decomposed into their harmonics in the frequency (or wave period) domain. In particular, such approaches allow for computation of the distribution of wave energy across a range of wave periods, which shows which periods contribute most to the overall energy. In Figure 4A, for example, at the outside location in the absence of kelp, much of the energy in the wave field is associated with waves of 16 second period, as indicated by the peak at 0.06 Hz. If kelp forests strongly attenuated wave energy one might then expect this peak to decline in the inside spectrum when kelp is present (i.e., one could look for stronger differences between the outside and inside spectra in the presence of kelp than when it was absent; Fig. 4). As is apparent in this representative figure, however, the extent of overlap between outside and inside spectra, regardless of the presence or absence of kelp, look similar.

Notably, however, although wave power spectra represent a common way to display information about sea state, they are less appropriate for assessing the capacity for kelp to damp waves. This point follows from the fact that it is the rate of energy transfer through space (the wave energy flux) that is conserved in the absence of dissipation, rather than energy per se. Indeed, as waves shoal, they increase in height as noted above, which increases their kinetic and potential energy per area. This process at first glance sounds nonphysical, because it indicates greater energy in waves that have propagated further shoreward and thus (superficially) implies a violation of conservation laws. What reconciles the inconsistency is that as waves shoal, their passage across space also slows, which leads to the conservation of wave energy flux. We therefore utilize, as outlined in the Methods, differences between the wave energy flux outside and inside as a metric for effects of kelp on waves.

### *Wave damping by kelp*

In the absence of kelp, the site at Marguerite Reef exhibited an average reduction of 12.1% in wave energy flux between the outside and inside locations (Fig. 5A, Table 2,  $p \leq 0.001$ ), attributed to effects of bottom friction. Importantly, an additional 7.2% was lost when kelp was present (Fig. 5A, Table 2,  $p \leq 0.001$ ). The distribution of reductions in energy flux also varied substantially in both the absence and presence of kelp. However, some component of the breadth of the distributions likely reflects burst-level statistical uncertainty (e.g., due to innate error associated with the spectral estimates), as evidenced by a portion of the distributions in Fig. 5B and 5C falling to the left of zero. Note that the rightward shift to higher losses in the kelp distribution highlights the additional loss in energy flux due to the presence of kelp (Fig. 5B-C).

The amount of kelp-driven energy dissipation depended subtly on wave height and period, as revealed in the linear regression analysis (Table 3). Although shorter period waves tended to lose relatively more energy while transiting between the outside and inside stations than longer period waves (note higher elevations in Fig. 6 of the leftmost portions of the curves), kelp-associated decreases in wave energy flux were greater for waves of longer periods (the lines for Kelp and No Kelp deviate more strongly for longer period waves; Fig. 6). There was also a minor effect of incident wave height, with stronger kelp damping of smaller waves ( $< 0.75$  m) on a percentage basis compared to larger waves ( $> 1$  m). This effect is apparent as a flattening of the Kelp slopes, relative to the No Kelp slopes, across panels of Fig. 6.

In contrast to detectable effects of wave height and period on levels of attenuation by kelp, we saw no evidence that the directional character of waves kilometers offshore of the site

strongly influenced the dissipation rates at our sensor locations (direction data derived from Datawell Waverider MkIII CDIP buoy 028; Fig. S2A). The pattern held despite strong seasonal variation in the basin-scale wave climate, characterized by a bimodal distribution of offshore wave directions, such that offshore waves originated more often from the west in the winter and more often from the south and southwest in the summer (Fig. S2A and S2C). As with the direction of waves while in deep water, regional wind fields (quantified using NDBC buoy station 46025) also appeared to play little role in influencing the levels of kelp damping (Fig. S2B and S2D).

## **DISCUSSION**

In this study, we were able to explicitly test the physical effect of kelp on the local wave field, by measuring wave activity in the same topographically static site before and during kelp forest presence. This approach allowed us to directly confront a persistent challenge to disentangling effects of kelp from other factors. In particular, it allowed us to separate kelp effects from those tied to seabed properties, the latter which often differ between kelp and non-kelp sites, due to the preference of kelp for rock outcrops versus less-consolidated substrata like cobble, sediment, or sand. In our case, we found that a *M. pyrifera* forest, in Palos Verdes, CA, had a detectable but limited capacity to damp wave energy. Wave interactions with the seafloor alone reduced wave energy flux, on average, by 12%, with an additional 7% reduction when an established kelp forest was present, over a propagation distance of 180 meters.

*Factors governing damping potential*

Although this study found that *Macrocystis pyrifera* forests have some capacity to damp waves, the magnitude of attenuation is small compared to that attributed to other forms of aquatic vegetation. Some kelps with stiffer support structures and which do not form floating surface canopies, such as *Laminaria hyperborea*, have been shown to substantially decrease wave heights (50%; Dubi and Torum 1996) and/or damp wave energy (70-85%; Mork 1996, though these latter estimates include effects of bottom dissipation). Mangroves, which are considerably stiffer than kelps and protrude out of the water, may attenuate up to 72% of incident wave energy (Horstman et al. 2012). Salt marsh vegetation, which also is emergent and only modestly flexible, has been shown to exhibit 60 to 80% reduction in wave energy (Knutson et al., 1982; Riffe et al. 2011; Möller et al. 2014). Seagrasses, which are more flexible, emergent sometimes, and found in substantially shallower waters relative to those in which *Macrocystis pyrifera* resides, have been shown to reduce wave energy by 20 to 40% (Fonseca and Cahalan 1992). We note, however, that these prior studies do not present information concerning vegetation-induced reductions in wave energy flux (as opposed to wave heights or wave energy per area), so direct comparison to the present study is difficult.

Assemblage or forest size, density, extent of submergence, morphology, and the stiffness of seaweed or plant structures are all expected to affect the damping potential of various types of aquatic vegetation (Tinoco et al. 2020). In particular, it is likely the exceptionally large size, positioning of considerable kelp biomass at the water's surface, and the capacity for *Macrocystis pyrifera* to sway appreciably with passing waveforms together influence its interaction with waves (see, e.g., scaling arguments of Denny et al. 1998). However, determining which of these features contribute most strongly to the low levels of attenuation of wave energy flux observed here, will require further study.

### *Wave versus current damping*

The relatively low levels of wave damping observed in the present study may fall at odds with expectations of some kelp workers, given the recognized ability of large forests to slow currents (e.g., Jackson and Winant 1983), and the common misconception that currents and waves will tend to interact similarly with aquatic vegetation. However, the assumption that currents and waves operate the same way is false. The time scale of currents and their reversals is distinctly different from that of wave-driven oscillations. In the case of nearshore currents, which typically change directions over hours in association with tides, considerable data indicate that these flows can indeed experience strong damping. This damping arises in aquatic vegetation as diverse as seagrass meadows (Fonseca et al. 1982; Koch and Gust 1999), turf and understory seaweeds (Carpenter and Williams 1993), and inside forests of large canopy-forming macroalgae (Jackson and Winant 1983; Gaylord et al. 2007; Rosman et al. 2007). A key issue is that tidal currents flow in the same direction for sufficiently long durations that even canopy-forming kelps can be fully drawn out in the direction of flow, such that drag can act on them quite strongly.

Waves, in contrast, oscillate over seconds, and reverse quickly enough that they are believed to have a much-reduced capacity to fully extend large, canopy-forming species to where they become stationary and subject to the maximal relative flow speeds that they can experience. This point has been discussed at length in the literature for many years (see, e.g., Koehl 1984). Nevertheless, such fundamental differences between currents and waves often get overlooked in considerations of how large canopy-forming kelps interact with water motions of different time scales.

### *Limitations of the study*

Although this study was able to detect an effect of kelp on wave energy flux, the underlying measurements were conducted in only a single forest. The degree to which a given *M. pyrifera* forest might modify wave energy flux could vary according to a number of site-specific and forest-specific characteristics. The forest used in this study, although within the range of plant and stipe densities characteristic of many *Macrocystis pyrifera* forests, was a moderately sized forest in terms of spatial extent (180 m in cross-shore width). A forest with greater cross-shore canopy extent would impose a greater total amount of damping, even given an identical rate of decrease in wave energy flux per meter of transit through a forest. We also acknowledge that Southern California generally experiences more benign sea state conditions than some other locales, and consequently the incident wave conditions observed throughout our study were limited mostly to modest-sized wave heights. That said, sea state conditions much in excess of those we recorded approach those that dislodge kelp from the substratum (Seymour et al. 1989). The potential for appreciably greater magnitudes of wave energy attenuation by giant kelp therefore appears limited.

### **CONCLUSION**

This study quantified the effect of a giant kelp forest on surface gravity waves using field measurements of waves at a single site in the absence and presence of kelp. Kelp-associated effects were isolated from those attributed to interactions with the seafloor using a before-after experimental design. Kelp-associated reductions in wave energy flux were detectable, but not

substantial, and varied with impinging wave heights and periods. Waves of smaller heights and longer periods exhibited the most damping in the presence of kelp. Although giant kelp does cause wave attenuation, the degree of damping is small, compared to multiple other types of aquatic vegetation. These findings reinforce and confirm previous work, conducted without the advantage of an explicit no-kelp/with-kelp experimental design, suggesting limited potential for wave attenuation. Benefits of *Macrocystis pyrifera* forests for shoreline protection therefore appear modest, other valuable features of such forests notwithstanding.

#### **ACKNOWLEDGEMENTS:**

This work was supported by the California State Coastal Conservancy [grant number 15-013], National Science Foundation (NSF) [grant number OCE-1636191], University of Southern California, Sea Grant [grant number NA180AR4170075], and Dolby Laboratories. K.E.E. was additionally supported by an NSF Graduate Research Fellowship, Bilinski Fellowship, and a Norcal Society of Environmental Toxicology and Chemistry grant. The authors are grateful to M. Anghera, A. Barilotti, H. Burdick, B. Burford, B. Cohn, K. Dubois, B. Grimes, T. Herzik, J. Hollarsmith, P. House, G. Ng, A. Ninokawa, J. Smart, B. Sterling, and G. Thompson for field and logistical assistance.

#### **LITERATURE CITED:**

Arkema, K.K., R. Griffin, S. Maldonado, J. Silver, J. Suckale, and A.D. Guerry. 2017. Linking social, ecological, and physical science to advance natural and nature-based protection for coastal communities. *Annals of the New York Academy of Sciences* 1399: 5-26, doi:10.1111/nyas.13322.

Carpenter, R.C., and S.L. Williams. 1993. Effects of algal turf canopy height and microscale substratum topography on profiles of flow speed in a coral forereef environment. *Limnology and Oceanography* 38: 687-694, doi:10.4319/lo.1993.38.3.0687.

Dalrymple, R.A., M. ASCE, J.T. Kirby, and P.A. Hwang. 1984. Wave diffraction due to areas of energy dissipation. *Journal of Waterway Port Coastal and Ocean Engineering* 110: 67-79, doi:10.1061/(ASCE)0733-950X(1984)110:1(67).

Darwin, C. 1839. *The Voyage of the Beagle*. (Reprinted in 1962, *The Harvard Classics*). P.F. Collier & Son Company, New York.

Dayton, P.K. 1972. Toward an understanding of community resilience and the potential effects of enrichments to the benthos at McMurdo Sound, Antarctica. *Proceedings of the Colloquium on Conservation Problems in Antarctica*, B.C. Parker (Ed.) Allen Press, 81-96.

Dayton, P.K., M.J. Tegner, P.E. Parnell, and P.B. Edwards. 1992. Temporal and spatial patterns of disturbance and recovery in a kelp forest community. *Ecological Monographs* 62: 421-445, doi:10.2307/2937118.

Denny, M.W. 1988. *Biology and the Mechanics of the Wave-Swept Environment*. Princeton, NJ: Princeton University Press.

Denny, M.W., B.P. Gaylord, E.A. Cowen. 1997. Flow and flexibility II. The roles of size and shape in determining wave forces on the bull kelp *Nereocystis luetkeana*. *Journal of Experimental Biology* 200: 3165-3183.

Denny, M., B. Gaylord, B. Helmuth, and T. Daniel. 1998. The menace of momentum: Dynamic forces on flexible organisms. *Limnology and Oceanography* 43: 955-968, doi:10.4319/lo.1998.43.5.0955.

Dubi, A., and A. Tørum. 1996. Wave energy dissipation in kelp vegetation. *Proceedings on Coastal Engineering* 3: 2625-2639, doi:10.1061/9780784402429.203.

Elwany, M.H.S., W.C. O'Reilly, R.T. Guza, and R.E. Flick. 1995. Effects of Southern California kelp beds on waves. *Journal of Waterway Port Coastal and Ocean Engineering* 121: 143-150.

Fonseca, M.S., J.S. Fisher, J.C. Zieman, and G.W. Thayer. 1982. Influence of the seagrass, *Zostera marina* L., on current flow. *Estuarine, Coastal, and Shelf Science* 15: 351-364, doi:10.1016/0272-7714(82)90046-4.

Fonseca, M.S., and J.A. Cahalan. 1992. A preliminary evaluation of wave attenuation by four species of seagrass. *Estuarine, Coastal, and Shelf Science* 35: 565-576, doi:10.1016/S0272-7714(05)80039-3.

Gaylord, B., and M.W. Denny. 1997. Flow and flexibility I. Effects of size, shape and stiffness in determining wave forces on the stipitate kelps *Eisenia arborea* and *Pterygophora californica*. *Journal of Experimental Biology* 200: 3141-3164.

Gaylord, B., B.B. Hale, and M.W. Denny. 2001. Consequences of transient fluid forces for compliant benthic organisms. *The Journal of Experimental Biology* 204: 1347-1360.

Gaylord, B., M.W. Denny, M.A. Koehl. 2003. Modulation of wave forces on kelp canopies by alongshore currents. *Limnology and Oceanography* 48: 860-871, doi:10.4319/lo.2003.48.2.0860.

Gaylord, B., D.C. Reed, L. Washburn, P.T. Raimondi. 2004. Physical-biological coupling in spore dispersal of kelp forest macroalgae. *Journal of Marine Systems* 49: 19-39, doi: 10.1016/j.jmarsys.2003.05.003.

Gaylord, B., J.H. Rosman, D.C. Reed, J.R. Koseff, J. Fram, S. MacIntyre, K. Arkema, C. McDonald, M.A. Brzezinski, J.L. Largier, S.G. Monismith, P.T. Raimondi, and B. Mardian. 2007. Spatial patterns of flow and their modification within and around a giant kelp forest. *Limnology and Oceanography* 52: 1838-1852, doi:10.2307/4502339.

Gaylord, B., M.W. Denny, M.A.R. Koehl. 2008. Flow forces on seaweeds: Field evidence for roles of wave impingement and organism inertia. *Biology Bulletin* 215: 295-308.

Gaylord, B., K.J. Nickols, L. Jurgens. 2012. Roles of transport and mixing processes in kelp forest ecology. *The Journal of Experimental Biology* 215: 997-1007, doi: 10.1242/jeb.059824.

Henderson, S.M. 2019. Motion of buoyant, flexible aquatic vegetation under waves: Simple theoretical models and parameterization of wave dissipation. *Coastal Engineering* 152: 103497, doi:10.1016/j.coastaleng.2019.04.009.

Hirsh, H.K., K.J. Nickols, Y. Takeshita, S.B. Traiger, D.A. Mucciarone, S. Monosmith, R.B. Dunbar. 2020. Drivers of biogeochemical variability in a Central California kelp forest: Implications for local amelioration of ocean acidification. *Journal of Geophysical Research: Oceans* 125: 1-22, doi: 10.1,29/2020JC016320.

Horstman, E.M., M. Dohmen-Janssen, P. Narra, N.J.F. Van den Berg, M. Siemerink, T. Balke, T. Bouma, and S. Hulscher. 2012. Wave attenuation in mangrove forests; field data obtained in trang, Thailand. *Coastal Engineering Proceedings* 1:40, doi:10.9753/icce.v33.waves.40.

Houser, C., S. Trimble, B. Morales. 2015. Influence of blade flexibility on the drag coefficient of aquatic vegetation. *Estuaries and Coasts* 38: 569-577, doi:10.1007/s12237-014-9840-3.

Jackson, G.A., C.D. Winant. 1983. Effect of a kelp forest on coastal currents. *Continental Shelf Research* 2: 75-80. doi:10.1016/0278-4343(83)90023-7.

Kinsman, B., 1965. *Wind Waves*. Dover Publications, New York, NY.

Knutson, P.L., R.A. Brochu, W.N. Seelig, M.R. Inskeep. 1982. Wave damping in *Spartina alterniflora* marshes. *Wetlands* 2: 87-104. doi:10.1007/BF03160548.

Kobayashi, N., A.W. Raichle, T. Asano. 1993. Wave attenuation by vegetation. *Journal of Waterway Port Coastal and Ocean Engineering* 119: 30-48. doi:10.1061/(ASCE)0733-950X(1993)119:1(30).

Koch, E.W. and G. Gust. 1999. Water flow in tide- and wave-dominated beds of the seagrass *Thalassia testudinum*. *Marine Ecology Progress Series* 184: 63-72. doi:10.3354/meps184063.

Koehl, M.A.R. 1984. How do benthic organisms withstand moving water? *American Zoologist* 24: 57-70, doi:10.1093/icb/24.1.57.

Lenth, R. 2020. emmeans: Estimated Marginal Means, aka Least-Squares Means. R package version 1.4.5. <https://CRAN.R-project.org/package=emmeans>

- Luhar, M., E. Infantes, H. Nepf. 2017. Seagrass blade motion under waves and its impact on wave decay. *Journal of Geophysical Research: Oceans* 122: 3736-3752, doi:10.1002/2017JC012731.
- Mendez, F.J. and I.J. Losada. 2004. An empirical model to estimate the propagation of random breaking and nonbreaking waves over vegetation fields. *Coastal Engineering* 51: 103-118, doi:10.1016/j.coastaleng.2003.11.003.
- Miller, R.J., K.D. Lafferty, T. Lamy, L. Kui, A. Rassweiler, and D.C. Reed. 2018. Giant kelp, *Macrocystis pyrifera*, increases faunal diversity through physical engineering. *Proceedings of the Royal Society B: Biological Sciences* 285: 20172571, doi:10.1098/rspb.2017.2571.
- Möller, I., M. Kudella, F. Rupprecht, T. Spencer, M. Paul, B.K. van Wesenbeeck, G. Wolters, K. Jensen, T.J. Bouma, M. Miranda-Lange, S. Schimmels. 2014. Wave attenuation over coastal salt marshes under storm surge conditions. *Nature Geosciences* 7:727-731, doi: <https://doi.org/10.1038/ngeo2251>.
- Mork, M. 1996. The effect of kelp in wave damping. *Sarsia* 80: 323-327.
- Morris, R.L., T.D.J. Graham, J. Kelvin, M. Ghisalberti, and S.E. Swearer. 2020. Kelp beds as coastal protection: wave attenuation of *Ecklonia radiata* in a shallow coastal bay. *Annals of Botany* 125: 235-246, doi:10.1093/aob/mcz127.
- Mullarney, J.C. and C.A. Pilditch. 2017. The differential response of kelp to swell and infragravity wave motion. *Limnology and Oceanography* 62: 2524-2537, doi:10.1002/lno.10587.
- North, W.J. 1971. The biology of giant kelp beds (*Macrocystis*) in California. *Nova Hedwigia* 32: 1-600.
- Paul M., T.J. Bouma, and C.L. Amos. 2012. Wave attenuation by submerged vegetation: combining the effect of organism traits and tidal current. *Marine Ecology Progress Series* 444: 31-41.
- Planet Team (2020). Planet Application Program Interface: In Space for Life on Earth. San Francisco, CA. <https://api.planet.com>.

R Core Team (2019). R: A language and environment for statistical computing. R Foundation for Statistical Computing, Vienna, Austria. URL <https://www.R-project.org/>.

Reed, D.C., and M.S. Foster. 1984. The effects of canopy shadings on algal recruitment and growth in a giant kelp forest. *Ecology* 65: 937-948, doi:10.2307/1938066.

Reed, D.C., A. Rassweiler, M.H. Carr, K.C. Cavanaugh, D.P. Malone, and D.A. Siegel. 2011. Wave disturbance overwhelms top-down and bottom-up control of primary production in California kelp forests. *Ecology* 92: 2108-2116, doi:10.2307/23034943.

Reidenbach, M.A., and E.L. Thomas. 2018. Influence of the seagrass, *Zostera marina*, on wave attenuation and bed shear stress within a shallow coastal bay. *Frontiers in Marine Science* 5: 397, doi:10.3389/fmars.2018.00397.

Riffe, K.C., S.M. Henderson, J.C. Mullarney. 2011. Wave dissipation by flexible vegetation. *Geophysical Research Letters* 38: L18607, doi:10.1029/2011GL048773.

Rodriguez, G.E., A. Rassweiler, D.C. Reed, and S.J. Holbrook. 2013. The importance of progressive senescence in the biomass dynamics of giant kelp (*Macrocystis pyrifera*). *Ecology* 94: 1848-1858, doi:10.1890/12-1340.1.

Rosman, J.H., J.R. Koseff, S.G. Monismith, and J. Grover. 2007. A field investigation into the effects of a kelp forest (*Macrocystis pyrifera*) on coastal hydrodynamics and transport. *Journal of Geophysical Research* 112: C02016, doi: 10.1029/2005JC003430.

Rosman, J.H., S.G. Monismith, M.W. Denny, and J.R. Koseff. 2010. Currents and turbulence within a kelp forest (*Macrocystis pyrifera*): Insights from a dynamically scaled laboratory model. *Limnology and Oceanography* 55: 1145-1158, doi:10.4319/lo.2010.55.3.1145.

Rosman, J.H., M.W. Denny, R.B. Zeller, S.G. Monismith, and J.R. Koseff. 2013. Interaction of waves and currents with kelp forests (*Macrocystis pyrifera*): Insights from a dynamically scaled laboratory model. *Limnology and Oceanography* 58: 790-802, doi:10.4319/lo.2013.58.3.0790.

Seymour, R.J. and D.M. Hanes. 1979. Performance analysis of tethered float breakwater. *Journal of The Waterway, Port, Coastal and Ocean Division* 105: 265-280.

Seymour, R.J., M.J. Tegner, P.K. Dayton, and P.E. Parnell. 1989. Storm wave induced mortality of giant kelp, *Macrocystis pyrifera*, in Southern California. *Estuarine, Coastal and Shelf Science* 28: 277-292.

Schiel, D.R., and M.S. Foster. 2015. *The Biology and Ecology of Giant Kelp Forests*. University of California Press Books, doi:0.1525/9780520961098.

Tinoco, R.O., J.E. San Juan, and J.C. Mullarney. 2020. Simplification bias: lessons from laboratory and field experiment on flow through aquatic vegetation. *Earth Surface Processes and Landforms* 45: 121-143, doi: 10.1002/esp.4743.

**TABLES**

Table 1. Akaike’s Information Criterion scores (AIC), their degrees of freedom, and predictors for each model in the backward step-wise model selection process. Final model selected is in bold. KelpCond is kelp forest condition (i.e., No Kelp or Kelp), Tp\_Out is wave period outside of the kelp forest, Hs\_Out is significant wave height outside of the kelp forest.

	<b>Model</b>	<b>df</b>	<b>AIC</b>
1	KelpCond*Tp_Out*Hs_Out	9	-301.7766
2	(KelpCond+Tp_Out+Hs_Out)^2	8	-302.1443
3	KelpCond*Tp_Out+Tp_Out*Hs_Out	7	-300.9562
4	KelpCond*Hs_Out+Tp_Out*Hs_Out	7	-295.7272
<b>5</b>	<b>KelpCond*Tp_Out+KelpCond*Hs_Out</b>	<b>7</b>	<b>-303.7119</b>
6	KelpCond*Tp_Out+Hs_Out	6	-300.5064
7	KelpCond*Hs_Out+Tp_Out	6	-296.6553

Table 2. Summary results for linear model testing the effect of kelp presence on the proportional loss in wave energy flux. Bold values are statistically significant.

<b>Parameter</b>	<b>Estimate</b>	<b>Std. error</b>	<b>t-value</b>	<b>p-value</b>
Multiple $R^2 = 0.04734$ ; Adjusted $R^2 = 0.04419$				
<b>Intercept (No Kelp)</b>	<b>0.12084</b>	<b>0.01262</b>	<b>9.577</b>	<b>&lt;0.001</b>
<b>Kelp</b>	<b>0.07177</b>	<b>0.01853</b>	<b>3.874</b>	<b>&lt;0.001</b>

Table 3. Summary results for linear model testing the effect of kelp presence, incident wave period ( $T_p$ ), and incident wave height ( $H_s$ ) on the proportional loss in wave energy flux and the Tukey HSD pairwise comparison.

Parameter	Estimate	Std. error	t-value	p-value
Multiple $R^2 = 0.2392$ ; Adjusted $R^2 = 0.2264$				

Intercept (No kelp)	0.294377	0.052366	5.622	<0.0001
Kelp	0.023085	0.083509	0.276	0.78241
$T_p$ Outside	-0.023637	0.003536	-6.685	<0.0001
$H_s$ Outside	0.110327	0.022474	4.909	<0.0001
Kelp Presence * $T_p$ Outside	0.014520	0.004837	3.002	0.00291
Kelp Presence * $H_s$ Outside	-0.133661	0.058916	-2.269	0.02400
Tukey HSD pairwise comparison with $H_s$ Outside= 0.944 meters; $T_p$ Outside=12.3 seconds; df=298				
Contrast	Estimate	Std. error	t-ratio	p-value
No Kelp - Kelp	-0.0755	0.0217	-3.478	0.0006

## FIGURES

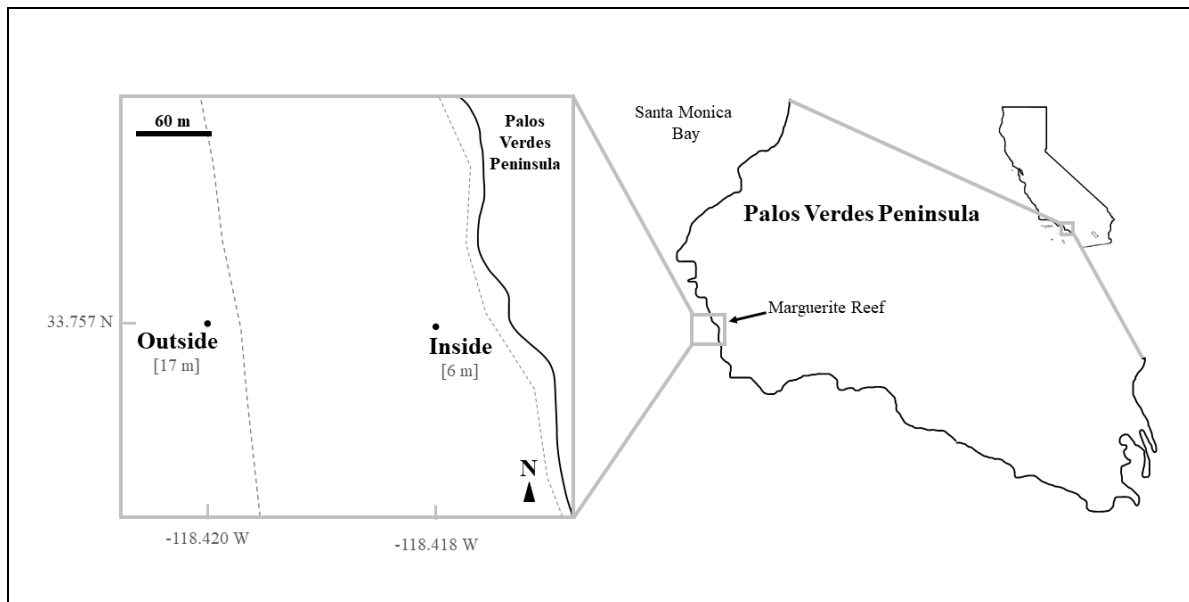


Fig. 1: Map of Marguerite Reef, Palos Verdes, California, USA, showing locations of the outside and inside pressure sensors, with their mean depths noted within brackets. The outer and inner edges of the kelp forest, which generally follow seabed isobaths, are represented by dashed lines. During times when the kelp forest was present at this site, it extended across and beyond the full north-south domain depicted in the inset.

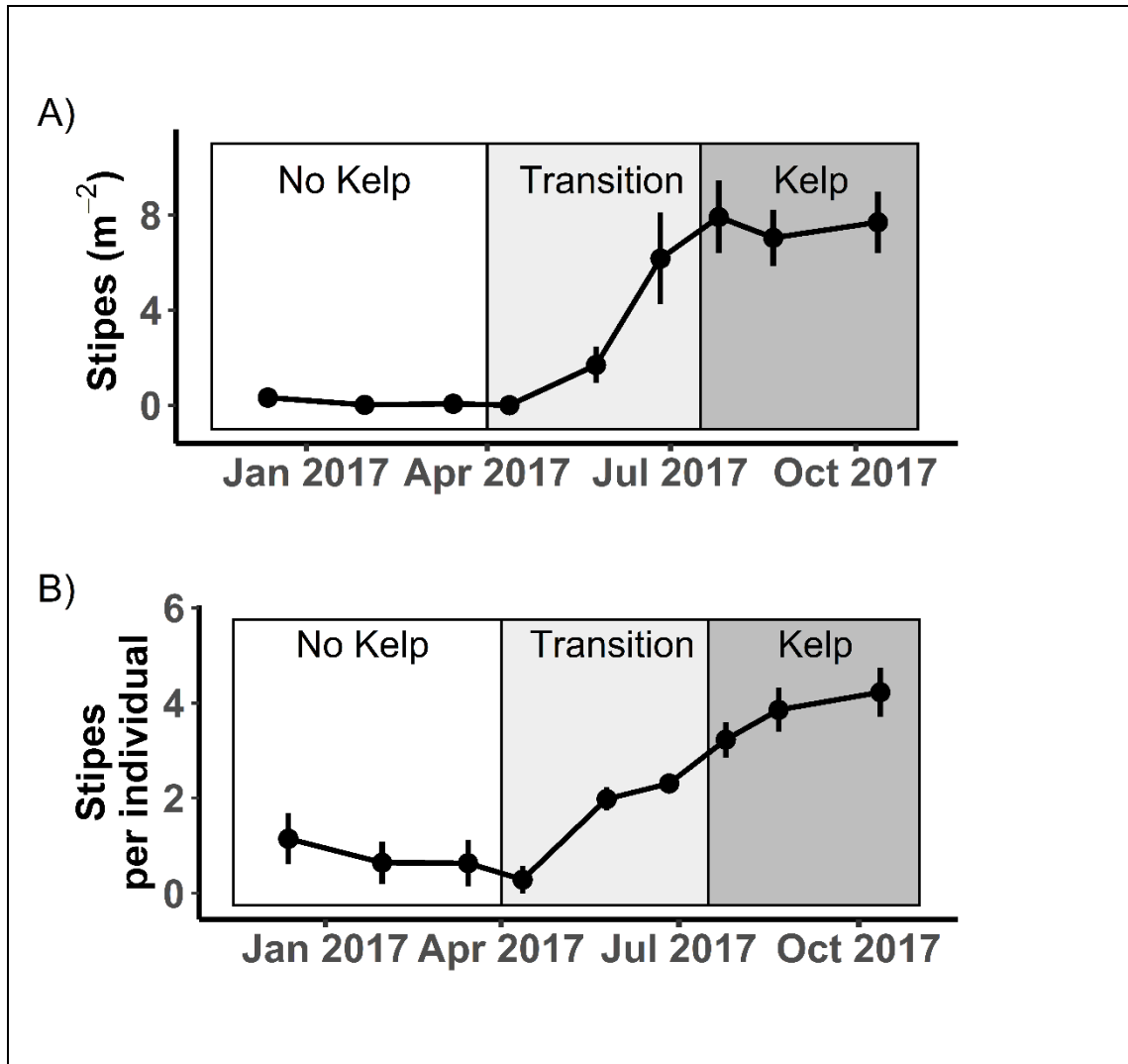
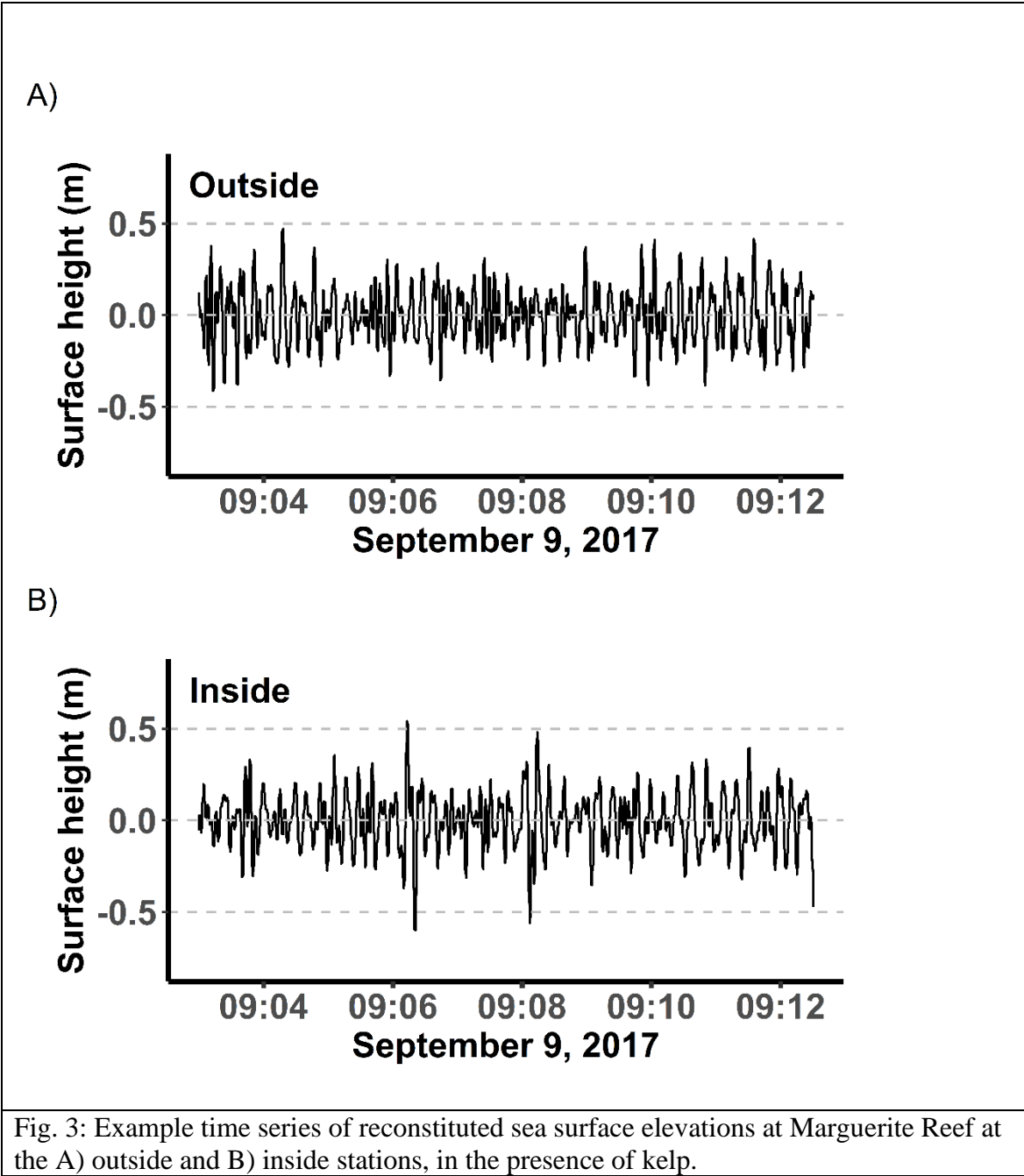


Fig. 2: Time series of A) *Macrocyctis pyrifera* stipes per meter squared and B) number of stipes per individual at Marguerite Reef throughout the duration of the study. Data points indicate means ( $\pm$ SE) averaged across the eight transects. Initial sightings of *M. pyrifera* recruits and onset of canopy formation determined the beginning of the partitioned Transition and Kelp periods, respectively.



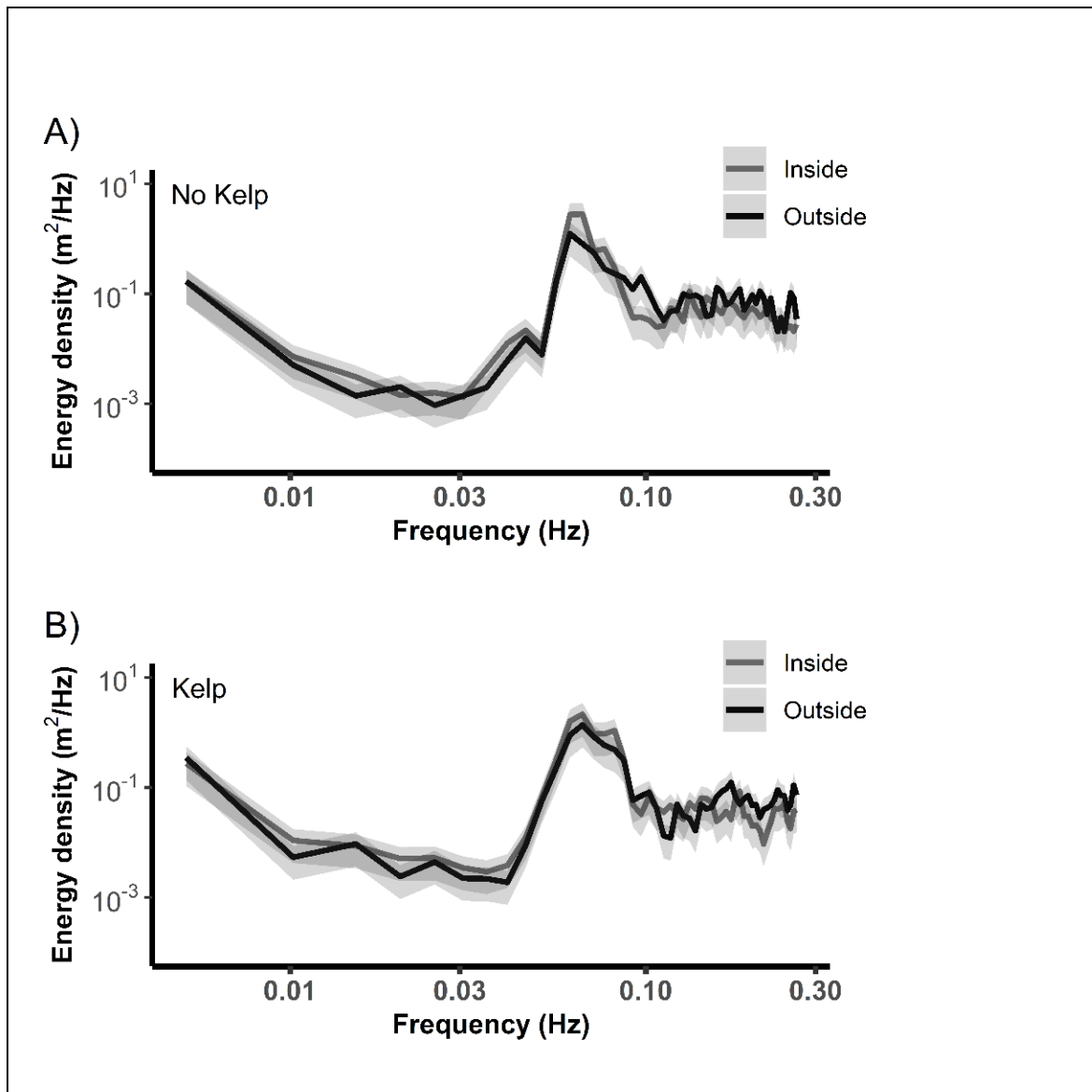


Fig. 4: Wave energy density spectra outside and inside of Marguerite Reef, in the absence (February 15, 2017 00:12) and presence (October 31, 2017 05:45) of kelp. Panels show A) outside in the absence of kelp in black ( $H_s = 0.70$  meters and  $T_p = 16.33$  seconds) and inside in the absence of kelp in grey ( $H_s = 0.88$  meters and  $T_p = 15.08$  seconds); B) outside in the presence of kelp in black ( $H_s = 0.73$  meters and  $T_p = 15.08$  seconds) and inside in the presence of kelp in grey ( $H_s = 0.84$  meters and  $T_p = 15.08$  seconds). Shading represents 95% confidence limits of the spectral estimates.

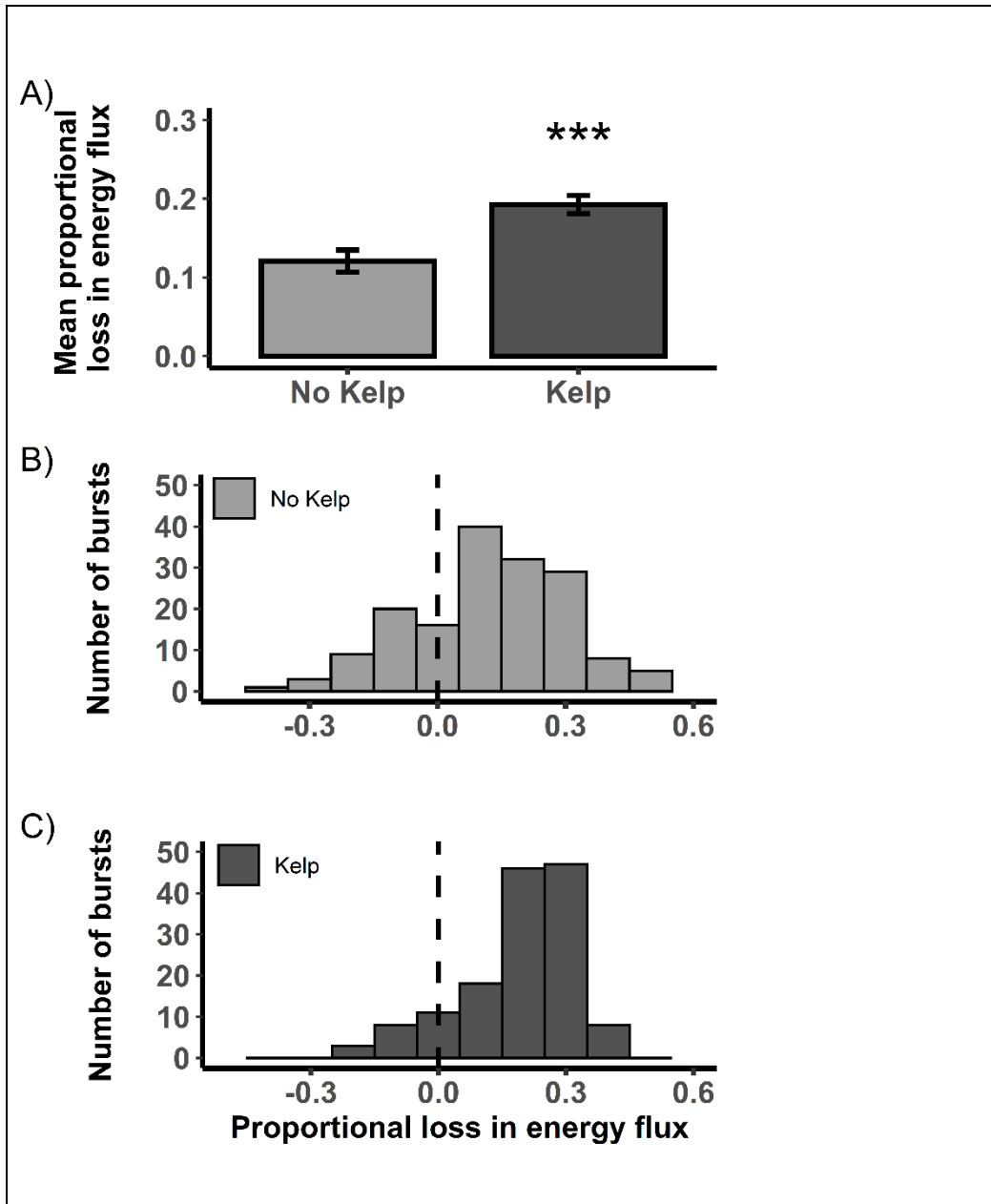


Fig. 5: Proportional loss in wave energy flux between outside and inside stations at Marguerite Reef in the absence and presence of kelp. A) Mean proportional loss in energy flux ( $\pm$ SE) averaged across all bursts from either the No Kelp or Kelp time periods. Asterisks indicate significant difference between kelp conditions ( $p \leq 0.001$ ,  $df=302$ ). B) Full distribution underlying the No Kelp period of (A), where  $n=163$  bursts. C) Full distribution underlying the Kelp period of (A), with  $n=141$ .

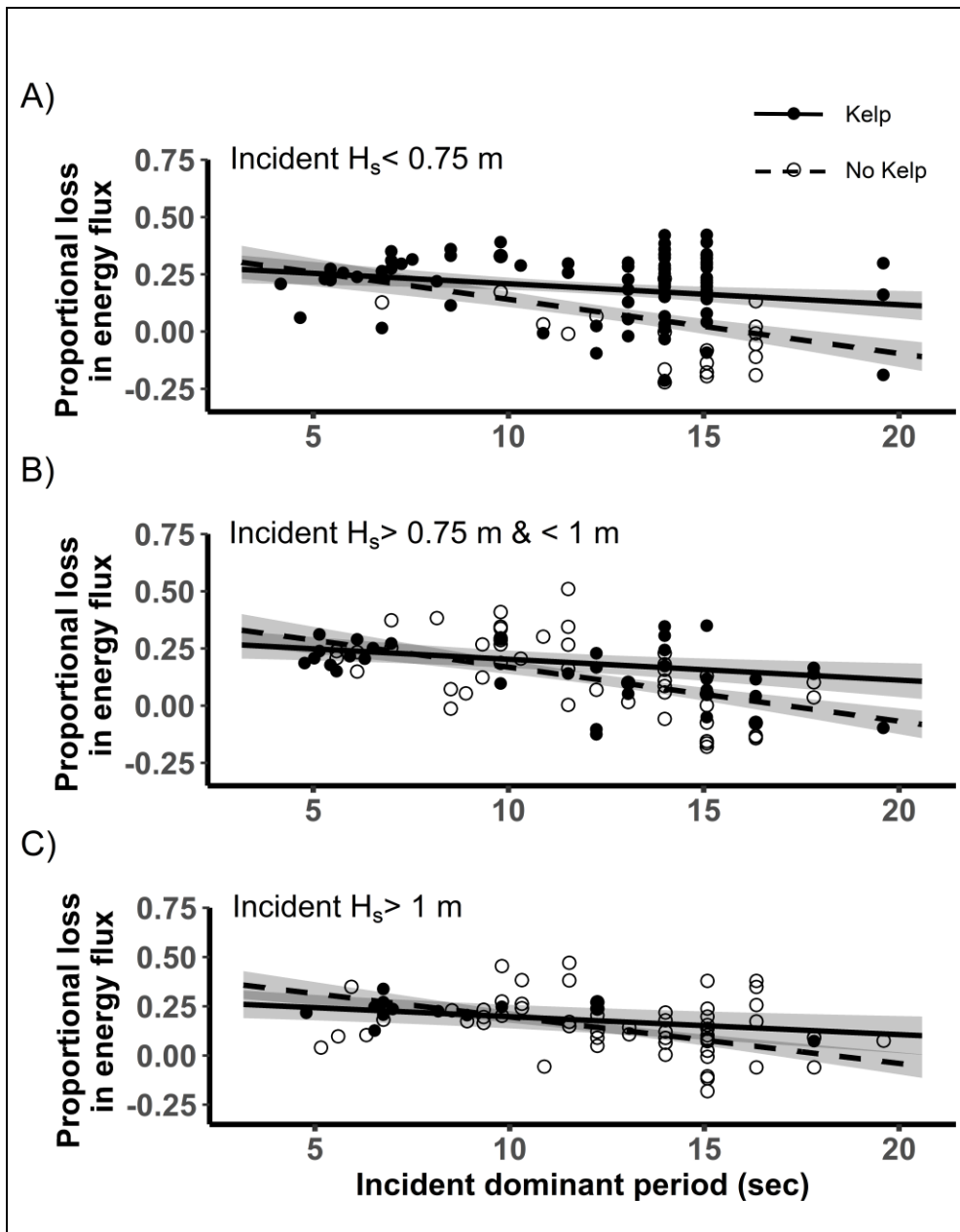
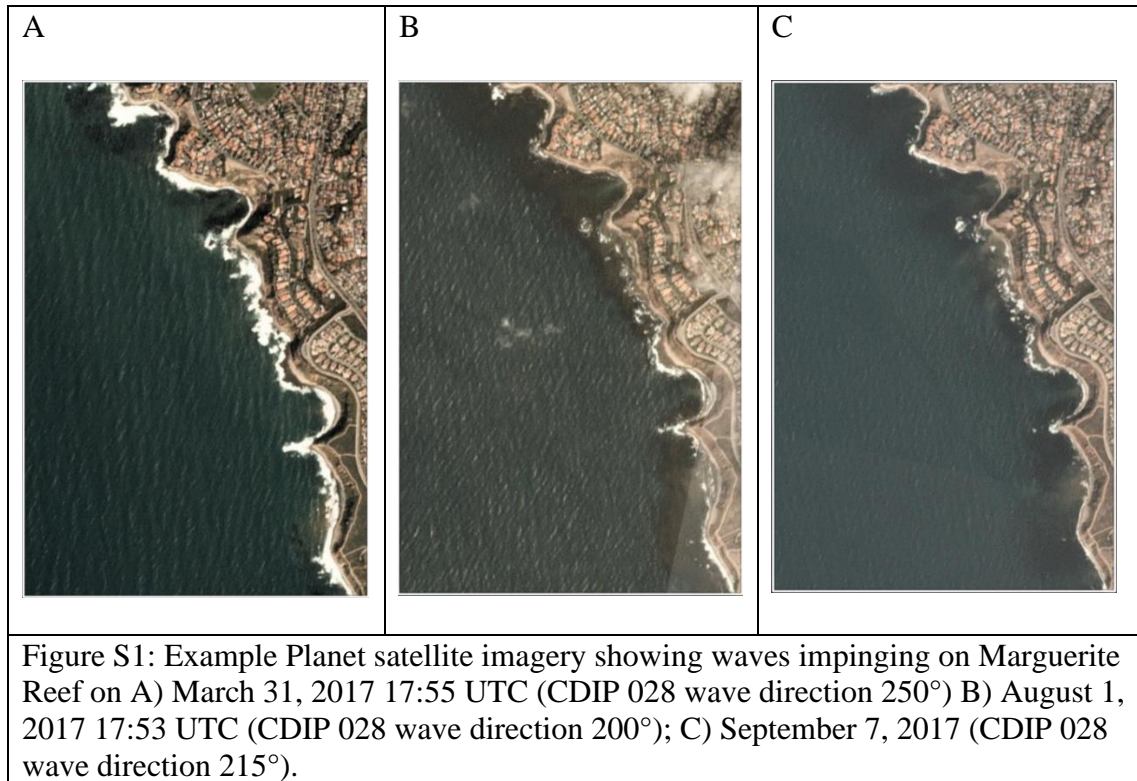


Fig. 6: Proportional loss in wave energy flux as a function of the dominant wave period at the outside station. Dashed lines represent No Kelp conditions and solid lines represent Kelp conditions. Trends are shown for multiple ranges of significant wave heights recorded at the outside station: A)  $H_s$  less than 0.75 meters, B)  $H_s$  from 0.76 to 1 meter, and C)  $H_s$  from 1.01 to 1.25 meters. Shaded regions indicate 95% confidence intervals. Solid and open data points correspond to Kelp and No Kelp conditions, respectively.

## APPENDICES



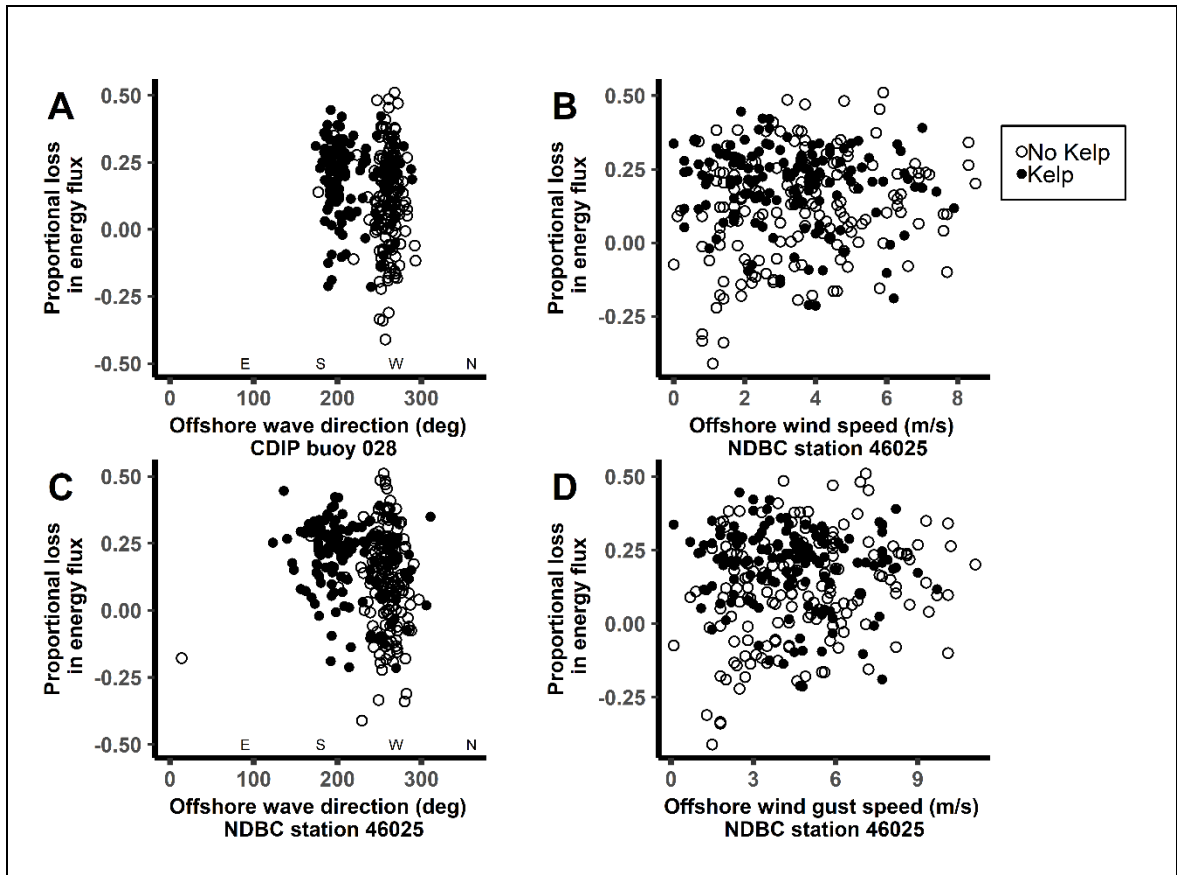


Figure S2: Proportional loss in wave energy flux as a function of A) the dominant offshore wave direction (degrees) at the 028 CDIP buoy; B) the offshore wind speed (meters per second) at the station 46025 NDBC buoy; C) the dominant offshore wave direction (degrees) at the NDBC buoy; D) the offshore wind gust speed (meters per second) at the NDBC buoy. Open circles represent No Kelp conditions and solid black circles represent Kelp conditions. Proportional wave energy losses showed no relationship with wind for Kelp conditions and varied minimally with wind in No Kelp conditions (slope 0.019, noting that a cluster of four data points exhibited disproportionate leverage). Wind effects were therefore neglected in other overarching analyses.

## **CHAPTER 2**

Macrocystis pyrifera forest development shapes the physical environment through current velocity reduction\*

---

\*Co-authors: Kerry J. Nickols, Tom Ford, Katherine C. Cavanaugh, Kyle C. Cavanaugh, Brian Gaylord

## ABSTRACT

Marine forests of the Giant Kelp, *Macrocystis pyrifera*, create biogenic habitat spanning the water column, within which hydrodynamic conditions can differ strongly from those outside. Such flow alteration has implications for physical, chemical, and ecological processes across multiple spatial scales. At the forest-wide scale, *M. pyrifera* has been shown to dramatically decrease alongshore current velocities, however, relatively little is known about how the attenuation of such currents evolves as new kelp forests emerge and mature. Here we quantify alongshore current velocities outside and within a temperate rocky reef environment that twice underwent a transition from a barren state to one in which a thick surface canopy was present. Findings suggest there is a threshold density during forest emergence at which much of the attenuation of alongshore depth-averaged velocity occurs – three stipes per square meter with a surface canopy present. Incremental increases in damping occur as the forest matures, highlighting that relatively young, thin forests can induce substantially reduced flows. Additionally, the presence of a young forest's subsurface canopy and its subsequent increase in height create a seasonally changing profile of reduced velocities through the water column. These results indicate greater complexity in how canopy-forming kelp influence nearshore flow properties than has often been recognized. Importantly, emerging forests can alter the nearshore environment through modulation of current speeds shortly following initial recruitment, with consequences for transport of larvae, nutrients, and sediment throughout the forest and adjacent habitats.

## INTRODUCTION

Currents play a critical role in shaping the biotic communities that inhabit coastal waters. Nearshore currents influence larval transport, dispersal, and retention patterns, which have consequences for genetic structure and connectivity of marine populations (Gaylord and Gaines 2000; Siegel et al. 2003, 2008; Nickols et al. 2012, 2015; Morgan et al. 2018). They also play an important role in delivering nutrients to nearshore habitats, driving growth rates of both pelagic and habitat-forming primary producers (Hurd 2000; McPhee-Shaw et al. 2007; Fram et al. 2008; Gaylord et al. 2012). Further, currents interact with waves and bottom topography to control particle suspension, deposition, and transport at the coastal edge (Gaylord et al. 2002, 2004). These and other interactions influence water clarity, benthic scouring, and reef burial, each of which have been shown to negatively impact benthic community members (Dayton et al. 1984; Watanabe et al. 2014).

Often referred to as an ecosystem engineer, *Macrocystis pyrifera*, the Giant Kelp, creates biogenic habitat spanning the benthos to the surface; its fronds consequently impose drag on currents throughout the water column. *M. pyrifera* has been shown to alter water movement at multiple spatial scales, with implications for physical, chemical, and ecological processes (Gaylord et al. 2012). Most notably, at the patch to forest-wide scale, *M. pyrifera* can dramatically decrease alongshore current velocities and, to a lesser degree, cross-shore current velocities (Jackson 1998; Gaylord et al. 2007; Rosman et al. 2007). Such modifications to flow not only have consequences for community residents but can result in bio-physical and bio-chemical feedbacks with the vegetation itself (Hurd 2000; Reed et al. 2006; Gaylord et al. 2012; Frieder et al. 2012; Koweek et al. 2017; Hirsh et al. 2020; Traiger et al. in review). For example, maintenance of sufficient nutrients relies on the delivery of new, nitrate-replete water throughout

the kelp forest. Reduced current velocities can impair such delivery, resulting in nutrient limitation that slows growth rates of the forest (Hurd 2000). Decreased cross-shore exchange, which can accompany reduced flows, further increases retention of nutrient-depleted waters, contributing to forest-wide senescence (Zimmerman and Kremer 1986; Rodriguez et al. 2013). Current velocities also modulate patterns of vertical mixing that affect kelp propagule sinking speeds and thus spore dispersal distances (Gaylord et al. 2002, 2006). Importantly, reduced current velocities result in shorter spore dispersal distances (Gaylord et al. 2004), which in turn, can increase the potential for self-fertilization with associated reductions in fitness (Raimondi et al. 2004; Reed et al. 2006).

Within-forest flows can be slower than incident ones by a magnitude or more (Jackson 1998, Gaylord et al. 2007, Rosman et al. 2007). However, studies quantifying kelp-associated current modification have been limited mostly to week- to month-long examinations in particular seasons. Forest density and canopy cover do exhibit general seasonal trends, reaching their peak in late summer months, and their low in the winter (Reed et al. 2009; Cavanaugh et al. 2011). Importantly, however, physical, and biological processes can operate individually, or in concert, to drive more irregular patterns of kelp forest succession, and consequently alter forest structure over a range of timescales (North 1971; Tegner et al. 1997; Graham et al. 2007; Rodriguez et al. 2013). The relative sparsity of longer-term hydrodynamic data gains even greater relevance given this dynamic character of *M. pyrifera* forests. A broader temporal understanding of kelp effects on flow is critical for determining long-term consequences for forest inhabitants, especially those that depend on water motion for the provision of food, for successful fertilization (as in broadcast spawners where egg and sperm meet through mixing), and for delivery of larvae required to sustain populations.

Giant kelp beds experience large changes in density, areal coverage, and even height, as new individuals emerge, add fronds and blades, and proliferate on the water's surface. The vertical distribution of kelp material within the water column (e.g., canopy height) inherently determines the profile of drag imposed on impinging currents, and likely influences the spatial patterns of attenuation throughout the water column. Nevertheless, previous *in situ* efforts have neglected much of this complexity, while focusing largely on comparisons of depth-averaged current velocities. Although some work has compared near-surface and near-bottom flows, noting important seasonal differences in the velocity gradient throughout the water column (Gaylord et al. 2007, Rosman et al. 2007), understanding of finer details remains incomplete. This information gap creates uncertainties in attempts to understand processes associated with certain vertical regions within a kelp forest. For example, *M. pyrifera* spores are released in the lower portion of the water column where this species' reproductive sporophylls reside, while sites of nutrient uptake occur primarily at the photosynthetic blades which are populated throughout the water column but concentrated at the surface. Detailed investigations of vertical velocity gradients within kelp forests are therefore warranted.

Given *M. pyrifera*'s well-documented capacity to substantially attenuate alongshore currents (and more so than those in the cross-shore direction), this study focuses on understanding the evolution of alongshore current attenuation throughout forest maturation. Here, we quantify current velocities outside and within a temperate rocky reef that twice underwent a transition from a barren state, in which the habitat was devoid of any vegetation, to one in which a thick surface canopy was present. Through this experimental framework, we address two specific questions: 1) to what extent does attenuation of alongshore current velocities depend on forest age as forest characteristics (stipe density, individual density, number

of stipes per individual, and surface canopy cover) change during forest development? and 2) to what extent does alongshore current attenuation differ throughout the water column as a subsurface canopy emerges and develops into a surface canopy?

## **METHODS**

### *Study site*

The focal site for this study, Marguerite Reef (33.75712, -118.41842), sits along the Palos Verdes Peninsula, within the central region of the Southern California Bight (Fig. 1), near Los Angeles, California, USA. The site is positioned along a roughly linear stretch of coastline, with a shoreline angle of 340° from north. In this region, subtidal currents primarily fluctuate along isobaths with amplitudes of 10-20 cm/s (Noble et al. 2009). Substrate at Marguerite Reef is comprised of bedrock and large boulders, interspersed with sand patches. At the onset of this study, the reef was dominated by purple urchins, *Strongylocentrotus purpuratus*, which were sufficiently abundant that the system had shifted into a “barren” state with little to no macrophytes present. As part of a broader kelp restoration project, the purple urchins were culled from Marguerite Reef in late 2016 and early 2017 and a *Macrocystis pyrifera* forest subsequently developed. Coincident with high sea surface temperatures and elevated turbidity due to a nearby landslide, the kelp forest again disappeared in late 2018, but reemerged in spring of 2019.

### *Kelp forest dynamics*

A combination of subtidal SCUBA surveys and satellite imagery were used to quantify changes in *M. pyrifera* forest structure throughout the study. Monthly subtidal swath surveys were conducted by divers over two experimental periods: November 2016 to May 2018 and April 2019 to October 2019, referenced as the 2017 and 2019 experiments, respectively. Between November 2016 and May 2018, surveys were conducted along 8 evenly spaced transects (30 m x 4 m, 30 m apart), oriented parallel to shore and spanning the cross-sectional area of the rocky reef (Fig. 1). From April 2019 to October 2019, the 8 transects had dimensions of 30 m x 2 m, but otherwise followed the same sampling protocol. Along each transect, *M. pyrifera* individuals taller than 1 meter and their respective stipes were counted to estimate the density of giant kelp. Qualitative observations of plant heights were recorded within 10 m x 2 m sections of each transect to assess the rapidly changing subsurface canopy height as the *M. pyrifera* forest developed. These observations included the presence of individuals less than 1 meter tall to capture the onset of new forest development. Raw images from PlanetScope were processed for surface canopy detection and distilled down to maximum monthly canopy coverage within the boundary of the subtidal survey area (Fig. 1) (Planet Team 2020). Maximum monthly coverage of surface canopy was then divided by the total boxed survey area (14,850 meters squared), to acquire the percentage of canopy cover that overlapped spatially with the subtidal kelp surveys.

#### *Alongshore current velocity measurements*

Water velocities along three axes (east, north, and up [ENU] coordinates) were measured outside (17 m depth, 33.75726 N, -118.41986 W) and inside (10 m depth, 33.75712 N, -

118.41842 W) the rocky substrate characterizing Marguerite Reef, using two acoustic Doppler current profilers (ADCP; 1200 kHz Workhorse Sentinel, Teledyne RD Instruments; Figure 1). ADCP deployments spanned the two experimental periods, from November 2016 through May 2018 and from April 2019 through September 2019. The ADCPs were mounted on the seafloor, looking upward, and recorded burst-averaged velocity profiles at 3-minute intervals, within 0.5 m vertical bins throughout the water column. The only exception to this protocol was that measurements collected in 2019 utilized a vertical bin size of 1 meter.

Raw velocity data were rotated to orient the horizontal Cartesian coordinates parallel and perpendicular to the coast, with positive values of  $u$  upcoast and negative values downcoast. Emphasis was on alongshore currents, as opposed to cross-shore currents, due to previous recognition of the former's greater degree of attenuation by kelp (Jackson 1998; Gaylord et al. 2007; Rosman et al. 2007). Velocity values in near-surface bins in the upper 10% of the water column were discarded due to data degradation associated with known side-lobe artifacts characteristic of acoustic profiles. Velocity records from the remaining 90% of the water column were then averaged over 30-minute blocks (Gunawan and Neary 2011).

#### *Influence of kelp on depth-averaged currents*

To examine *M. pyrifera*'s effect on the alongshore current velocities, 30-minute-averaged alongshore velocity data were depth-averaged and then partitioned into paired blocks of 10 days duration, one outside and one inside the reef habitat, each straddling a given kelp survey date. For each pair of 10-day time series, depth-averaged velocities outside of the reef were then regressed against those within the reef using major axis (MA) regression. This approach

provided a quantitative assessment of the fractional decline in current speed on the reef in comparison to the simultaneous current speed outside of the reef habitat. A 1:1 slope would indicate no reduction in current speed on average when comparing the reef station to the station outside, while a smaller regression slope would indicate greater reduction of within-kelp current speeds compared to those outside. The slopes were then plotted as a function of stipe density to quantify the relationship between forest properties and the extent of damping. Note that because the topography and bathymetry between the two sensor locations remained static throughout the study, the regression slopes corresponding to the zero-stipe case serve as reasonable reference points from which to compare further modifications due to kelp. Slopes were converted to a percentage of velocity reduction using:

$$P_i = (1 - slope_i) * 100 \quad (2)$$

where  $P_i$  is the percentage of velocity reduced within the inner region of the reef,  $slope$  is the slope of the major axis regression of velocities outside versus inside the reef, and  $i$  is the stipe density (unique for each kelp survey date). Percentages of velocity reduction were then compared across stipe densities, which varied through time, to determine the relationship between kelp forest structure and reductions in depth-averaged current speeds. A Šidák correction was applied to account for conducting multiple comparisons across the respective slopes. All statistical tests were accomplished in R version 4.0.2 (R Core Team, 2021), with regressions and pairwise comparisons conducted using the package *smatr* (Warton et al. 2012).

### *Influence of subsurface canopy on alongshore currents*

To quantify alongshore velocity reductions as the subsurface canopy emerged and extended up to the surface, MA regression slopes were computed using 30-minute-averaged alongshore velocity data from the 0.5-meter vertical bin corresponding to the 25<sup>th</sup>, 50<sup>th</sup>, and upper 75<sup>th</sup> percentile of the water column relative to the bottom, in addition to depth-averaged velocity data. Because the previous 10-day mini time series could obscure important patterns at shorter time scales relevant to subsurface canopy development, alongshore velocity data were re-partitioned into pairs of mini time series, one outside and one inside the reef, each spanning a three-day period within each week for the dates ranging between April 20, 2017, and July 14, 2017. For each weekly 3-day time series, velocities outside of the reef were then regressed against those within the reef using major axis (MA) regression to produce a slope for each of the three percentiles of the water column (e.g., 25<sup>th</sup>, 50<sup>th</sup>, and 75<sup>th</sup>). Slopes were compared through time and for each water column percentile to determine the timing and degree of attenuation with respect to the subsurface canopy. Pairwise comparisons of the respective slopes were conducted using a Šidák correction. All statistical tests were accomplished in R version 4.0.2 (R Core Team, 2021), with MA regressions and pairwise comparisons conducted using the package *smatr* (Warton et al. 2012).

## **RESULTS**

### *Kelp forest dynamics*

The structure of the *Macrocystis pyrifera* forest at Marguerite Reef varied considerably throughout the duration of this study. In late 2016 and into early 2017, the reef was devoid of vegetation. New *M. pyrifera* recruits began to appear on the benthic substrate in mid-April 2017 and grew rapidly, first reaching the water surface in late June 2017 (Figure 2A). Canopy cover spanning the subtidal survey area was detected by satellite image analysis in July 2017, which was in accordance with diver observations. The percentage of maximum canopy cover averaged 51.3 (SE +/- 3.9) % between July 2017 and February 2018, after which the canopy roughly doubled its coverage, averaging 90.1 (SE +/- 0.68) %. The site reached a maximum of 92% canopy cover in April 2018 (Figure 2A). The kelp forest disappeared entirely in late 2018, resulting in the reef being, once again, devoid of vegetation. Canopy cover was detected again by satellite image analysis in June 2019, which was in accordance with diver observations. The percentage of canopy cover increased from 14.4% in June 2019 to 34.6% in November 2019, with an average of 26.8 (SE +/- 3.7) % coverage over that timeframe (Figure 2A).

Stipe density increased sharply from 0 stipes per square meter in mid-April 2017 to 6.2 (SE +/- 1.9) stipes per square meter in late June 2017 and reached a maximum of 7.9 (SE +/- 1.5) stipes per square meter in late July 2017 (Figure 2B). The forest subsequently underwent a period of self-thinning, as indicated by a reduction in both stipe density and kelp density – the number of kelp individuals per square meter – from late Fall 2017 into early 2018 (Figure 2B, 2C). While stipe and kelp densities slowly decreased into the Fall of 2017, the size of remaining kelp individuals continued to increase into early spring of 2018, as indicated by a gradual increase in the number of stipes per individual, from 2 (SE +/- 0.2) stipes per individual in late May 2017 to a maximum of 7.6 (SE +/- 0.8) stipes per individual in late May 2018 (Figure 2D). Such a pattern indicates a shift in the structural composition of the forest (i.e., a shift from a

forest composed of many plants each supporting a handful of stipes, to one composed of fewer, but larger individuals). In late 2018, Marguerite Reef experienced a complete loss of its subtidal vegetation.

In the spring of 2019, Marguerite Reef again transitioned from a reef composed of bare rock to one supporting a forest with surface canopy. Stipe density increased from 0 stipes per square meter in April 2019 to 3.8 (SE +/- 2.0) stipes per square meter in June 2019 and averaged 3.4 (SE +/- 0.2) stipes per square meter between June and October 2019. Densities of kelp individuals initially increased to 1.4 (SE +/- 0.6) individuals per square meter in June 2019, and then subsequently decreased to 0.5 (SE +/- 0.3) individuals per square meter by October 2019. The size of the kelp individuals gradually increased throughout forest development, reaching a maximum of 4 (SE +/- 0.9) stipes per individual by October 2019. While general forest growth patterns were similar between the two experimental periods (2017 and 2019), the magnitude of peak plant and stipe densities, as well as canopy coverage, in 2019 were approximately one third to one half of those observed in the 2017 experiment. Peak forest densities in both 2017 and 2019 experiments were within typical ranges of mature *M. pyrifera* forests in California (1.9-15 stipes m<sup>-2</sup> and up to 3 plants m<sup>-2</sup>, North 1971).

#### *Influence of kelp on depth-averaged alongshore currents*

Alongshore current velocities within the reef were lower than those outside of the reef in the absence of kelp (stipe density < 0.2), and then were further reduced once the kelp forest developed. Kelp had a striking effect on alongshore current velocities within the reef, as readily seen by the abrupt collapse in velocities observed at the inner sensor station (Figure 3,

represented in yellow), contrasted with the roughly unchanging pattern of velocities at the sensor station outside of the reef (Figure 3, represented in blue). Sharp reductions in alongshore velocities within the inner region of the reef coincided with an increase in kelp stipe densities in both 2017 and 2019. In contrast, alongshore velocities remained high and variable outside of the reef habitat. Slow alongshore velocities persisted within the reef throughout the summer months and into the Fall of each year, highlighted by the slower and less variable velocities observed at the inner sensor station and overlaid on the faster and more variable velocities observed at the outer sensor station (Figure 3).

Comparison of root means square (rms) velocities outside and within the reef throughout forest development provide a general quantitative metric for characterizing kelp's influence on average alongshore current speeds. For example, alongshore rms velocities at the inner sensor station remained slow (i.e., less than 1 cm/s) throughout the summer and into Fall 2017, while rms velocities outside the reef fluctuated between 3 to 5 cm/s (Table 1). Similarly, throughout the summer and into Fall 2019, alongshore rms velocities inside the reef remained less than 1.5 cm/s, while rms velocities outside the reef ranged between 3.7 cm/s to 6.1 cm/s (Table 1).

While informative, comparisons of rms velocities do not fully capture the underlying physical relationship between the two sensor stations. As such, comparing major axis regression slopes of velocities outside and within the reef provides a more direct metric by which to calculate percent velocity reduction due to the presence of kelp (Figure 4). Velocity reductions that occur in the absence of kelp can be attributed to frictional losses due to interactions with the benthos and differences in sensor station depths within the coastal boundary layer (Nickols et al. 2012). Further velocity reductions can be attributed to the presence of kelp at a given stipe density (or forest structure).

An acute change in velocity reductions occurred at a threshold forest structure of 3 stipes per square meter, at which much of the depth-averaged velocity reduction occurred (Figure 4). In the absence of kelp (stipe densities  $\leq 0.173$ ), regression slopes ranged from 0.46 to 0.85, representative of current reductions associated with seafloor friction and broader coastal boundary layer effects. In contrast, once the forest reached 3 stipes per square meter and the canopy was at the surface, slope regressions dropped uniformly to values below 0.12, indicating that velocities within the reef were of order 12% of those outside of the reef. Further reductions in depth-averaged velocities also arose with increasing stipe density (Figure 5). Interestingly, when stipe densities were low (i.e., 1.7 stipes per square meter) and the forest canopy had not yet reached the surface, depth-averaged velocity reductions were not detectably different from the no-kelp regressions.

#### *Influence of subsurface canopy on alongshore currents*

While depth-averaged velocity reductions were detectable only after a surface canopy began to form, reduced velocities were readily visible in the lower region of the velocity profile beforehand (Figure 6). A subsurface canopy “shadow” characterized by reduced velocities was apparent within the inner region of the reef, and rapidly changed in height as the canopy grew toward the surface.

Distinct regions of the water column exhibited temporal lags in their respective percentages of velocity reduction over the course of subsurface canopy development. Initial observations of single-bladed kelp recruits blanketing the benthos occurred in mid-April 2017. Alongshore velocities in the 25<sup>th</sup> percentile of the water column (near-bottom) were reduced by

100% by 57 days post recruitment (Figure 7). Conditions of near-100% velocity reduction in the 50<sup>th</sup> (middle) and 75<sup>th</sup> (near-surface) percentiles took an additional 14 and 21 days, respectively.

## DISCUSSION

In this study, we quantified reductions in alongshore current velocities across successional stages of a restored *M. pyrifera* forest at Marguerite Reef, Palos Verdes, California. Over the course of the study, the reef twice underwent a transition from a barren state, devoid of vegetation, to one in which a kelp forest was present. Depth-averaged alongshore velocities within the reef decreased abruptly upon initial formation of the surface canopy and stipe density reaching roughly 3 stipes per square meter. Stipe density exhibited a positive relationship with depth-averaged velocity attenuation. Temporal and spatial lags of velocity reduction occurred throughout the water column as the subsurface canopy developed in spring of 2017. Velocity attenuation in the upper region of the water column lagged behind that of the lower region of the water column by a little over one month, revealing a rapidly changing velocity profile that could have important implications for community residents and for kelp itself.

### *Forest structure*

Stipe density governs much of the attenuation of alongshore current velocity observed at Marguerite Reef, however, there are likely additional drivers at play. Forest age and size of the kelp plants are also important. For example, Marguerite Reef exhibited a lesser degree of velocity reduction when the kelp forest was “older” and composed of fewer, but larger individuals, for a given stipe density. These data suggest that two forests supporting the same

stipe density, but different “ages”, likely would not exhibit the same degree of alongshore current attenuation – all else being equal, the “younger” forest would likely exhibit a greater degree of attenuation. Therefore, the level of forest maturation may be a largely overlooked driver of alongshore current damping potential.

Additionally, while the presence of a surface canopy appeared to be critical to the detection of kelp-associated reductions in depth-averaged velocity, additional canopy cover did not correspond with increased velocity reductions. As such, canopy cover, per se, may not be a dominant determinant of the degree of current attenuation, as alluded in previous studies (Rosman et al. 2007), and perhaps is a less useful metric for predicting current attenuation of mature forests at finer temporal scales (e.g., intra-annual). Collinearity among stipe density, kelp density, kelp size, and canopy cover measured in this study, however, limits the capacity to quantitatively determine effects of differing forest structures on the degree of velocity reduction and warrants future investigation. Additionally, while changes in kelp canopy cover likely impact surface flows, acoustic Doppler current profilers are unable to reliably characterize surface current velocities, necessitating an alternative experimental approach in future work to understand drivers of attenuation of surface currents.

Although the presence of kelp upcoast or downcoast of Marguerite Reef may have contributed to velocity reductions observed over the course of our study, absence of strong differences in damping between times when currents are oriented upcoast versus downcoast (Figure 4) suggest either that the presence of neighboring kelp was symmetrical up and down the coast of Marguerite Reef, or that effects of adjacent forests were minor. Potential roles of neighboring kelp forests warrant future exploration.

### *Subsurface canopy*

Depth-specific velocity reductions within the reef align temporally and spatially with anticipated changes in subsurface canopy height. In late May 2017, velocity reductions detected at the bottom 25<sup>th</sup> percentile position of the water column coincided with an increase in velocities in the middle of the water column, as represented by a decrease followed by a sharp increase in velocity reduction in the middle 50<sup>th</sup> percentile position in Figure 7. As alongshore velocities encounter an obstacle, in this case a subsurface canopy, the water must either re-route laterally around the obstacle, or vertically, above the obstacle. While water is likely also re-routed laterally, the spike in velocities in the region above the subsurface canopy, observed in late May 2017 at the middle 50<sup>th</sup> percentile position of the water column and to a lesser degree in late June 2017 at the upper 75<sup>th</sup> percentile position of the water column, indicates water is being re-routed vertically, such that it manifests in an acceleration of velocities just above the subsurface canopy. In the case of an established forest supporting a surface canopy, vertical re-routing is physically constrained by the sea surface, and thus water is redirected around the lateral edges of the forest, manifesting as accelerated velocities along the forest edges, as observed in previously studied *M. pyrifera* forests (Jackson and Winant 1983; Jackson 1998; Gaylord et al. 2007).

Relevance of the physical process of rerouted water is not limited to emerging kelp forests. Established and multi-year-old giant kelp forests, such as those commonly found in Southern California, experience a seasonal surge of new recruits come springtime. Data shown here suggests that roughly annual pulses of new kelp recruits could further modify the profile of alongshore velocity reductions. This could be of particular importance to not only the kelp itself,

via altered nutrient transport, but to the myriad of community members that occupy the kelp forest. For example, many benthic invertebrates are broadcast spawners and rely on water motion to facilitate fertilization of eggs and sperm (Crimaldi and Zimmer 2014), as well as transport of their larvae across multiple temporal and spatial scales (Pineda et al. 2007). As such, alterations of the spatial patterns of current velocities can have consequences for the fate of both local dispersers with short larval durations, such as the orange cup coral, *Balanophyllia elegans*, and longer distance dispersers with long larval durations, such as the purple urchin *Strongylocentrotus purpuratus*. Further, while benthic suspension feeders rely on water motion to deliver phytoplankton and other suspended food sources to near-bed regions of the water column where they live (Pequegnat 1964, Page et al. 2008), other planktivores, such as rockfish, rely on the delivery of zooplankton to regions higher in the water column, where adults and juveniles of some species reside (Pequegnat 1964, Gaines and Roughgarden 1987).

### *Residence time*

Modifications to the alongshore current velocity profile can also have profound effects on the residence time of water, particularly in lower regions of the water column as cohorts of new kelp recruits emerge. Reduced current velocities, as observed in this study, can lengthen residence times of water internal to the kelp forest, which in turn, can lead to increases in chemical stratification and nutrient-depletion. For example, slower flows increase the amount of time kelp is in contact with a given pool of water, determining the capacity of kelp to chemically modify the water properties through photosynthetic uptake of CO<sub>2</sub> and production of oxygen (Traiger et al. in review; Hirsh et al. 2020). Because much of the kelp-driven chemical alteration

occurs in the surface waters, where the photosynthetic biomass is concentrated, the water column can become chemically stratified, creating chemically distinct regions within the water column (Traiger et al. in review). Severely reduced velocities, such as those observed following surface canopy formation in both the 2017 and 2019 experiments, can further exacerbate differences in water column chemistry. Additionally, entrapment of poorly oxygenated waters can occur within depressions of the rocky reef, creating “internal tide pools,” which can be particularly consequential for kelp forest organisms residing in the lower region of the water column (Leary et al. 2017). Residence time of low-oxygen water within these pools is likely increased in scenarios such as those observed throughout June of 2017, when the emerging subsurface canopy attenuated much of the alongshore velocities in the lower region of the water column. Further, reductions in near-bottom current velocities can limit the influx and lateral transport of nutrient-replete waters throughout the forest (Fram et al. 2008), which can drive temporal and spatial patterns of forest recovery following restoration, as well as forest growth more broadly (Stewart et al. 2009). Each of these biophysical and biochemical processes contribute to the patchy mosaic of water column properties experienced by kelp forest community members. Importantly, attenuation of flows occurs to varying degrees in different regions of the water column, depending on forest growth and structure, which in turn, can exacerbate or ameliorate stressors, such as ocean acidification, hypoxia, or nutrient-repletion.

#### *Transport of particulates and detritus*

Currents can interact with kelp to control sediment transport and suspension of particles within the water column, influencing patterns of kelp persistence and benthic community

composition through processes such as benthic scour, reef burial, and reduced light penetration (Eckman et al. 1989; Watanabe et al. 2014; Foster and Schiel 2015). While strong current velocities can result in sediments being transported long distances across reefs (Ferré et al. 2010), the presence of a kelp forest likely impedes alongshore sediment transport and facilitates localized sediment accretion through attenuation of currents. Reduced alongshore transport of sediments can be of particular concern for rocky reef communities found adjacent to coastal regions prone to erosion and landslides, such as the Palos Verdes Peninsula (Ferré et al. 2010). For example, sediment plumes following landslides can reduce species diversity and biomass as well as shift benthic community composition in adjacent impacted kelp forest communities (Kiest 1993). Beyond direct burial of existing benthic community members, increased sedimentation can limit recruitment of kelp and other benthic species by obstructing substrate attachment, scouring new individuals, or inhibiting light; the latter of which is particularly consequential for early life stages of primary producers (Watanabe et al. 2014). Interestingly, such consequences of altered sediment transport and particle suspension likely contributed to the temporal patterns of kelp forest structure observed in this study. The complete loss of subtidal vegetation at Marguerite Reef in late 2018 coincided with a landslide that occurred just up the coast. Partial reef burial and increase in water column particulates persisted at the site throughout the 2019 experiment. Subsequent forest recovery observed in the 2019 experiment was significantly less than what was observed in the 2017 experiment and likely driven in part by biophysical feedbacks among kelp, alongshore currents, and sediment influx. While giant kelp forests have little capacity for coastal protection by way of attenuation of surface waves (Elwany et al. 1995; Elsmore et al. in review), they may contribute significantly to processes of sediment entrainment and deposition within the coastal zone through modulation of alongshore currents.

## **CONCLUSION**

This study quantified reductions in alongshore velocities within reef habitat that twice underwent a transition from a barren state to one supporting a kelp forest with a surface canopy. Reductions in depth-averaged velocities increased with increasing stipe density, once a surface canopy was present. Subsurface canopy development resulted in temporal and spatial lags in current attenuation spanning the vertical space of the water column. Velocity reductions were first observed in the lower portion of the water column, prior to detection within the depth-averaged velocities. These findings reinforce existing literature showing giant kelp forests have the capacity to substantially modify alongshore currents and provide new insights into the role forest structure plays in determining the degree of flow reduction and its spatial and temporal patterns. Findings have implications for larval, nutrient, detrital, and sediment transport in the nearshore environment.

## **ACKNOWLEDGEMENTS**

This work was supported by the California State Coastal Conservancy [grant number 15-013], National Science Foundation (NSF) [grant number OCE-1636191], University of Southern California, Sea Grant [grant number NA180AR4170075], and Dolby Laboratories. K.E.E. was additionally supported by an NSF Graduate Research Fellowship, Bilinski Fellowship, and a Norcal Society of Environmental Toxicology and Chemistry grant. The authors are grateful to A. Barilotti, H. Burdick, B. Cohn, C. Dibble, K. Dubois, G. Elsmore, B. Grimes, T. Herzik, J.

Hollarsmith, P. House, A. Ninokawa, D. Panos, A. Saley, A. Sparks, B. Sterling, G. Thompson, A. Ullmann, and M. Ward for field and logistical assistance.

## LITERATURE CITED

Crimaldi, J.P., and R.K. Zimmer. 2014. The physics of broadcast spawning in benthic invertebrates. *Annual Review of Marine Science*. 6:141-65, doi: 10.1146/annurev-marine-010213-135119

Dayton, P.K., V., Currie, T., Gerrodette, B.D., Keller, R. Rosenthal, D.V. Tresca. 1984. Patch dynamics and stability of some California kelp communities. *Ecological Monographs*. 54(3):253-289.

Dayton, P.K., M.J. Tegner, P.E. Parnell, and P.B. Edwards. 1992. Temporal and spatial patterns of disturbance and recovery in a kelp forest community. *Ecological Monographs* 62: 421-445, doi:10.2307/2937118.

Denny, M.W. 1988. *Biology and the Mechanics of the Wave-Swept Environment*. Princeton, NJ: Princeton University Press.

Eckman, J.E., D.O. Duggins, and A.T. Sewell. 1989. Ecology of understory kelp environments. I. Effects of kelps on flow and particle transport near the bottom. *Journal of Experimental Biology and Ecology*. 129:173-187.

Elsmore, K.E., K.J. Nickols, L. Miller, M. Denny, T. Ford, B. Gaylord. In Review. Wave damping by giant kelp, *Macrocystis pyrifera*.

Elwany, M.H.S., W.C. O'Reilly, R.T. Guza, and R.E. Flick. 1995. Effects of Southern California kelp beds on waves. *Journal of Waterway Port Coastal and Ocean Engineering* 121: 143-150.

Ferré, B. A.R. Sherwood, and P.L. Wiberg. 2010. Sediment transport on the Palos Verdes shelf, California. *Continental Shelf Research*. 30:761-780.

Fram, J.P. and H.L. Stewart. 2008. Physical pathways and utilization of nitrate supply to the giant kelp, *Macrocystis pyrifera*. *Limnology and Oceanography*. 53(4):1589-1603.

Frieder, C.A., S.H. Nam, T.R., Martz, L.A. Levin. 2012. High temporal and spatial variability of dissolved oxygen and pH in a nearshore California kelp forest. *Biogeosciences*. 9:3917-3930, doi: 10.5194/bg-9-3917-2012

Gaines, S.D., and J. Roughgarden. 1987. Fish in offshore kelp forests affect recruitment to intertidal barnacle populations. *Science*. 235(4787):479-481.

Gaylord, B., and S.D., Gaines. 2000. Temperature or transport? Range limits in marine species mediated solely by flow. *The American Naturalist*. 155(6):769-789.

Gaylord, B., D.C., Reed, P.T. Raimondi, L. Washburn, S. R. Mclean. 2002. A physically based model of macroalgal spore dispersal in the wave and current-dominated nearshore. *Ecology*. 83(5):1239-1251.

Gaylord, B., D.C. Reed, L. Washburn, P.T. Raimondi. 2004. Physical-biological coupling in spore dispersal of kelp forest macroalgae. *Journal of Marine Systems* 49: 19-39, doi:10.1016/j.jmarsys.2003.05.003.

Gaylord, B., D.C. Reed, P.T., Raimondi, L. Washburn. 2006. Macroalgal spore dispersal in coastal environments: mechanistic insights revealed by theory and experiment. *Ecological Monographs*. 76(4):481-502.

Gaylord, B., J.H. Rosman, D.C. Reed, J.R. Koseff, J. Fram, S. MacIntyre, K. Arkema, C. McDonald, M.A. Brzezinski, J.L. Largier, S.G. Monismith, P.T. Raimondi, and B. Mardian. 2007. Spatial patterns of flow and their modification within and around a giant kelp forest. *Limnology and Oceanography* 52: 1838-1852, doi:10.2307/4502339.

Gaylord, B., K.J. Nickols, L. Jurgens. 2012. Roles of transport and mixing processes in kelp forest ecology. *The Journal of Experimental Biology* 215: 997-1007, doi:10.1242/jeb.059824.

Gunawan, B., and V.S. Neary. 2011. ORNL ADCP Post-processing guide and MATLAB algorithms for MHK site flow and turbulence analysis.

Hirsh, H.K., K.J. Nickols, Y. Takeshita, S.B. Traiger, D.A. Mucciarone, S. Monosmith, R.B. Dunbar. 2020. Drivers of biogeochemical variability in a Central California kelp forest: Implications for local amelioration of ocean acidification. *Journal of Geophysical Research: Oceans* 125: 1-22, doi:10.1029/2020JC016320.

Hurd, C.L. 2000. Water motion, marine macroalgal physiology, and production. *Journal of Phycology*. 36:453-472.

Jackson, G.A. 1998. Currents in the high drag environment of a coastal kelp stand off California. *Continental Shelf Research*. 17(15):1913-1928.

Jackson, G.A., C.D. Winant. 1983. Effect of a kelp forest on coastal currents. *Continental Shelf Research* 2: 75-80. doi:10.1016/0278-4343(83)90023-7.

Kiest, K. 1993. The Influence of sediment from landslide plumes on sessile kelp forest assemblages. Master's Theses. 634. San Jose State University. doi: <https://doi.org/10.31979/etd.4sb5-4k87>

Kowec, D.A., K.J. Nickols, P.R. Leary, S.Y. Litvin, T.W. Bell, T. Luthin, S. Lummis, D.A. Mucciarone, R.B. Dunbar. 2017. A year in the life of a central California kelp forest: physical and biological insights into biogeochemical variability. *Biogeosciences*. 14:31-44, doi:10.5194/bg-14-31-2017

Leary, P.R., C.B. Woodson, M.E. Squibb, M.W. Denny, S.G. Monosmith, and F. Micheli. 2017. "Internal tide pools" prolong kelp forest hypoxic events. *Limnology and Oceanography*. 62:2864-2878.

McPhee-Shaw, E.E., D.A. Siegel, L. Washburn, M.A. Brzeinski, J.L. Jones, A. Leydecker, J. Melak. 2007. *Limnology and Oceanography*. 52(5) 1748-1766.

Miller, R.J., K.D. Lafferty, T. Lamy, L. Kui, A. Rassweiler, and D.C. Reed. 2018. Giant kelp, *Macrocystis pyrifera*, increases faunal diversity through physical engineering. *Proceedings of the Royal Society B: Biological Sciences* 285: 20172571, doi:10.1098/rspb.2017.2571.

Morgan, S.G., S.H. Miller, M.J. Robart, and J.L. Largier. 2018. Nearshore larval retention and cross-shelf migration of benthic crustaceans at an upwelling center. *Frontiers in Marine Science*. 5:161.

Nickols, K.J., B. Gaylord, J.L. Largier. 2012. The coastal boundary layer: predictable current structure decreases alongshore transport and alters scales of dispersal. *Marine Ecology Progress Series*. 464:17-35.

Nickols, K.J., J.W. White, J.L. Largier, and B. Gaylord. 2015. Marine population connectivity: Reconciling large-scale dispersal and high self-retention. *The American Naturalist*. 185(2):196-211

Noble, M.A., K.J. Rosenberger, P. Hamilton, and J.P. Xu. 2009. Coastal ocean transport patterns in the central Southern California Bight, in Lee, H.J., and Normark, W.R., eds., *Earth Science in the Urban Ocean: The Southern California Continental Borderland*: Geological Society of America Special Paper 454, p. 193–226, doi: 10.1130/2009.2454(3.3)

North, W.J. 1971. The biology of giant kelp beds (*Macrocystis*) in California. *Nova Hedwigia* 32: 1-600.

Page, H.M., D.C. Reed, M.A. Brzezinski, J.M. Melack, and J.E. Dugan. 2008. Assessing the importance of land and marine sources of organic matter to kelp forest food webs. *Marine Ecology Progress Series* 360:47-62.

Pequegnat, W.E. 1964 The epifauna of a California siltstone reef. *Ecology*. 45(2):272-283.

Pineda, J., J.A. Hare, and S. Sponaugle. 2007. Larval transport and dispersal in the coastal ocean and consequences for population connectivity. *Oceanography*. 20(3):22-39.

Planet Team (2020). Planet Application Program Interface: In Space for Life on Earth. San Francisco, CA. <https://api.planet.com>.

R Core Team (2021). R: A language and environment for statistical computing. R Foundation for Statistical Computing, Vienna, Austria. URL <https://www.R-project.org/>.

Raimondi, P.T., D.C. Reed, B. Gaylord, and L. Washburn. 2004. Effects of self-fertilization in the giant kelp, *Macrocystis pyrifera*. *Ecology*. 85(12):3267-3276.

Reed, D.C. and M.S. Foster. 1984. The effects of canopy shadings on algal recruitment and growth in a giant kelp forest. *Ecology* 65: 937-948, doi:10.2307/1938066.

Reed, D.C., B.P. Kinlan, P.T. Raimondi, L. Washburn, B. Gaylord, and P.T. Drake. 2006. A metapopulation perspective on the patch dynamics of giant kelp in Southern California. Pages 352-386 in J. Kritzer and P. Sale, editors. *Marine metapopulations*. Academic Press, San Diego, California, USA.

Rodriguez, G.E., A. Rassweiler, D.C. Reed, and S.J. Holbrook. 2013. The importance of progressive senescence in the biomass dynamics of giant kelp (*Macrocystis pyrifera*). *Ecology* 94: 1848-1858, doi:10.1890/12-1340.1.

Rosman, J.H., J.R. Koseff, S.G. Monismith, and J. Grover. 2007. A field investigation into the effects of a kelp forest (*Macrocystis pyrifera*) on coastal hydrodynamics and transport. *Journal of Geophysical Research* 112: C02016, doi: 10.1029/2005JC003430.

Rosman, J.H., S.G. Monismith, M.W. Denny, and J.R. Koseff. 2010. Currents and turbulence within a kelp forest (*Macrocystis pyrifera*): Insights from a dynamically scaled laboratory model. *Limnology and Oceanography* 55: 1145-1158, doi:10.4319/lo.2010.55.3.1145.

Rosman, J.H., M.W. Denny, R.B. Zeller, S.G. Monismith, and J.R. Koseff. 2013. Interaction of waves and currents with kelp forests (*Macrocystis pyrifera*): Insights from a dynamically scaled laboratory model. *Limnology and Oceanography* 58: 790-802, doi:10.4319/lo.2013.58.3.0790.

Schiel, D.R., and M.S. Foster. 2015. *The Biology and Ecology of Giant Kelp Forests*. University of California Press Books, doi:0.1525/9780520961098.

Siegel, D.A., B.P. Kinlan, B. Gaylord, and S.D. Gaines. 2003. Lagrangian descriptions of marine larval dispersion. *Marine Ecology Progress Series*. 260:83-96.

Siegel, D.A., S. Mitarai, C.J. Costello, S.D. Gaines, B.E. Kendall, R.R. Warner, and K.B. Winters. 2008. *Proceedings of the National Academy of Sciences*. 105(26):8974-8979.

Stewart, H.L., J.P. Fram, D.C. Reed, S.L. Williams, M.A. Brzezinski, S. MacIntyre, B. Gaylord. 2009. Differences in growth, morphology, and tissue carbon and nitrogen of *Macrocystis pyrifera* within and at the outer edge of a giant kelp forest in California, USA. *Marine Ecology Progress Series*. 375:101-112.

Traiger, S.B., B. Cohn, D. Panos, M. Daly, M. Martone, I. Gutierrez, D.A. Mucciarone, Y. Takeshita, S.G. Monosmith, R.B. Dunbar, and K.J. Nickols. In Review. Biogeochemical modification of surface waters by kelp forest canopies: Influence of kelp metabolism and site-specific hydrodynamics.

Warton, D.I., R.A. Duursma, D.S. Falster, and S. Taskinen. 2012. smatr 3 – an R package for estimation and inference about allometric lines. *Methods in Ecology and Evolution*. 3(2):257-259, doi:10.1111/j.2041-210X.2011.00153.x.

Watanabe, H., M. Ito, A. Matsumoto, and H. Arakawa. 2014. Effects of sediment influx on the settlement and survival of canopy-forming macrophytes. *Scientific Reports*. 6:18677, doi:10.1038/srep18677.

Zimmerman, R.C. and J.N. Kremer. 1986. In situ growth and chemical composition of the giant kelp, *Macrocystis pyrifera*: Response to temporal changes in ambient nutrient availability. *Marine Ecology Progress Series*. 27(3):277-285, doi:10.3354/meps027277.

**TABLES**

Table 1: Summary statistics for depth-averaged alongshore velocities (cm/s) outside and inside the reef. Statistics including root mean square velocity (rms), arithmetic mean (mean), minimum velocity (min), and maximum velocity (max) were computed for the 10-day timeseries associated with each subtidal kelp survey.

Depth-averaged alongshore velocity (cm/s)									
Experiment	Date	rms		mean		min		max	
		outside	inside	outside	inside	outside	inside	outside	inside
2017	2017-01-29	4.167	2.693	-0.384	-0.556	-10.141	-9.850	18.417	9.003
2017	2017-04-11	3.916	3.761	-0.052	-1.234	-17.490	-15.948	11.856	8.659
2017	2017-05-24	4.340	3.024	-0.368	-0.105	-12.814	-11.227	10.990	11.324
2017	2017-06-25	4.893	0.817	0.736	-0.468	-10.941	-2.845	14.455	1.254
2017	2017-07-24	4.008	0.640	-0.249	-0.359	-12.044	-2.181	15.546	1.227
2017	2017-08-20	4.670	0.684	-0.182	-0.090	-13.168	-2.771	15.989	2.152
2017	2017-10-11	3.195	0.766	-0.821	-0.298	-8.407	-2.521	10.072	2.001
2017	2017-11-20	3.408	0.786	-0.936	-0.330	-11.542	-2.683	7.249	1.296
2017	2018-01-31	3.443	0.834	-1.025	-0.457	-13.141	-2.838	7.442	1.992
2017	2018-03-19	4.101	1.422	0.911	-0.682	-9.524	-4.329	17.557	2.135
2017	2018-05-22	3.383	1.555	-0.882	-1.285	-11.406	-4.448	6.237	1.299
2019	2019-04-18	4.705	3.281	-0.083	0.395	-11.930	-9.372	16.614	8.598
2019	2019-05-23	4.346	3.359	0.109	-0.118	-13.551	-15.438	11.045	7.101
2019	2019-06-24	3.665	1.067	-0.169	-0.093	-10.855	-3.655	11.131	3.408
2019	2019-07-23	4.858	1.241	-0.105	-0.206	-12.171	-3.827	18.781	5.099
2019	2019-09-26	6.130	1.420	0.033	-0.528	-32.020	-5.126	22.255	4.016
2019	2019-11-13	5.521	1.310	-0.064	-0.312	-13.500	-3.654	20.326	4.206

## FIGURES

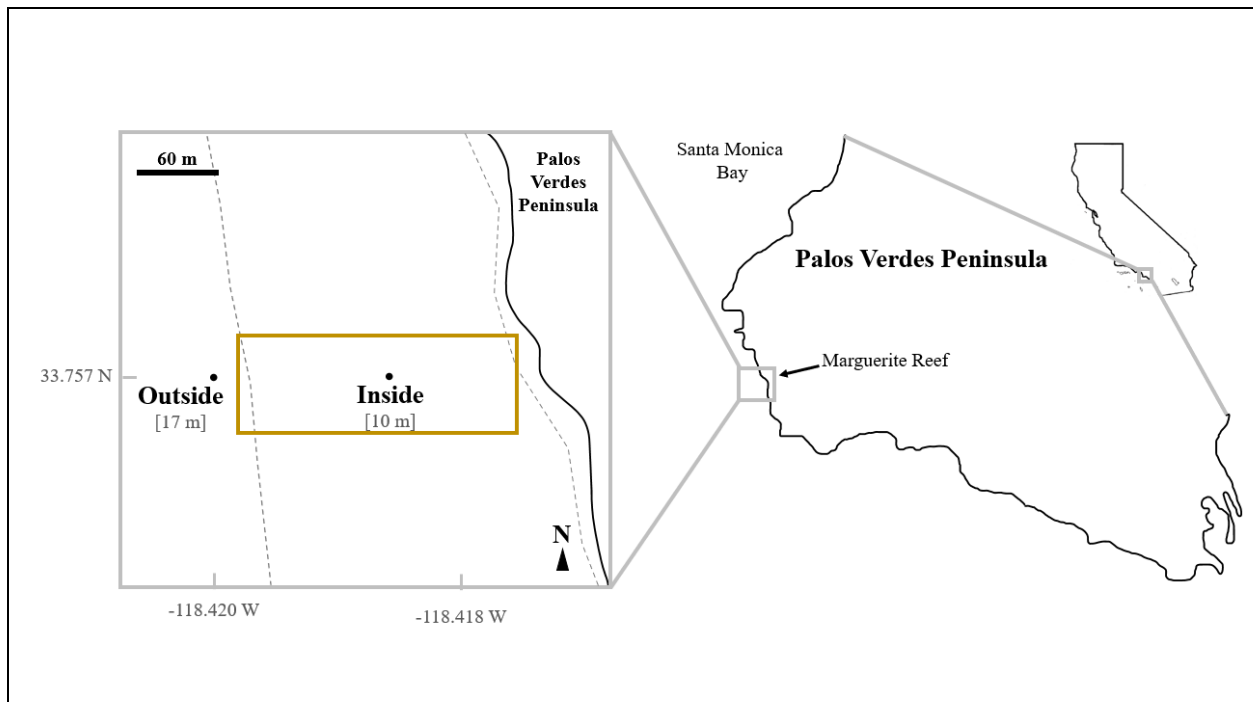


Figure 1: Map of Marguerite Reef, Palos Verdes, California, USA, showing locations of the outside and inside instruments, with their mean depths noted within brackets. The outer and inner edges of the kelp forest, which generally follow seabed isobaths, are represented by dashed lines. The yellow box delineates the spatial extent within which kelp parameters were quantified.

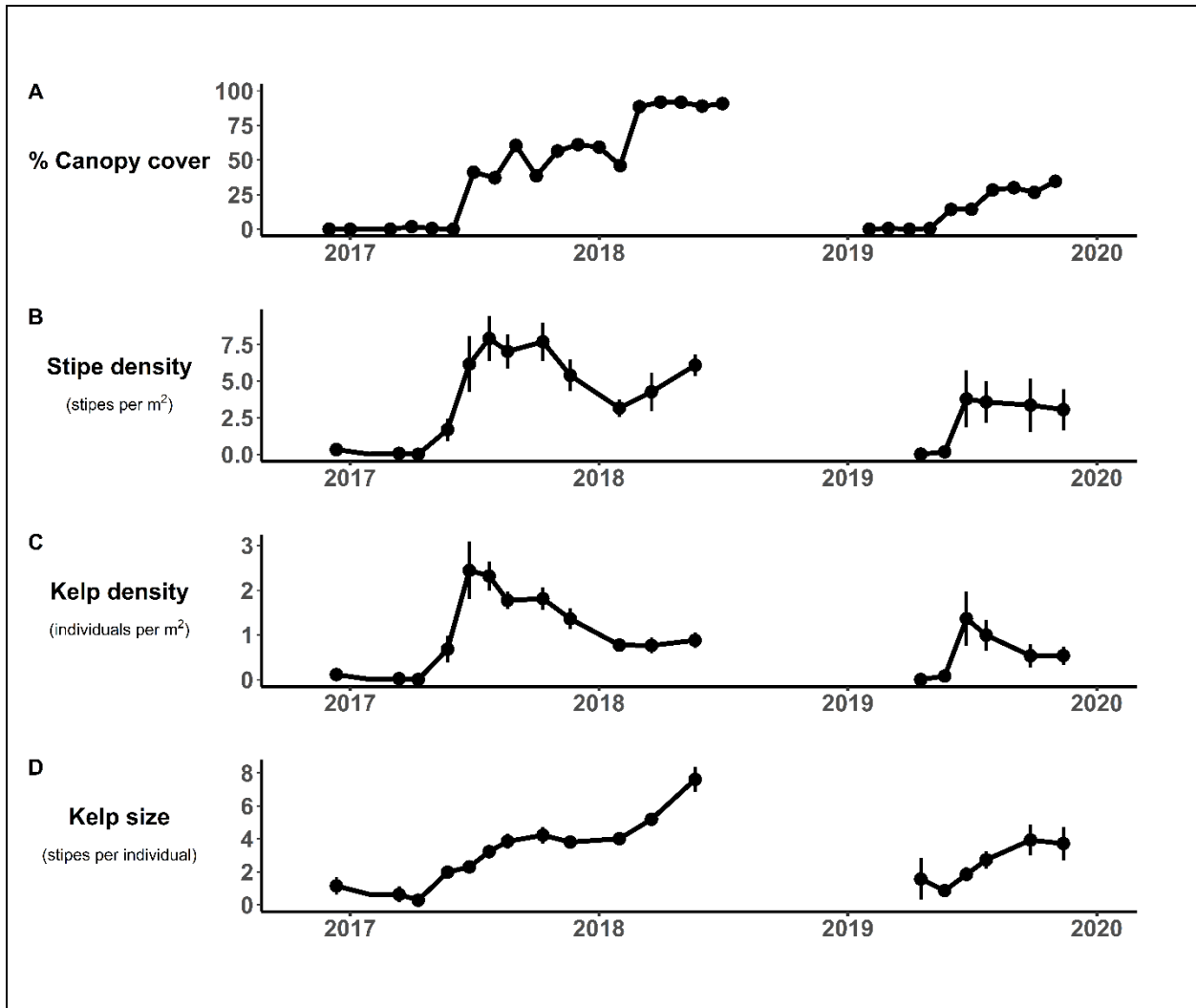


Figure 2: Changes in the *M. pyrifera* kelp forest structure at Marguerite Reef, Palos Verdes, CA, over the duration of the study: A) percentage of canopy cover at the surface, B) plant density, C) stipe density, and D) stipes per plant. Points indicate the mean across transects and vertical bars indicated +/- SE. Canopy coverage is the percent of kelp coverage over a rectangular area, overlapping with the subtidal kelp surveys; rectangular area is shown and labeled in Figure 1.

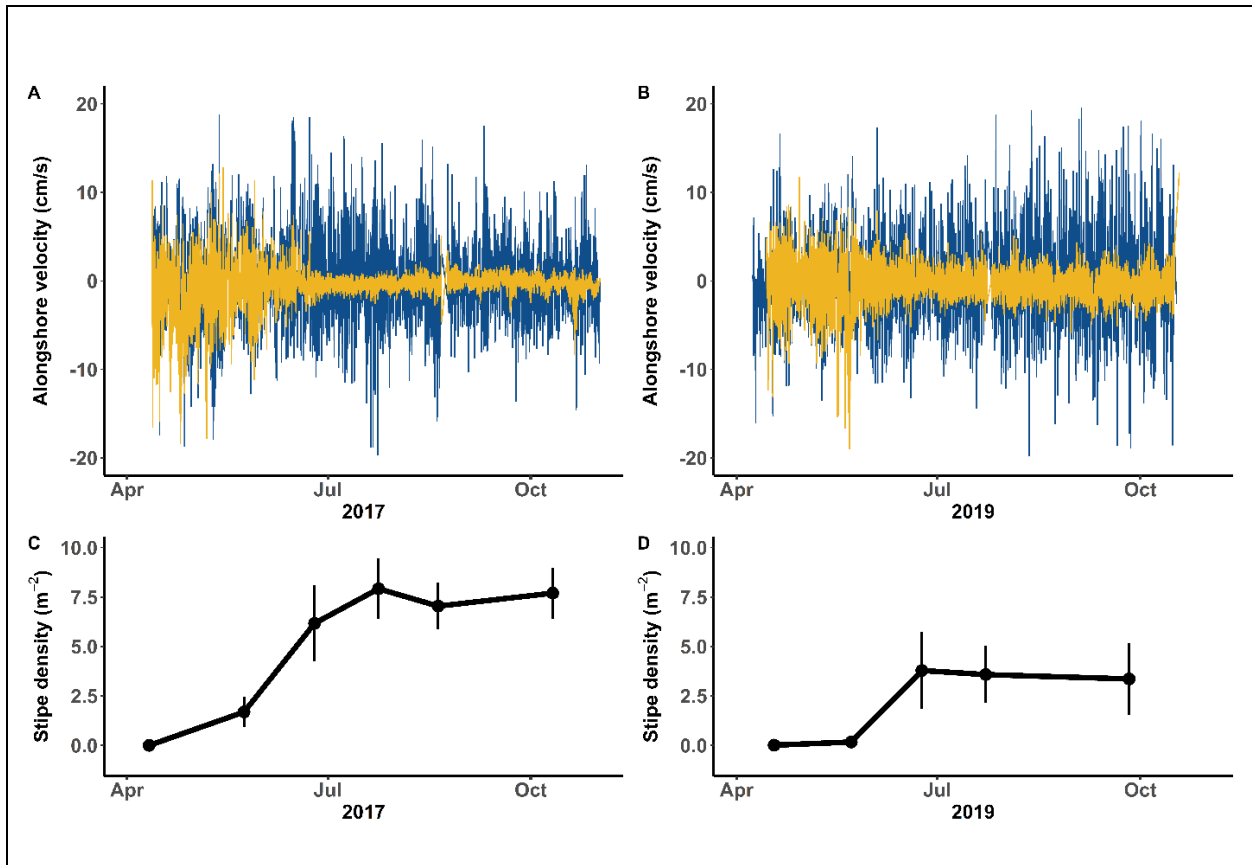


Figure 3: Depth-averaged alongshore velocities outside (blue lines) and inside (yellow lines) Marguerite Reef as a new kelp forest emerged between April and October of A) 2017 and B) 2019. *Macrocystis pyrifera* stipe densities at Marguerite Reef between April and October of C) 2017 and D) 2019. Points indicate the mean across transects and vertical bars indicated +/- SE.

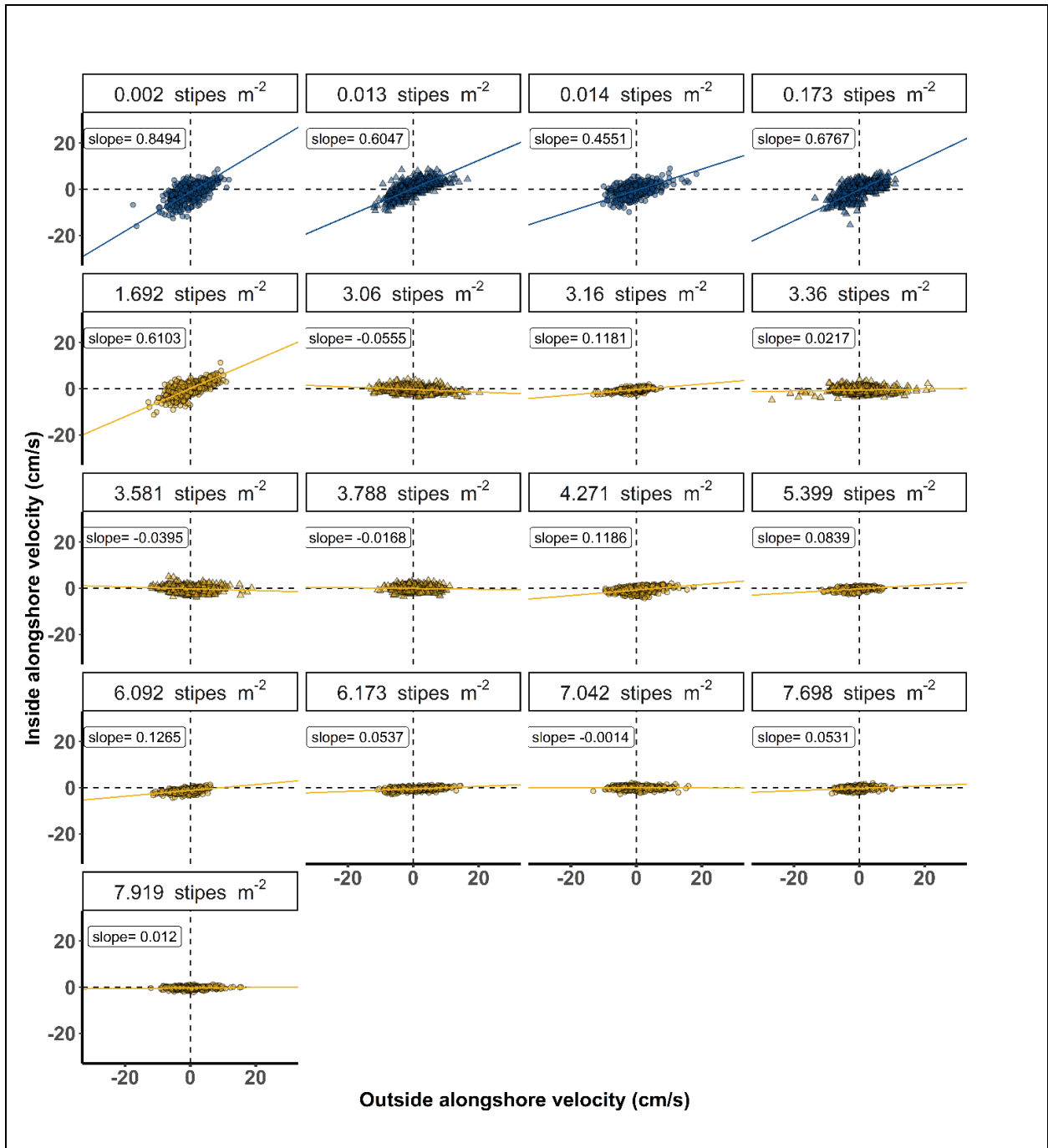


Figure 4: Major axis regressions of depth-averaged alongshore velocities (cm/s) outside and inside Marguerite Reef, across stipe densities (stipes per square meter). Plots are ordered and labeled by stipe density. Lines represent the major axis regression slope, points represent depth-averaged velocities corresponding with a given survey date. Blue coloration indicates relationships when negligible kelp was present (stipe density <0.2) and golden-brown coloration indicates relationships when kelp was present (stipe density >0.2). Circles represent data from the 2017 experiment and triangles represent data from the 2019 experiment.

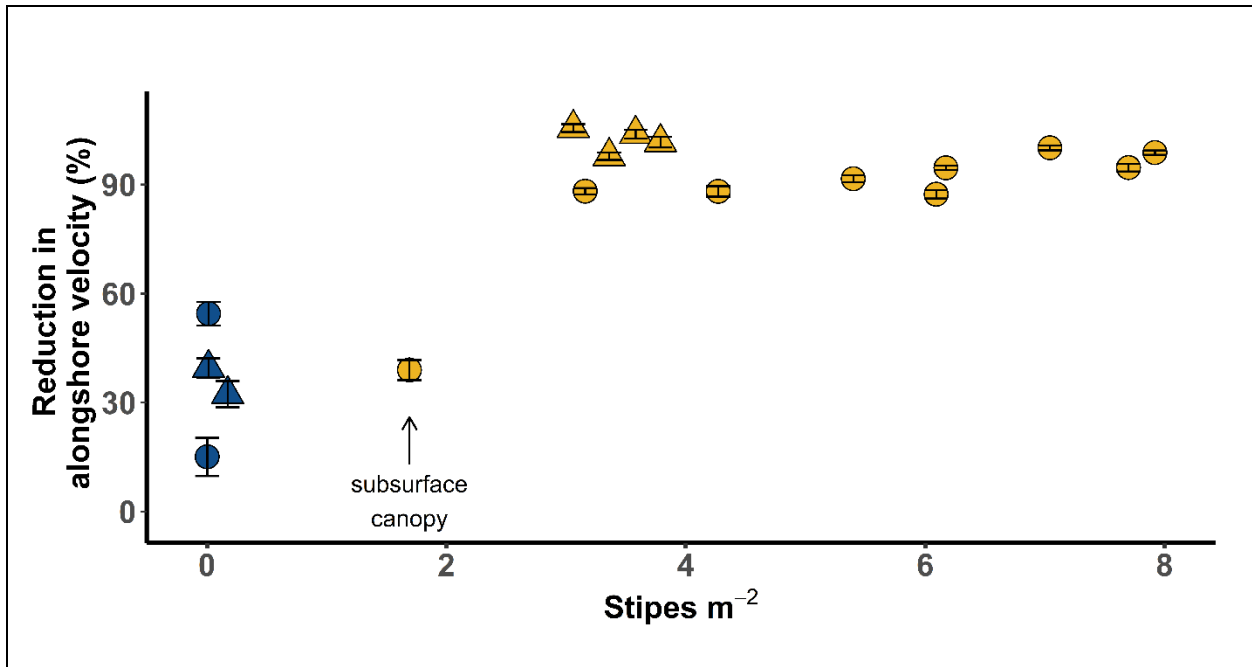


Figure 5: Reduction in alongshore velocities within Marguerite Reef across stipe densities (stipes per square meter). Points represent percent velocity reductions (computed from major axis regression slopes) associated with each stipe density. Vertical bars indicate their respective standard errors. Blue points indicate no kelp was present (stipe density  $< 0.2$ ) and yellow points indicate kelp was present (stipe density  $> 0.2$ ). Circles represent data from the 2017 experiment and triangles represent data from the 2019 experiment. Arrow labeled “subsurface canopy” indicates when kelp was present, but not yet at the surface.

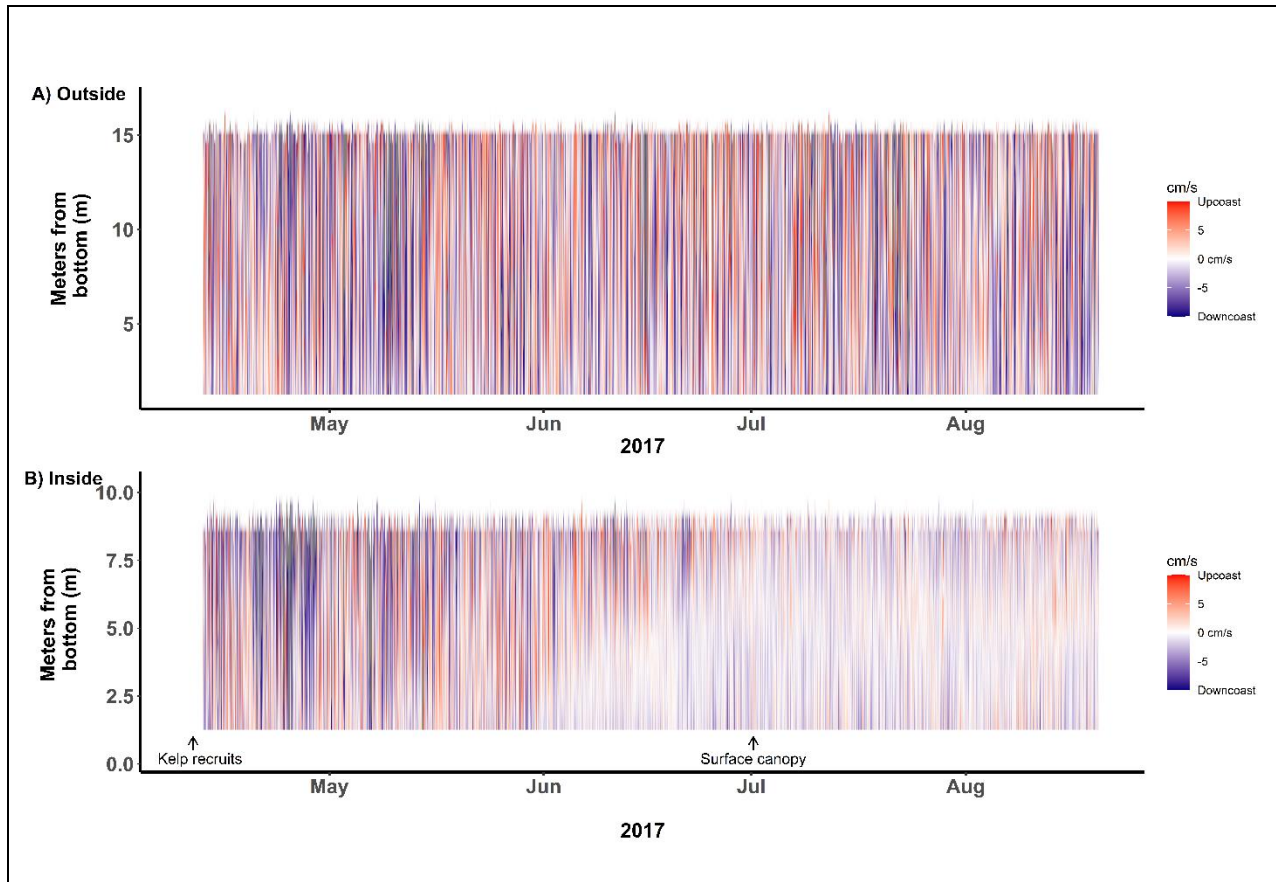


Figure 6: Time series of alongshore velocity profiles A) outside and B) inside Marguerite Reef, spanning the transition from a barren reef to one supporting a kelp forest with a surface canopy. Red colors correspond to flows upcoast and blue colors correspond to flows downcoast. Darker shades indicate greater velocities and lighter shades indicate slower velocities, with white representing 0 cm/s. Vertical arrows indicate when single-bladed kelp recruits and the surface canopy were each first observed.

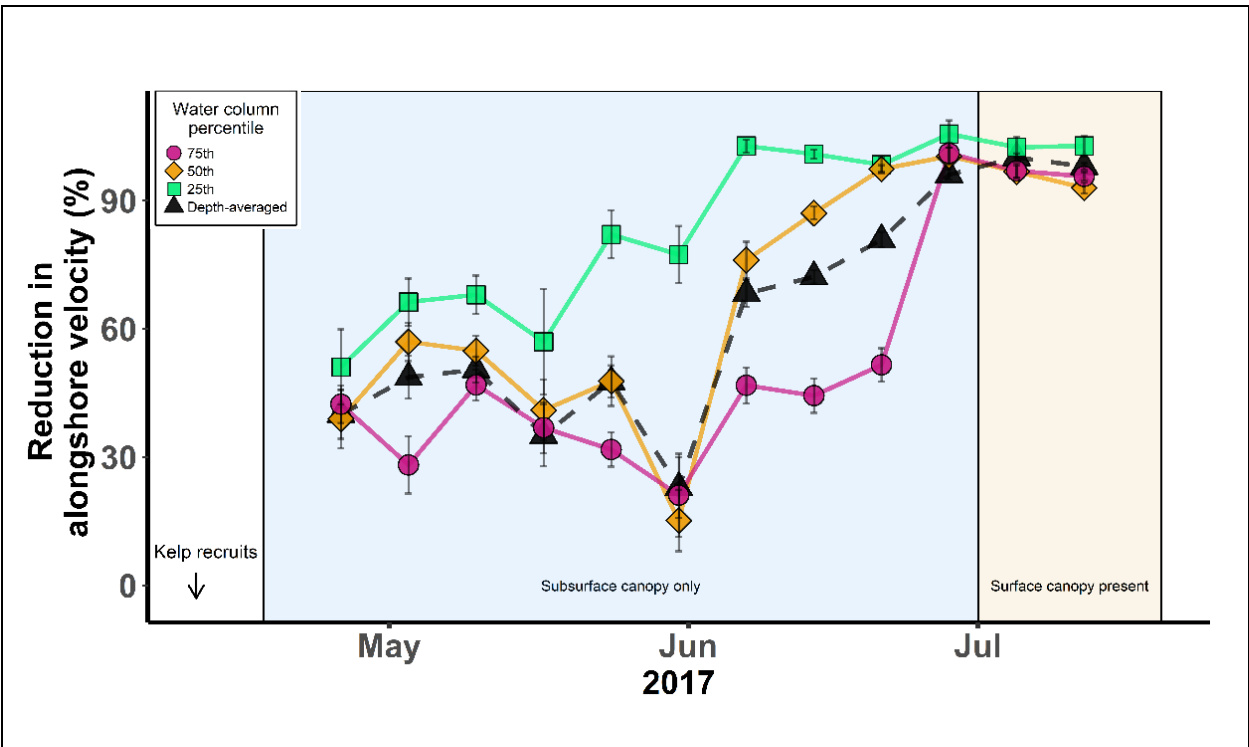


Figure 7: Reduction in alongshore velocities within Marguerite Reef, throughout the 2017 transition from a barren state to a kelp forest state supporting a surface canopy. Points represent weekly percent velocity reductions. Vertical bars indicate their respective standard errors. Black triangles represent depth-averaged (DA) data, green squares, orange diamonds, and pink circles represent data from velocities at the 25<sup>th</sup>, 50<sup>th</sup> and 75<sup>th</sup> percentile positions of the water column, respectively. Blue shading indicates no surface canopy was present and yellow shading indicates surface canopy was present at Marguerite Reef. Arrow indicates when single-bladed kelp recruits were first observed.

### **CHAPTER 3**

Jaw-test allometry of two temperate urchin species across habitat conditions\*

---

\*Co-authors: Tristin Anoush McHugh, Jan Freiwald, Brian Gaylord

## ABSTRACT

Sea urchins are of great importance ecologically, economically, and culturally worldwide. They have the capacity to dramatically alter the structural complexity of ecosystems, support lucrative commercial fisheries, and have been a part of the human diet for thousands of years. As such, patterns of urchin growth have provided insights into mechanisms of large-scale ecosystem shifts, improvement of present-day fisheries management, and reconstruction of historical harvesting practices dating back to the Holocene. Sea urchin growth has been studied extensively across taxa and systems and while some generalities exist, differences among species and local environmental conditions have been shown to strongly influence patterns of urchin growth, specifically in growth of urchin gonads (reproduction and energy storage), tests (skeletal structure), and jaws (feeding apparatus). Here we characterize relationships among gonad production, size (i.e., test diameter), and jaw morphology (i.e., length, width, shape, weight) between *Strongylocentrotus purpuratus* and *Mesocentrotus franciscanus*, two dominant urchin species of California's temperate rocky reefs. We also explore the extent to which those allometric relationships change across differing habitat conditions, classified as bull kelp (*Nereocystis luetkeana*) forest, reef with understory algae-only (no surface kelp canopy), and urchin barren, to better understand the role of habitat context on species-specific gonad, test, and jaw allometry. Both species of urchin exhibited greater production of gonad material in the kelp and understory habitats than the barren habitat, highlighting the stark differences in food availability across the habitats. The relationship between jaw length and test diameter did not differ between habitat conditions, in contrast to what has been documented in other kelp-barren systems (e.g., *Macrocystis pyrifera* forests and barrens of Monterey Bay, CA) and with other urchin species around the world (e.g.,

*Heliocidaris erythrogramma*). Further, *M. franciscanus* exhibited relatively wider jaws than *S. purpuratus* in the kelp habitat, however, such species-specific differences disappeared in the barren habitat, challenging the use of jaw shape to distinguish species within fossil records in lieu of habitat context. However, because *M. franciscanus* had relatively heavier jaws than *S. purpuratus* across all habitats, the relationship between jaw weight and test diameter could be leveraged to parse out distinct species from urchin remains. These results indicate greater complexity in the allometric relationships of urchin tests and their jaws, specifically when comparing between species and across differing or unknown habitat conditions. Habitat context should be considered when building growth models using jaw-test relationships for fisheries management, specifically for *S. purpuratus*, and when inferring species from midden and fossil records for reconstruction of human harvesting patterns across space and through time.

## INTRODUCTION

Sea urchins reside in and can influence a broad range of ecosystems, with distributions ranging from the poles to the equator and extending from the quiescent depths of the sea to the hydrodynamically charged intertidal zone. Particularly in the nearshore environment, shifts in urchin population size and behavior can dramatically alter community structure and function (Steneck 2020; Smith et al. 2021). For example, population outbreaks of sea urchins and associated overgrazing have induced rapid transitions from tropically and physically complex systems, dominated by coral reefs, seagrass meadows, and kelp forests, to ones that are “barren,” largely devoid of aquatic vegetation (Maciá and Lirman 1999; O’Leary and McClanahan 2010; Filbee-dexter and Scheibling 2014; Vergés et al. 2016).

Further, sea urchins are of direct relevance to humans, as they are harvested for food, commercially and traditionally, and used for social and ceremonial purposes (Andrew et al. 2002; Department of Fisheries and Oceans Canada, 2019; Rogers-Bennett and Okamoto 2020). Commonly referred to as “roe”, or “uni”, the gonad material of urchins serves as the primary site for reproduction and energy storage (Gonor 1973), is rich in glycogen, protein, and lipids (McBride 2005), and is consumed worldwide, with Japan and France making up most of the current global market (Azad 2011). In particular, California’s red urchin (*Mesocentrotus franciscanus*) fishery is quite lucrative and predominantly exports highly valued product to Japan (Workman 1999; Azad 2011). Indigenous Peoples of the western coast of North America have also harvested urchins for thousands of years, with some records of urchin remains dating back to the Holocene (Erlandson et al. 2005; Campbell 2008; Ainis 2020).

Reconstruction of historical urchin fishing records has been possible through use of relationships between urchin test diameter and jaw morphology (Campbell 2008; Ainis 2020).

Archeologists have used jaw-test allometry to infer the size frequencies of urchins harvested by Indigenous Channel Islanders throughout the Holocene (Ainis 2020). Such analyses provide improved estimates of urchin exploitation and enhance understanding of the relative importance of multiple components of the diets of ancient humans spatially, seasonally, and across longer timescales. For example, size reconstructions revealed Indigenous Islanders focused harvesting efforts on the smaller purple urchin, *Strongylocentrotus purpuratus*, and to a lesser extent on the red urchin, *M. franciscanus*, in contrast to present day fishing practices where the reverse is true. Further, though untested, it has been suggested that such reconstructed harvest records can be used to infer past environmental conditions within nearshore habitats (i.e., water temperatures or algal cover) (Campbell 2008; Ainis 2020).

While variable, urchin gonad production exhibits generally seasonal patterns, with peak production occurring in the Fall throughout California and Oregon for *S. purpuratus* and *M. franciscanus* (Ebert et al. 2011; Claisse et al. 2013; Teck et al. 2018). Harvesting efforts of *M. franciscanus* follow a similar temporal trend, with larger urchin landings occurring during the peak reproductive season (Teck et al. 2018). Periods of low gonad production correspond to reduced fishing effort and lower price per landing, suggesting lower quality gonad product (Teck et al. 2018). Historical harvesting efforts likely also corresponded with urchin reproduction cycles, with harvesters preferentially selecting urchins at times when gonad production was highest. Low gonad production occurs seasonally, following spawning which typically occurs in early spring (Gonor 1973). However, sharp, and prolonged shifts in temperature or food availability (e.g., loss of a kelp forest) can also lead to reduced gonad production (Azad 2011; Claisse et al. 2013; Okamoto 2014). Such environmental perturbations can cause gonad production, and thus harvesting efforts, to fall out of sync with seasonal

patterns and/or depress annual harvesting yields which could be reflected in historical landings data as well as middens or fossil records.

Following ecosystem shifts from a kelp forest to barren state, urchins can experience prolonged periods of starvation, necessitating acclimatization, morphological plasticity, and/or tradeoffs in fitness in order to survive. Both urchin tests and jaws grow continuously throughout their lifetime, however the rate of such growth can vary with environmental context (Cutress 1965; Ebert 1980; Ling and Johnson 2009). As such, modifications to urchins' feeding apparatuses relative to their test size, in the context of limited food availability, has garnered much attention (e.g., Ebert 1980, 2014; Pederson and Johnson 2007; deVries et al. 2019). Food-deprived urchins tend to have larger jaws for a given test size (or smaller tests for a given jaw size) than those of well-fed urchins (Ebert 1980, 2014; Pederson and Johnson 2007; deVries et al. 2019). However, the mechanism by which this difference occurs is still not fully understood. Some argue that larger jaws facilitate increased feeding efficiency, which could be particularly important when food is scarce (Ebert 1980, 2014; Pederson and Johnson 2007). Other studies suggest that both test and jaw size vary with energetic state in urchins, and that a focus on jaw plasticity as a beneficial response to low food may be misleading. In particular, one recent study found that while jaw length to test diameter ratios were greater in food-deprived purple urchins, this difference was driven by modifications to test size rather than jaw size (deVries et al. 2019). Additionally, it was suggested that maintenance of barren populations may not derive from increased feeding efficiencies, but rather by the urchins' ability to achieve reproductive success despite unfavorable conditions (i.e., food-limited barrens). Such a hypothesis is especially interesting given the notion that organisms only have so much energy to operate in the environment. The manner in which urchins use such fixed amounts of energy, which are

presumably depressed within barrens (Spindel et al. 2021), is thought to influence broader population dynamics, the tendency for urchins to instigate kelp forest destruction, and the maintenance of barrens once created.

Species-specific differences in jaw morphology have been described for California's two dominant urchin species, *S. purpuratus* and *M. franciscanus*, though allometric relationships were derived from relatively small sample sizes and thus, could benefit from further parameterization (Campbell 2008). Robust characterization of jaw morphology between these two species could improve estimates of their relative contributions to the diets of coastal Indigenous Peoples dating back to the Holocene. Much of the literature exploring jaw-test allometry in *S. purpuratus* has been with urchins sourced from intertidal and very shallow subtidal habitats, leaving room to explore potential differences for urchins originating from subtidal habitats where food sources and environmental conditions differ. Further, while jaw-test allometry of red urchins have been examined previously, patterns were only explored in urchins derived from habitats with plentiful food. Potential differences in jaw-test allometry due to food-deprivation could have consequences for growth models that are important for fisheries management and aquaculture.

Urchin jaws have been used to improve species-specific growth models that are critical to effective fisheries management (Ebert and Russell 1993; Rogers-Bennett et al. 2003). For instance, measurements of jaw growth from a mark-recapture study revealed that red urchins (*Mesocentrotus franciscanus*) were much older than otherwise would be predicted based on their test diameter alone (Ebert and Russell 1993). Previous estimates of ages in *M. franciscanus*, using test diameter alone, suggested red urchins entered the fishery as young as four years old (Kato and Schroeter 1985). Studies using jaw measurements to construct growth

models found instead that *M. franciscanus* required at least 7 years of growth before reaching harvestable size (Rogers-Bennett et al. 2003). Accompanying studies of sea urchin tests, using radiocarbon markers as timestamps, also revealed the exceptional longevity of red sea urchins, which can reach a century (Ebert and Southon 2003). Importantly, however, it is unclear how limited food availability may impact these growth estimates, through alteration of the jaw length – test diameter relationship. Parameterization of the jaw length – test diameter relationship in *M. franciscanus* under well-fed and food-deprived conditions (i.e., kelp forest vs. barren habitats) would elucidate the extent to which historical habitat context would need to be considered in species-specific growth models.

Along the northern coast of California, sea urchins have contributed recently to widespread declines in nearshore kelp forests and the transition to a barren state. In 2014, forests of *Nereocystis luetkeana* (the bull kelp) were subjected to what scientists have called the “perfect storm” of conditions, resulting in catastrophic loss of this canopy-forming species (Rogers-Bennett and Catton 2019; McPherson et al. 2021). While not completely understood, the suite of conditions that aligned to facilitate a loss of 95% of California’s bull kelp forests were three-fold: 1) elevated seawater temperatures, which weakened bull kelp individuals 2) sea star wasting disease, which led to the decimation of the sunflower sea star (*Pycnopodia helianthoides*), an important predator in the kelp forest system, and 3) most relevant here, an explosion of purple urchins (*Strongylocentrotus purpuratus*), which notoriously overgraze kelp forests when in high numbers (Rogers-Bennett and Catton 2019; McPherson et al. 2021). Only remnant patches of kelp have persisted through this die-off and urchin barrens have replaced what were once large stretches of forests. Unlike barrens in southern California, which are dominated by *S. purpuratus*, recent development of barrens in northern California are composed

of a mix of *S. purpuratus* and *M. franciscanus* (Reef Check, unpublished data). Importantly, within the barrens, the two urchin species are directly competing for already depleted resources, which could further influence growth of (or lack of) skeletal and reproductive material (i.e., test, jaw, gonad production). Such a scenario presents a unique opportunity to directly compare jaw-test allometry of *S. purpuratus* and *M. franciscanus* to one another and their respective relationships with food availability.

We expand here upon previous research to better understand the jaw-test relationships of *Strongylocentrotus purpuratus* and *Mesocentrotus franciscanus* across a gradient of habitat conditions. We quantify gonad production, jaw morphology, and their respective relationships to test diameter, in these two species from subtidal rocky reefs that support a range of community states. The community states include barren sites, locations with understory macroalgae only, or sites with an intact surface kelp canopy plus an understory community. Through this experimental framework, we address three questions: 1) to what extent does gonad production (proxy for energy reserve) differ across habitat types (kelp, understory, barren) for *S. purpuratus* and *M. franciscanus*? 2) how does the relationship between jaw-test morphology compare between *S. purpuratus* and *M. franciscanus*? and 3) to what extent do those relationships differ depending on the condition of the habitat they came from (kelp, understory, barren)?

## **METHODS**

### *Urchin collections*

In the Fall of 2020, a total of 152 purple urchins (*Strongylocentrotus purpuratus*) and 152 red urchins (*Mesocentrotus franciscanus*) were collected from four sites within Mendocino County in northern California – Portuguese Beach, Point Arena, Noyo, and Caspar (Figure 1;

Table 1). The four sites were classified into one of three categories, based on the amount and type of aquatic vegetation present: “kelp,” “understory,” or “barren,” which were determined by the dominant community structure. The reef at Portuguese Beach (39.30258, -123.80284), classified as a kelp site, supported a thick *Nereocystis luetkeana* forest, while the reef at Point Arena (38.92940, -123.73278), classified as an understory site, had no surface canopy, but supported a community of understory alga. The reefs at Noyo (39.43019, -123.81406) and Caspar (39.36430, -123.82113), classified as barren sites, were devoid of vegetation and were densely populated by purple and red urchins. A range of sizes for each urchin species were collected from the respective sites and subsequently measured and dissected upon return to shore.

#### *Morphological measurements*

Test diameters were measured with vernier calipers ( $\pm 0.01$  mm), and wet masses were quantified using a portable balance ( $\pm 0.01$  g). Gonads were then dissected and weighed using the same balance. In the lab, jaws were dissected and placed in a 5% hypochlorite solution for 24 hours to remove all tissue. The remaining calcified material was then rinsed with deionized water, and air-dried. One jaw (demi-pyramid) per urchin was weighed using a balance ( $\pm 0.0001$  g) and photographed from a fixed distance with a scale bar within each image. The length and width of each jaw were then determined using ImageJ software (v. 1.8) (Figure 2). A jaw shape parameter was calculated by dividing the jaw width by the jaw length. Jaw length, width, and shape parameters were not measured or calculated for urchins from the understory habitat.

### *Statistical analysis*

To test for differences in gonad mass across habitat conditions in each species, a linear regression was constructed with gonad mass (g) as the response variable, and test diameter (mm; continuous), species (i.e., *Strongylocentrotus purpuratus* and *Mesocentrotus franciscanus*; categorical), and habitat condition (i.e., kelp, barren, understory; categorical), as well as their associated interactions, as predictors. To check for overfitting, a backward stepwise model selection was conducted to determine the best fitting model. Associated AIC scores and models tested are shown in Table S1. The residuals in the model were assessed visually for normality and heteroscedasticity.

To test for differences in jaw morphology across habitat conditions in each species, three separate linear regressions were constructed with jaw length (mm), jaw width (mm), and jaw shape (defined as jaw width : jaw length ratio), each as a response variable for their given model. For each linear regression, test diameter (mm; continuous), species (i.e., *Strongylocentrotus purpuratus* and *Mesocentrotus franciscanus*; categorical), and habitat condition (i.e., kelp, barren, understory; categorical), as well as their associated interactions, were used as predictors. To check each model for overfitting, a backward stepwise model selection was conducted to determine the best fitting model. Associated AIC scores and models tested for each of the three regressions are shown in Table S2. The residuals in each model were assessed visually for normality and heteroscedasticity to inform appropriateness of each of the respective models. All statistical tests were accomplished in R version 4.0.2 (R Core Team, 2020) and pairwise comparisons were conducted using the package emmeans (Lenth 2020).

## RESULTS

### *Urchin test morphology*

Test diameters of the urchins collected ranged between 26 – 83 mm and 20 – 124 mm for *S. purpuratus* and *M. franciscanus*, respectively (Figure 3). For each species, diameter ranges were similar across habitat types. Because urchins were collected to capture a broad size range, the frequencies shown in Figure 3 are not reflective of the natural population within each habitat type. The fitted regressions between wet mass and test diameter did not differ across habitats or between species (Figure 4).

### *Gonad production*

Gonad production increased with test diameter for both species, regardless of habitat condition (Figure 5). Red urchins exhibited more massive gonads than the purple urchins in the kelp habitat (Figure 5E), however, gonad production did not differ between red and purple urchins in either the barren or understory habitats (Figure 5C-D). Both red and purple urchins exhibited greater gonad production in the kelp habitat than in the barren habitat (Figure 5A-B; Table S3). While gonad production was also greater in the understory habitats than in the barren habitats for both species, gonad production by the purple urchin found in understory habitats was not significantly different from that produced in the kelp habitat. In contrast, gonad production by the red urchin found in understory habitats was less than what was produced in the kelp habitat (Figure 5; Table S3).

### *Jaw morphology*

Jaw morphology differed between species and across habitats. Each jaw parameter (i.e., length, width, shape, and mass) increased with increasing test diameter, regardless of species or habitat. The relationship between jaw length and test diameter did not differ across habitats or between species, with the exception of a significant difference between purple urchins from a kelp habitat and red urchins from a barren habitat (Figure 6; Table S4).

In contrast, the relationship between jaw width and test diameter differed between species and across habitats (Figure 7; Table S5). In the kelp habitat, red urchins had wider jaws than their purple counterparts for a given test diameter (Figure 7D). Interestingly, however, jaw widths were indistinguishable between the purple and red urchins from the barren habitat (Figure 7C). Barren-derived urchins of both species exhibited wider jaws for a given test diameter, than those derived from the kelp habitat (Figure 7A-B).

Similarly, jaw shape (width-to-length ratio) for a given test diameter, differed between species and across habitats (Figure 8; Table S6). Within the kelp habitat, red urchins had a broader jaw shape than their purple counterparts (Figure 8D). However, as with the jaw width parameter, species-specific differences in jaw shape were not observed in the barren habitat (Figure 8C). Jaws of barren-derived purple urchins exhibited a broader shape for a given test diameter than those from the kelp habitat (Figure 8A; Table S6). However, jaw shape did not differ between barren-derived and kelp-derived red urchins (Figure 8B; Table S6).

The jaw mass – test diameter relationship differed between species and across habitats (Figure 9; Table S7). Within each habitat type, red urchins had relatively more massive jaws than purple urchins (Figure 9 C-E). However, when comparing a given species across habitat

types, both red and purple barren-derived urchins had relatively more massive jaws for a given test diameter (or smaller test diameters for a given jaw mass) than those derived from either a kelp or understory habitat (Figure 9A-B; Table S7). Additionally, the jaw mass – test diameter relationship did not differ between kelp and understory habitats for either species. The jaw mass – test diameter relationship from barren-derived purple urchins were also indistinguishable from those of red urchins derived from kelp or understory habitats.

## **DISCUSSION**

In this study, we quantified the extent to which relationships among urchin gonad production and jaw morphology varied by species and habitat condition (kelp, understory-only, barren) in Mendocino County, northern California. Overall, the red urchin produced more massive gonad material in the kelp habitat than in the understory habitat, with the lowest gonad production occurring in the barren habitat. There was no difference in purple urchin gonad production between kelp and understory habitats, however, more massive gonads were produced in kelp and understory habitats than in the barren habitat. In general, red urchins had relatively wider, broader, and heavier jaws for a given test diameter than their purple urchin counterparts (Table 2). However, this species-specific pattern only held within the kelp habitat. The species-specific jaw-test relationships differed depending on the condition of the habitat they came from. Importantly, while the two species were distinguishable within the kelp habitat by their test diameter and jaw width, shape and weight relationships, no differences between jaw length, width, or shape were detected between the two species within barren habitats. Jaw width and length were not measured for urchins from understory-only habitats. Interestingly,

the jaw length – test diameter relationship did not differ between kelp and barren habitats (Table 3). In contrast, urchins from the barren habitat exhibited relatively wider, heavier jaws than those from the kelp habitat. Observed differences in gonad production and jaw morphology between species and across habitat types complicates previous understanding and use of jaw-test allometry across disciplines.

### *Species-specific differences*

Differences in gonad production between red and purple urchins collected from the kelp habitat could be attributed to species-specific differences in test shape and/or diet. In this study, red urchins produced relatively more massive gonads than purple urchins within the kelp habitat, for a given test diameter. In general, red urchin tests tend to be more spherical in shape, while purple urchin tests tend to be squatter. Differences in overall body shape can lead to red urchins exhibiting relatively greater internal volumes than a purple urchin of the same test diameter, and consequently provide more internal volume for gonad material to occupy. While test height was not measured in this study, it is possible observed differences in gonad production could be driven by differences in the overall test volume (via differences in test height). Further, metabolic processes involved in gonad production are tightly linked to food availability and diet (Foster et al. 2015; Rogers-Bennett and Okamoto 2020), and thus species-specific differences in consumption may have contributed to the differences in gonad production observed here. While red and purple urchins were collected simultaneously at each habitat type, theoretically with equal access to food, it is possible their diets were not identical in volume or composition. Prior studies have shown purple urchins consume macroalga at half

the rate of red urchins (Vadas 1977). Additionally, while purple urchins consume macroalgal species indiscriminately, red urchins have been shown to preferentially consume *Nereocystis* (Vadas 1977). Differences in nutritional value of macroalgal species available for consumption (Foster et al. 2015), in conjunction with species-specific diet preferences (Vadas 1977), could contribute to differential gonad production in red and purple urchins from the same location.

Species-specific differences in jaw shape have been previously documented for *S. purpuratus* and *M. franciscanus*, and thus jaw shape has been suggested as a metric by which to distinguish urchin species among urchin remains (i.e., middens or fossil records; Campbell 2008). Generally, red urchins had wider jaws for a given test diameter than did purple urchins (Campbell 2008). However, data presented here highlight a previously unrecognized complexity to this relationship. These findings indicate that the extent to which urchin species can be distinguished via jaw shape depends on their respective habitat type (barren or kelp), which is associated with food availability. In this study, species-specific differences in jaw shape are apparent in urchins derived from well-fed kelp habitat and align well with previously observed patterns, such that red urchins exhibit relatively broader jaws (Campbell 2008). However, these species-specific differences in jaw shape disappear under food-deprived conditions, as observed here in the barren-derived urchins (Figure 8; Table S6). In lieu of additional environmental context, it may not be possible to distinguish red and purple urchins from one another using jaw length or shape metrics of urchin remains from middens or fossils (i.e., in Ainis 2020).

Previous work has not included jaw mass as a parameter by which to compare and possibly distinguish echinoid species from one another in midden and fossil remains, however, patterns observed in this study suggest the jaw mass to test diameter relationship may provide

an alternative distinguishing metric; however, habitat context again presents challenges. The two urchin species are distinguishable by jaw weight when compared within a given habitat context (i.e., kelp, understory, barren). For example, red urchins from barrens exhibit heavier jaws for a given test diameter than purple urchins from barrens, and red urchins from kelp and understory habitats exhibit heavier jaws than purple urchins from kelp and understory habitats. However, jaw weights of purple urchins from barrens were indistinguishable from those of red urchins from both kelp and understory habitats. It may be possible, though yet untested, to use a combination of the jaw shape and jaw mass relationships with test diameter to tease apart both urchin species and habitat context. It is likely the heavier jaws of red urchins observed here are driven by the relatively greater amount of material along the jaw's width-axis. However, species-specific differences in age at a given test size may play a role as well. For example, red urchins tend to have slower growth rates such that for a given test size, a red urchin is older than a purple urchin. The older red urchin may develop relatively denser jaws through more compact deposition of calcium carbonate material onto the jaw over time. Further analyses quantifying jaw densities of the two species would be needed to explicitly tease apart the role of urchin age and density of calcium carbonate deposition versus deposition via greater jaw area.

#### *Habitat-specific differences*

Differences in gonad production across habitat types are likely driven by food availability and composition within each habitat, though other factors may be at play, including the degree of imported (allochthonous) drift alga and inter- and intra-specific competition for

food. For example, while there was no *Nereocystis luetkeana* canopy present in the understory-only habitat, drift alga sourced from adjacent kelp forests could have been delivered to the habitat by way of currents, supplementing the diet of understory alga. Such a scenario could explain the intermediate level of gonad production by red urchins from the understory habitat. Given that red urchins preferentially consume *N. luetkeana* (Vadas 1977) and are prone to sedentarily wait for algal drift (Lowe et al. 2015), it is possible they were not consuming much of the attached understory species, and consequently produced submaximal gonad material (in comparison to their kelp-derived counterparts). In contrast, gonad production by purple urchins between the understory and kelp habitats did not differ. It is possible this was driven, at least in part, by the indiscriminatory feeding behavior exhibited by purple urchins (Vadas 1977), such that they were likely consuming locally-derived macroalga – regardless of access to drift kelp or surface canopy presence. Little to no gonad production within the barren habitat indicates that external subsidies of drift alga were likely absent or insufficient to support gonadal development for either species. Further, competition with conspecifics and other grazers (e.g., abalone) for local macroalgal resources (Leighton 1966; Centoni 2018) likely contribute to localized consumption patterns that can, in turn drive site-specific gonad production patterns.

In addition to influencing gonad production, food availability and feeding efficiency have been shown to influence other axes of urchin growth, such as urchin tests and jaws. Specifically, the relationship of jaw length and test diameter has been linked to habitat condition in sea urchin species found around the world (Ebert 1980, 2014; Black et al. 1982; Pederson and Johnson 2007; Hernandez and Russell 2010; deVries et al. 2019). In general, food-limited urchins exhibit longer jaws for a given test diameter than their well-fed counterparts (Ebert 1980; deVries et al. 2019; Smith and Garcia 2021). These differences may arise through

changes in the morphologically plastic jaws, as larger jaws could facilitate increased feeding efficiency, which could in turn be critical to survival in low-food environments (Ebert 1980, 2014; Pederson and Johnson 2007; Smith and Garcia 2021). However, recent experiments testing this theory found that changes in the jaw length : test diameter ratio were driven by strong reductions in growth of both jaw and test diameter (and especially of the latter) under low-food conditions, as opposed to an increase in jaw growth compared to test diameter (deVries et al. 2019). Moreover, differences in jaw-test ratios did not appreciably influence feeding efficiency, suggesting the patterns observed in jaw-test allometry are a consequence of food deprivation, not a plastic response with an adaptive benefit, per se (deVries et al. 2019).

Patterns of habitat-specific jaw-test relationships observed in this study differ from what has been documented in the literature. Most notably, jaw length – test relationships of purple urchins measured in this study did not differ between habitats with distinct food-availability. This was somewhat surprising, given the many studies exemplifying this effect of habitat condition on the jaw length-test diameter relationship for purple urchins (Ebert 1980, 2014; Fansler 1983; deVries et al. 2019; Smith and Garcia 2021). The similar jaw lengths between habitat conditions observed here were anticipated for red urchins, however, given their characteristically slow growth (Ebert and Southon 2003; Rogers-Bennett et al. 2003). Changes in test diameter and jaw length of urchins are measurable over timescales of several months to a year (Rogers-Bennett et al. 2003; Foster et al. 2015; deVries et al. 2019), which are quite short, relative to the lifespan of a red urchin, which can be upwards of a century (Ebert and Southon 2003). Further, larger, older urchins exhibit slower growth rates, making habitat-induced changes to skeletal growth (e.g., test diameter, jaw length) harder to detect. Importantly, habitat perturbations, such as widespread kelp canopy loss, would likely need to

persist for several years in order to transcend to measurable changes in urchin skeletal structures, and presumably longer for detectability in large, old, red urchins.

Macroalgal diet composition can influence both jaw and test growth in purple urchins (Foster et al. 2015). For example, purple urchins fed *Macrocystis pyrifera*, *Chondracanthus corymbiferus*, and a mixed diet each showed higher growth of test diameters, wet weight, and jaw length, whereas purple urchins fed *Pterygophora californica* and *Rhodomeniacalifornica* each showed lower test diameter, wet weight, and jaw growth (Foster et al. 2015). As such, regional differences in the dominant canopy-forming kelp species may contribute to the jaw shape relationships observed in this and other studies (e.g., Smith and Garcia 2021). Here, differences in jaw width and shape manifested in purple urchins, such that barren-derived urchins had relatively wider jaws than their well-fed counterparts. These patterns differed from findings of a recent study on purple urchins in Monterey Bay, where jaw shape did not differ between urchins from kelp and barren habitats (Smith and Garcia 2021). Interestingly, central California primarily supports *M. pyrifera* forests, while northern California supports *N. luetkeana* forests. Feeding experiments explicitly testing the influence on *M. pyrifera* and *N. luetkeana* diets on jaw-test relationships among purple urchins would help elucidate macroalgal diet as a potential driver.

Previous work exploring allocation of <sup>45</sup>calcium to the various skeletal components of *S. purpuratus* found an overall depression of calcification in starved urchins relative to those well-fed (Lewis et al. 1990). While differences in calcification rates may have occurred here (between the barren and kelp/understory habitats), it is unclear the degree to which they contributed to the heavier jaws observed among barren urchins. Relative differences in purple and red urchin jaw masses across habitat types were most likely driven by differences in total

jaw area, specifically along the width-axis, rather than differences in density of calcium carbonate in the jaw. However, further analyses of the density and distribution of calcium carbonate across the jaws would be necessary to directly address such a pattern.

Test shrinkage, or “degrowth,” has been proposed as a possible mechanism by which the jaw-test allometry changes in low-food conditions. Urchin tests grow through two main pathways: by an increase in size of existing skeletal plates and by addition of new plates at the aboral margin (i.e., the “top” of the urchin), which are modulated by simultaneous dissolution of “older” plates at the oral margin (Cutress 1965). As such, the aforementioned pathways of growth also point to possible pathways of test shrinkage. For example, starved urchins exhibit reduced calcification rates (Lewis et al. 1990), which likely impede both the expansion of existing skeletal plates and the development of new aboral plates. Continuous dissolution of oral plates coinciding with reduced growth of new aboral plates could result in test shrinkage over time, however such a process has not yet been observed for red or purple urchins. Resorption of test material (i.e., calcite) has been proposed as an additional pathway of test shrinkage. However, experiments testing metabolic changes in calcium due to starvation found no evidence for calcium resorption from old skeletal material being used to build new skeletal material (Lewis et al. 1990). Further, extreme starvation of purple urchins under laboratory conditions, did not result in changes to the test diameter (Ebert et al. 2014), implying shrinkage or degrowth may not be the primary mechanism of persistence under such stress-inducing conditions.

### *Implications for management*

The recent, widespread loss of canopy-forming kelp throughout the northern California coast has resulted in severe consequences for the nearshore ecosystem and those that rely on it for their livelihood. Initiated in 2014, the region transitioned from a kelp-dominated system to one in which barrens spanned large swaths of the coastline. These urchin barrens persisted for six years prior to this study and are still present to date. Severely reduced gonad production by urchins from these barren habitats (Figure 5C) highlight ecosystem consequences that can cascade to profound fisheries impacts. With much of the coastline remaining in a barren, food-deprived state, the already localized commercial red urchin fishery (Kalvass and Hendrix 1997) has experienced further truncation and loss of income, so much so that in 2017, the fishery filed for disaster relief from the Federal government (Rogers-Bennett and Okamoto 2020). Remnant patches of kelp, such as those found at Portuguese Beach (Figure 1), provide few, concentrated regions in which red urchins are able to maintain marketable gonad production (Figure 5E). While it is poorly understood why and how the remaining kelp has been able to persist, it is possible these concentrated fishing efforts have, at least in part, helped through maintaining low grazing pressure (via urchin harvesting). Commercial urchin divers have a keen eye on locations where gonad production is greatest, and these fishery hotspots likely shift through time as nearshore subtidal communities respond to biotic and abiotic pressures (e.g., food availability, predator abundance, changing temperatures). In partnership with commercial urchin divers, continued monitoring of gonad production across the region could provide resource managers a bioindicator of habitat quality and condition with greater spatial coverage and temporal frequency than the existing subtidal ecosystem monitoring surveys, which occur at select locations roughly annually (e.g., Reef Check, PISCO).

Test diameter is often used as a proxy for age and is important in determining lower size limits of harvestable urchins (Rogers-Bennett et al. 2003; Ainis 2020). While there is currently no commercial fishery for purple urchins along the California coast, there is growing interest in expanding aquaculture infrastructure as a management tool by which to facilitate and encourage extraction of purple urchins from dense barrens (California Ocean Protection Council, 2021; Urchinomics). Potential benefits of targeted extractions of purple urchins from barren-dominated sites is two-fold; it alleviates grazing pressure in hopes of facilitating kelp recovery while simultaneously creating an economically viable market for the otherwise discarded urchins. As infrastructure for a new purple urchin fishery develops, robust growth models for purple urchins will be needed for effective fisheries management. The jaw length – diameter relationship may support a conservative growth model for the purple urchin. However, habitat condition history should be considered if and when a growth model is developed for a purple urchin market. While habitat context is likely less important for quantifying growth rates of purple urchins from Mendocino County, it may alter growth rate estimates in other regions that observe differing jaw lengths by habitat (e.g., Monterey; see Smith and Garcia 2021).

Further, urchin barrens can persist for decades (Claisse et al. 2013), and one suggested mechanism for this persistence is increased feeding efficiency of urchins in barren habitats through production of longer jaws. While this may occur in some systems, it does not appear to be a key driver of barren maintenance at the sites studied here. Jaw lengths did not differ between barren and kelp habitats (Figure 6), suggesting that either jaw length is not linked to feeding efficiency (supported by findings in deVries et al. 2019) or food deprivation was not severe enough to trigger efforts to enhance feeding efficiency. Understanding both the

mechanisms behind urchin barren maintenance and the thresholds and consequences of urchin starvation are key to managing and enhancing the remaining kelp stocks in California's North Coast.

## ACKNOWLEDGEMENTS

This work was supported by the Bilinski Fellowship. The authors are grateful to M. deVries, D. Dann, J. Fitzgerald, J. Herum, V. Hickman, K. Hope, S. Kawana, M. Murphy-Cannella, K. Nickols, A. Ninokawa, I. Norton, A. Saley, S. Stein, F. Torres, commercial urchin divers of Fort Bragg, CA, and Reef Check dockside volunteers for lab, field, and logistical assistance.

## LITERATURE CITED

Ainis, A.F. 2020. Using sea urchin remains to infer the health of kelp forest ecosystems in the past: Identification, quantification, and allometric reconstructions of harvested sea urchin (*Strongylocentrotus* spp.) on California's Channel Islands. *The Journal of Island and Coastal Archaeology*. 13:1-28, doi:10.1080/15564894.2020.1774445.

Andrew, N.L., Y. Agatsuma, E. Ballesteros, A.G. Bazhin, E.P. Creaser, D.K.A. Barnes, L.W. Botsford, A. Bradbury, A. Campbell, J.D. Dixon, S. Einarsson, P.K. Gerring, K. Hebert, M. Hunter, S.B. Hur, C.R. Johnson, M.A. Juinio-Menez, P. Kalvass, R.J. Miller, C.A. Moreno, J.S. Palleiro, D. Rivas, S.M.L. Robinson, S.C. Schroeter, R.S. Steneck, R.L. Vadas, D.A. Woodby, and Z. Xiaoqi. 2002. Status and management of world sea urchin fisheries. *Oceanography and Marine Biology: An Annual Review*. 40:343-425.

Azad, A.K. 2011. Factors influencing adult gonad production and larval growth and survival of the purple sea urchin (*Strongylocentrotus purpuratus*). Dissertation. Department of Animal Sciences, University of British Columbia, Vancouver, Canada.

Black, R., M.S., Johnson J.T., Trendall. 1982. Relative size of Aristotle's lantern in *Echinometra mathaei* occurring at different densities. *Marine Biology*. 71(1):101–106, doi:10.1007/BF00396997.

California Ocean Protection Council. 2021. Interim Action Plan for Protecting and Restoring California's Kelp Forests.

Campbell, G. 2008. A preliminary study of methods for identifying archaeological sea urchin remains in the Pacific Northwest. *Canadian Zooarchaeology* 25:15–35.

Carr, M.H. 1989. Effects of macroalgal assemblages on the recruitment of temperate zone reef fishes. *Journal of Experimental Marine Biology and Ecology* 126:59-76.

Centoni, J. 2018. Negatively correlated abundance suggests competition between red abalone (*Haliotis rufescens*) and red sea urchins (*Mesocentrotus franciscanus*) inside and outside established MPAs closed to commercial sea urchin harvest in Northern California. Master's Thesis. Humboldt State University.

Claisse, J. T., J. P. Williams, T. Ford, D. J. Pondella II, B. Meux, and L. Protopapadakis. 2013. Kelp forest habitat restoration has the potential to increase sea urchin gonad biomass. *Ecosphere* 4(3):38.

Cutress, B.M. 1965. Observations on growth in *Eucidaris tribuloides* (Lamarck), with special reference to the origin of the oral primary spines. *Bulletin of Marine Science*. 15(4):797-834.

Dayton, P.K. 1972. Toward an understanding of community resilience and the potential effects of enrichments to the benthos at McMurdo Sound, Antarctica. *Proceedings of the Colloquium on Conservation Problems in Antarctica*, B.C. Parker (Ed.) Allen Press, 81-96.

Department of Fisheries and Oceans Canada, 2019. Pacific Region Integrated Fisheries Management Plan—Red Sea Urchin—August 1, 2018-July 31, 2019. Department of Fisheries and Oceans Canada, Vancouver, B.C., Canada.

deVries, M.S., S.J. Webb, J.R.A. Taylor. 2019. Re-examination of the effects of food abundance on jaw plasticity in purple sea urchins. *Marine Biology*. 166:141.

Ebert, T.A. 1980. Relative growth of sea urchin jaws: an example of plastic resource allocation. *Bulletin of Marine Science*. 30:467–474.

Ebert, T.A. and M.P. Russell. 1993. Growth and mortality of subtidal red sea urchins (*Strongylocentrotus franciscanus*) at San Nicolas Island, California, USA: problems with models. *Marine Biology*. 117:79-89.

Ebert, T.A. and J.R. Southon. 2003. Red sea urchins (*Strongylocentrotus franciscanus*) can live over 100 years: confirmation with A-bomb 14carbon. *Fish Bull* 101:915-922.

Ebert, T.A., J.C. Hernandez, and M.P. Russell. 2011. Problems of the gonad index and what can be done: analysis of the purple sea urchin *Strongylocentrotus purpuratus*. *Marine Biology*. 158:47–58.

Ebert, T.A., J.C. Hernández, and S. Clemente. 2014. Annual reversible plasticity of feeding structures: cyclical changes of jaw allometry in a sea urchin. *Proceedings of the Royal Society B* 281:20132284, doi:<https://doi.org/10.1098/rspb.2013.2284>.

Erlandson, J.M., T.C. Rick, J.A. Estes, M.H. Graham, T.J. Braje, and R.L. Vellanoweth. 2005. Sea otters, shellfish, and humans: 10,000 years of ecological interaction on San Miguel Island, California. *Proceedings of the Sixth California Islands Symposium, 2005*, edited by D. K. Garcelon and C. A. Schwemm, pp. 9-21. Arcata, CA: National Park Service Technical Publication CHIS-05-01.

Fansler SC. 1983. Phenotypic plasticity of skeletal elements in the purple sea urchin, *Strongylocentrotus purpuratus*. Master Thesis. Department of Biology, San Diego State University, San Diego, CA, USA.

Filbee-Dexter, K. and R.E. Scheibling. 2014. Sea urchin barrens as alternative stable states of collapsed kelp ecosystems. *Marine Ecology Progress Series*. 495:1–25, doi:10.3354/meps10573.

Foster, M.C., J.E.K. Byrnes, D.C. Reed. 2015. Effects of five southern California macroalgal diets on consumption, growth, and gonad weight, in the purple sea urchin *Strongylocentrotus purpuratus*. *PeerJ*. doi:<https://doi.org/10.7717/peerj.719>.

Hernandez, J.C. and M.P. Russell. 2010. Substratum cavities affect growth-plasticity, allometry, movement and feeding rates in the sea urchin *Strongylocentrotus purpuratus*. *The Journal of Experimental Biology*. 213:520-525, doi:10.1242/jeb.029959.

Kalvass, P.E. and J.M. Hendrix. 1997. The California red sea urchin, *Strongylocentrotus franciscanus*, Fishery: Catch, effort, and management trends. *Marine Fisheries Review*. 59(2)1-17.

Kato, S. and S.C. Schroeter. 1985. Biology of the red sea urchins, *Strongylocentrotus franciscanus*, and its fishery in California. *Marine Fisheries Review* 47:1–20.

Kriegisch, N., S.E. Reeves, E.B. Flukes, C.R. Johnson, and S.D. Ling. 2019. Drift-kelp suppresses foraging movement of overgrazing sea urchins. *Oecologia* 190:665–677.

Kroh, A. and R. Mooi. 2011. World Echinoidea database. Available online at: <http://www.marine-species.org/echinoidea>

Leighton, D.L. 1966. Studies of food preference in algivorous invertebrates of southern California kelp beds. *Pacific Science*. 20:104-113.

- Lenth, R. 2020. emmeans: Estimated Marginal Means, aka Least-Squares Means. R package version 1.4.5. <https://CRAN.R-project.org/package=emmeans>
- Lewis, C.A., T.A. Ebert, and M.E. Boren. 1990. Allocation of <sup>45</sup>calcium to body components of starved and fed purple sea urchins (*Strongylocentrotus purpuratus*). *Marine Biology*, 105:213-222.
- Ling, S.D. and C.R. Johnson. 2009. Population dynamics of an ecologically important range-extender: kelp beds versus sea urchin barrens. *Marine Ecology Progress Series*. 374:113–125, doi:<https://doi.org/10.3354/meps07729>.
- Lowe, A.T, R. Whippo, A.W.E. Galloway, K.H. Britton-Simmons, and M. Dethier. 2015. Sedentary urchins influence benthic community composition below the macroalgal zone. *Marine Ecology*. 36:129-140.
- Maciá, S. and D. Lirman. 1999. Destruction of Florida Bay seagrasses by a grazing front of sea urchins. *Bulletin of Marine Science*. 65(2):593-601.
- McBride, S.C. 2005. Sea Urchin Aquaculture. *American Fisheries Society Symposium*. 46:179-208.
- McPherson, M.L., D.J.I. Finger, H.F. Houskeeper, T.W. Bell, M.H. Carr, L. Rogers-Bennett, R.M Kudela. 2021. Large-scale shift in the structure of a kelp forest ecosystem co-occurs with an epizootic and marine heatwave. *Communications Biology*. 4:298 doi:<https://doi.org/10.1038/s42003-021-01827-6>
- Miller, R.J., K.D. Lafferty, T. Lamy, L. Kui, A. Rassweiler, and D.C. Reed. 2018. Giant kelp, *Macrocystis pyrifera*, increases faunal diversity through physical engineering. *Proceedings of the Royal Society B: Biological Sciences* 285: 20172571.
- O’Leary, J.K. and T.R. McClanahan. 2010. Trophic cascades result in large-scale coralline algae loss through differential grazer effects. *Ecology*. 91(2):3584-3597.
- Pearse, J.S. and V.B. Pearse. 1975. Growth zones in the echinoid skeleton. *American Zoologist* 15(3):731–753.
- Pederson, H.G. and C.R. Johnson. 2008. Growth and age structure of sea urchins (*Heliocidaris erythrogramma*) in complex barrens and native macroalgal beds in eastern Tasmania. *ICES J Marine Science*. 65:1–11.
- R Core Team. 2020. R: A language and environment for statistical computing. R Foundation for Statistical Computing, Vienna, Austria. URL <https://www.R-project.org/>.
- Rogers-Bennett, L., D.W. Rogers, W.A. Bennett, and T.A. Ebert. 2003. Modeling red sea urchin growth using six growth models. *Fisheries Bulletin* 101:614–26.

Rogers-Bennett, L. and C.A. Catton. 2019. Marine heat wave and multiple stressors tip bull kelp forest to sea urchin barrens. *Scientific Reports*. 9:1–9.

Rogers-Bennett, L., and D. Okamoto. 2020. *Mesocentrotus franciscanus* and *Strongylocentrotus purpuratus*. *Developments in Aquaculture and Fisheries Science*. 43:593-608.

Smith, J.G. and S.C. Garcia. 2021. Variation in purple sea urchin (*Strongylocentrotus purpuratus*) morphological traits in relation to resource availability. *PeerJ*. 9:e11352, doi:10.7717/peerj.11352.

Steneck, R.S. 2020. Regular sea urchins as drivers of shallow benthic marine community structure. *Developments in Aquaculture and Fisheries Science*. 43:255-279.

Spindel, N.B., L.C. Lee, and D.K. Okamoto. 2021. Metabolic depression in sea urchin barrens associated with food deprivation. *bioRxiv* 2020.11.28.402156, doi:<https://doi.org/10.1101/2020.11.28.402156>.

Springer, Y.P., C.G. Hays, M.H. Carr, and M.R. Mackey. 2010. Toward ecosystem-based management of marine Macroalgae—The bull kelp, *Nereocystis luetkeana*. *Oceanography and Marine Biology: An Annual Review*, 48, 1-42.

Teck, S.J., J. Lorda, N.T. Shears, T. Ben-Horin, R.E. Toseland, S.T. Rathbone, D. Rudie, and S.D. Gaines. 2018. Quality of a fished resource: Assessing spatial and temporal dynamics. *PLoS ONE*. 13(6):e0196864. doi: 10.1371/journal.pone.0196864. PMID: 29874229; PMCID: PMC5991392.

Turner, N.J. 2001. "Coastal peoples and marine plants on the northwest coast", <https://hdl.handle.net/1912/2545>.

Urchinomics. 2021. Urchinomics. Available online at: <https://www.urchinomics.com/> (accessed May 9, 2021).

Vadas, R.L. 1977. Preferential Feeding: An optimization strategy in sea urchins. *Ecological Monographs*. 47(4):337-371.

Vergés A., C. Doropoulos, H.A. Malcolm, M. Skye, M. Garcia-Piza, E.M. Marzinelli, A.H. Campbell, E. Ballesteros, A.S. Hoey, A. Vila-Concejo, Y. Bozec, and P.D. Steinberg. 2016. Long-term empirical evidence of ocean warming leading to tropicalization of fish communities, increased herbivory, and loss of kelp. *Proceedings of the National Academy of Sciences*. 113:13791–13796.

**TABLES**

Table 1. Sample collection information for each site.

Site Name	Site Code	Latitude, Longitude	Habitat Classification	Sample size (n)	
				<i>Strongylocentrotus purpuratus</i>	<i>Mesocentrotus franciscanus</i>
Noyo Harbor	NH	39.43019, -123.81406	Barren	29	41
Caspar Cove	CC	39.36430, -123.82113	Barren	21	28
Portuguese Beach	PB	39.30258, -123.80284	Kelp	72	53
Point Arena	PA	38.92940, -123.73278	Understory	30	30

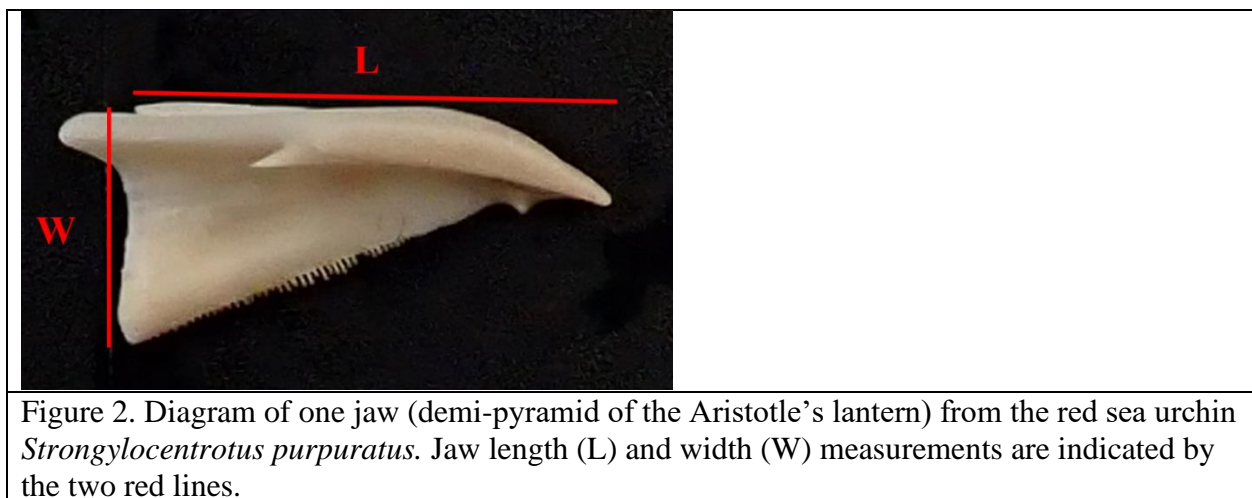
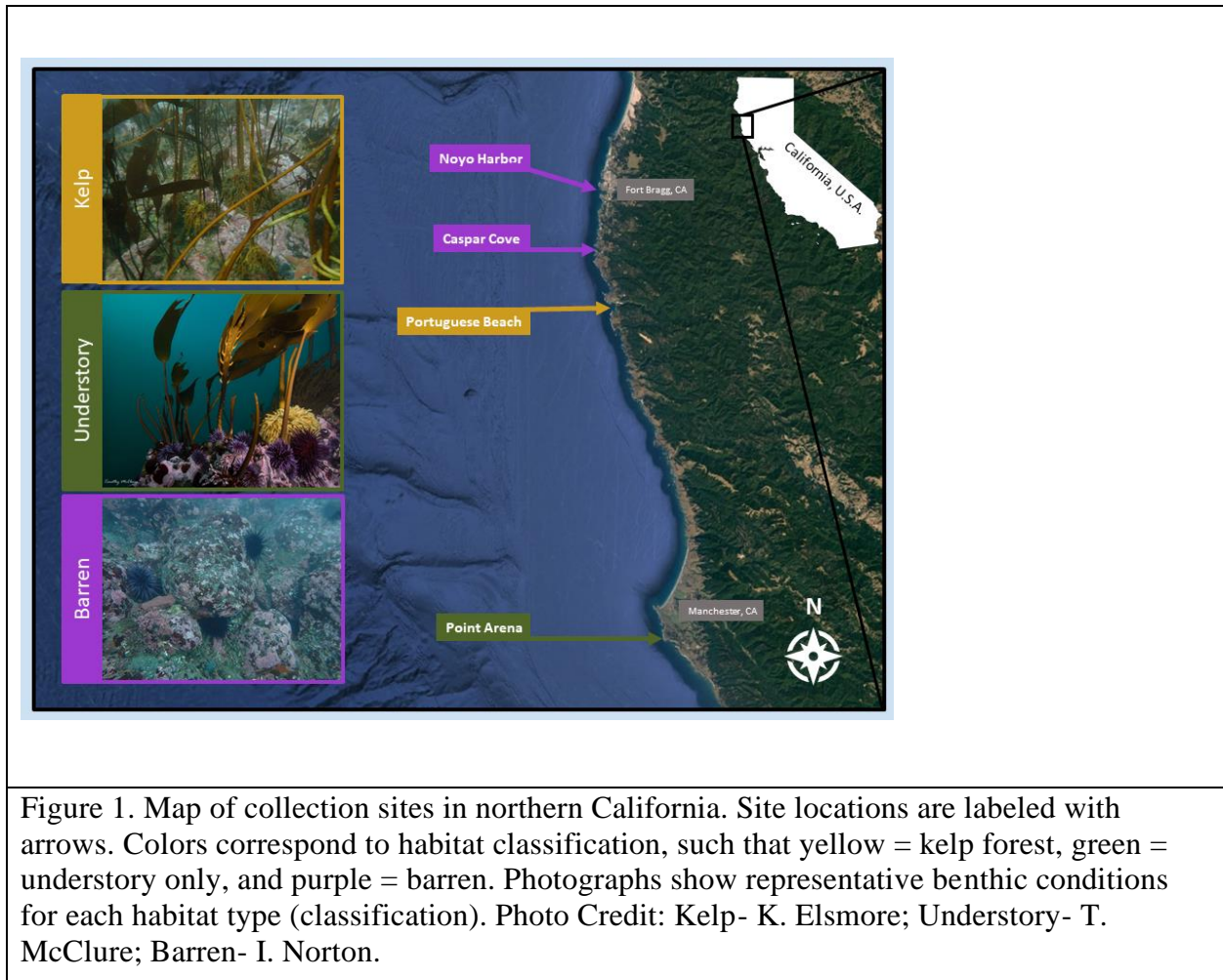
Table 2 Summary of species-specific comparisons across all urchin parameters measured. Each sign (>,<=) describes the general relationship between the purple urchin, *S. purpuratus*, and the red urchin, *M. franciscanus*, for a given parameter.

Species Comparison		
Parameter	Habitat	Relationship between: <i>S. purpuratus</i> _ <i>M. franciscanus</i>
Gonad weight (g)	Kelp	<
	Understory	=
	Barren	
Jaw length (mm)	Kelp	=
	Barren	
Jaw width (mm)	Kelp	<
	Barren	=
Jaw shape (width:length)	Kelp	<
	Barren	=
Jaw weight (g)	Kelp	<
	Understory	
	Barren	

Table 3 Summary of habitat-specific comparisons across all urchin parameters measured. Each sign (>,<=) describes the general relationship between the pairs of habitats examined (kelp, understory, barren), for a given urchin species (*S. purpuratus*, *M. franciscanus*). NA indicates that the given parameter was not measured for one of the habitats in the pairing.

Habitat Comparison				
Parameter	Species	Relationship between:		
		Kelp _ Barren	Kelp _ Understory	Understory _ Barren
Gonad weight (g)	<i>S. purpuratus</i>	>	=	>
	<i>M. franciscanus</i>		>	
Jaw length (mm)	<i>S. purpuratus</i>	=	NA	
	<i>M. franciscanus</i>			
Jaw width (mm)	<i>S. purpuratus</i>	<	NA	
	<i>M. franciscanus</i>			
Jaw shape (width:length)	<i>S. purpuratus</i>	<	NA	
	<i>M. franciscanus</i>	=		
Jaw weight (g)	<i>S. purpuratus</i>	<	=	<
	<i>M. franciscanus</i>			

## FIGURES



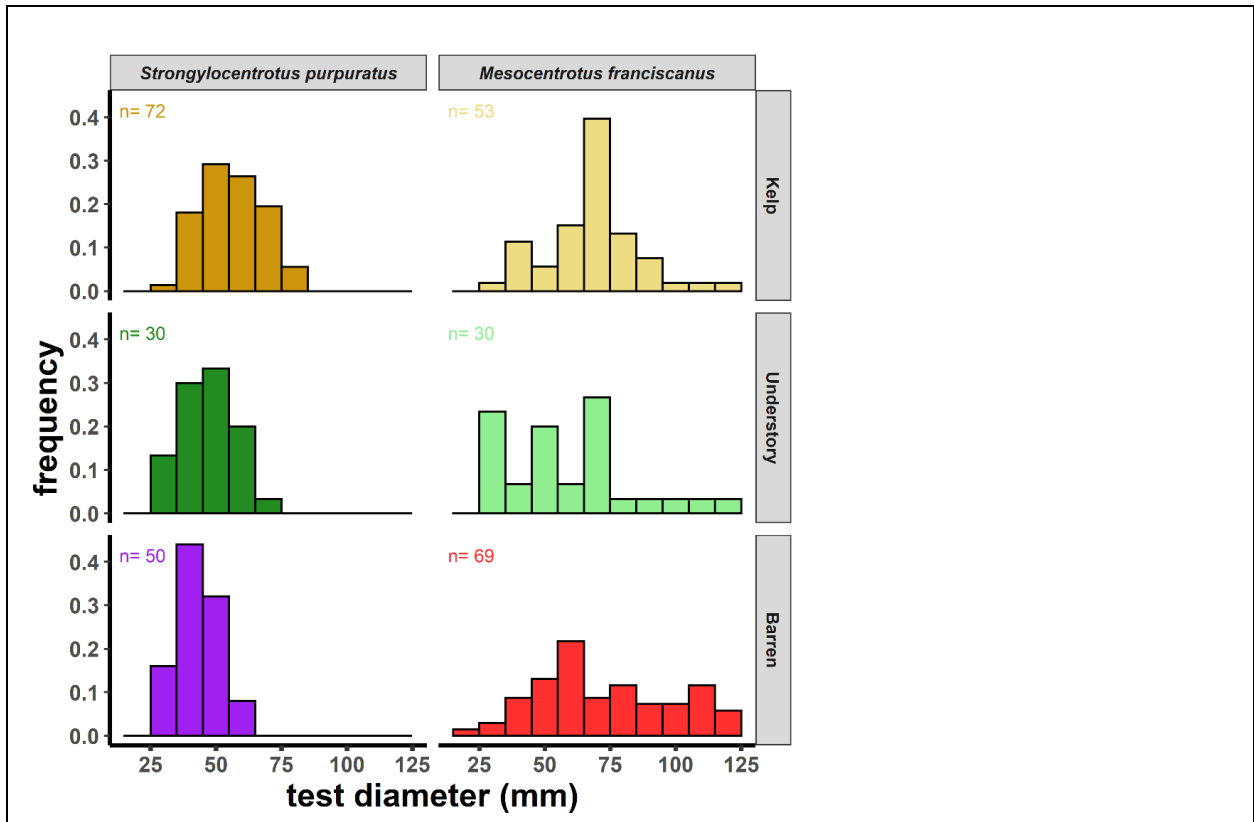


Figure 3. Urchin test diameter (mm) frequency of *Strongylocentrotus purpuratus* and *Mesocentrotus franciscanus* collected from habitats characterized as kelp (dark yellow for *S. purpuratus*, light yellow for *M. franciscanus*), understory (dark green for *S. purpuratus*, light green for *M. franciscanus*), and barren (purple for *S. purpuratus*, red for *M. franciscanus*).

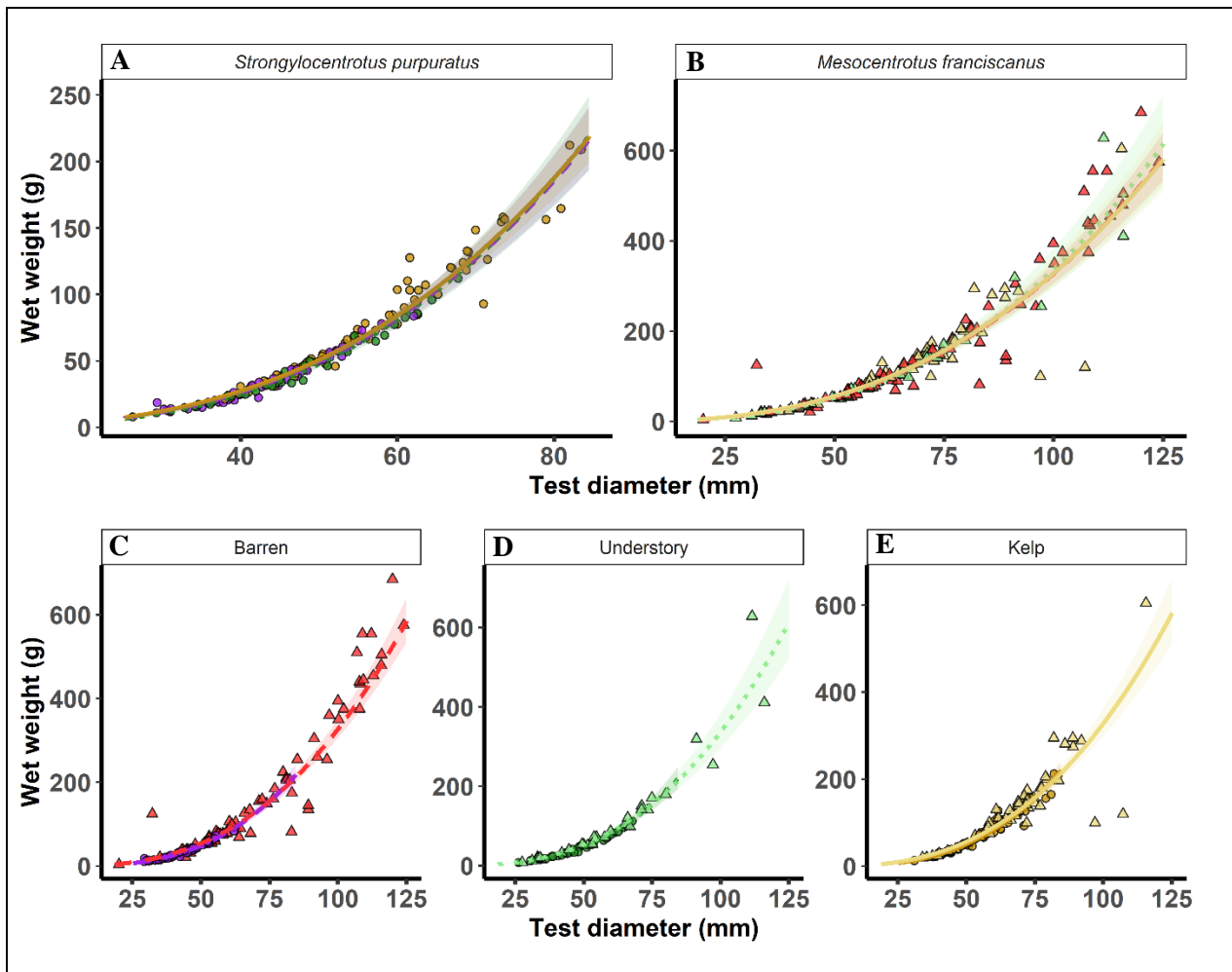


Figure 4. Relationships between urchin total wet mass (g) and test diameter (mm) for all A) *Strongylocentrotus purpuratus* and B) *Mesocentrotus franciscanus* individuals collected, and from habitats characterized as C) barren (purple for *S. purpuratus*, red for *M. franciscanus*), D) understory habitat (dark green for *S. purpuratus*, light green for *M. franciscanus*), and E) kelp habitat (dark yellow for *S. purpuratus*, light yellow for *M. franciscanus*). Points indicate raw data (circles for *S. purpuratus* and triangles for *M. franciscanus*). Lines represent model fit for each habitat type (long dash for barren, dotted for understory, and solid for kelp) and shading represents the respective standard error. No differences were detected across habitat categories or between the two species.

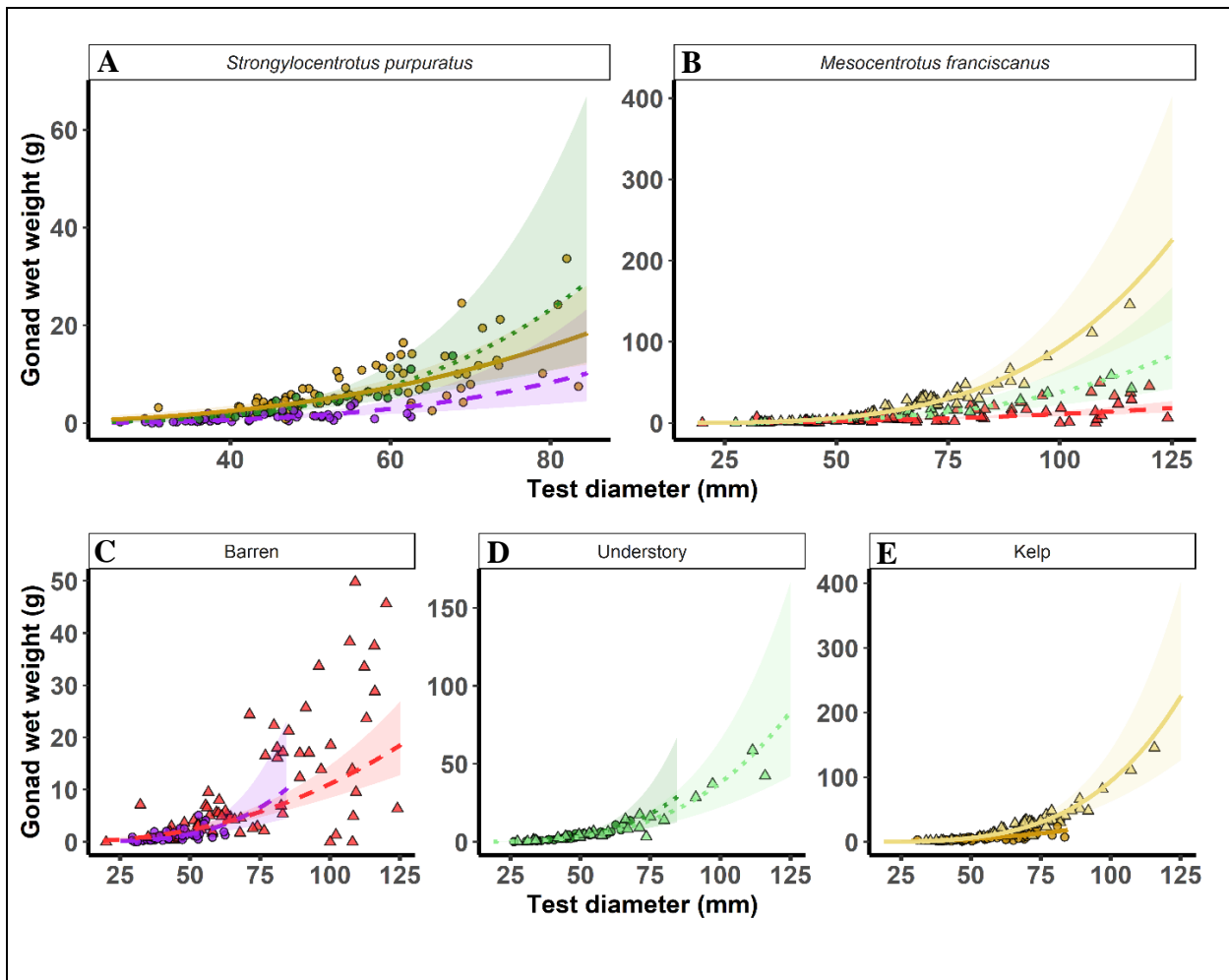


Figure 5. Relationship between urchin gonad wet mass (g) and test diameter (mm) for all A) *Strongylocentrotus purpuratus* and B) *Mesocentrotus franciscanus* individuals collected, and from habitats characterized as C) barren (purple for *S. purpuratus*, red for *M. franciscanus*), D) understory habitat (dark green for *S. purpuratus*, light green for *M. franciscanus*), and E) kelp habitat (dark yellow for *S. purpuratus*, light yellow for *M. franciscanus*). Points indicate raw data (circles for *S. purpuratus* and triangles for *M. franciscanus*). Lines represent model fit for each habitat type (long dash for barren and solid for kelp) and shading represents the respective standard error.

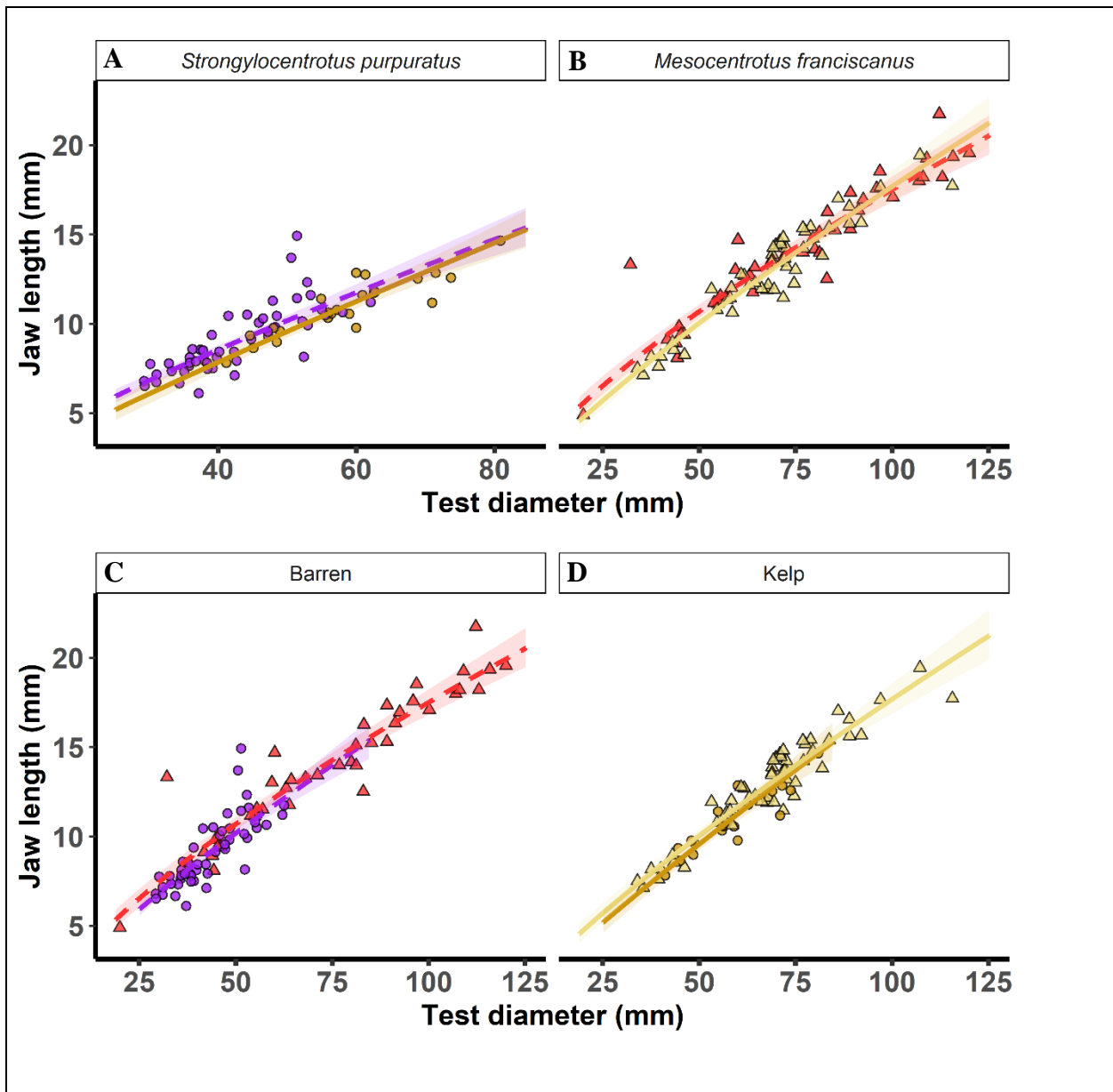


Figure 6. Relationship between urchin jaw length (mm) and test diameter (mm) for A) *Strongylocentrotus purpuratus* and B) *Mesocentrotus franciscanus* individuals collected, and from habitats characterized as C) barren (purple for *S. purpuratus*, red for *M. franciscanus*), and D) kelp habitat (dark yellow for *S. purpuratus*, light yellow for *M. franciscanus*). Points indicate raw data (circles for *S. purpuratus* and triangles for *M. franciscanus*). Lines represent model fit for each habitat type (long dash for barren and solid for kelp) and shading represents the respective standard error.

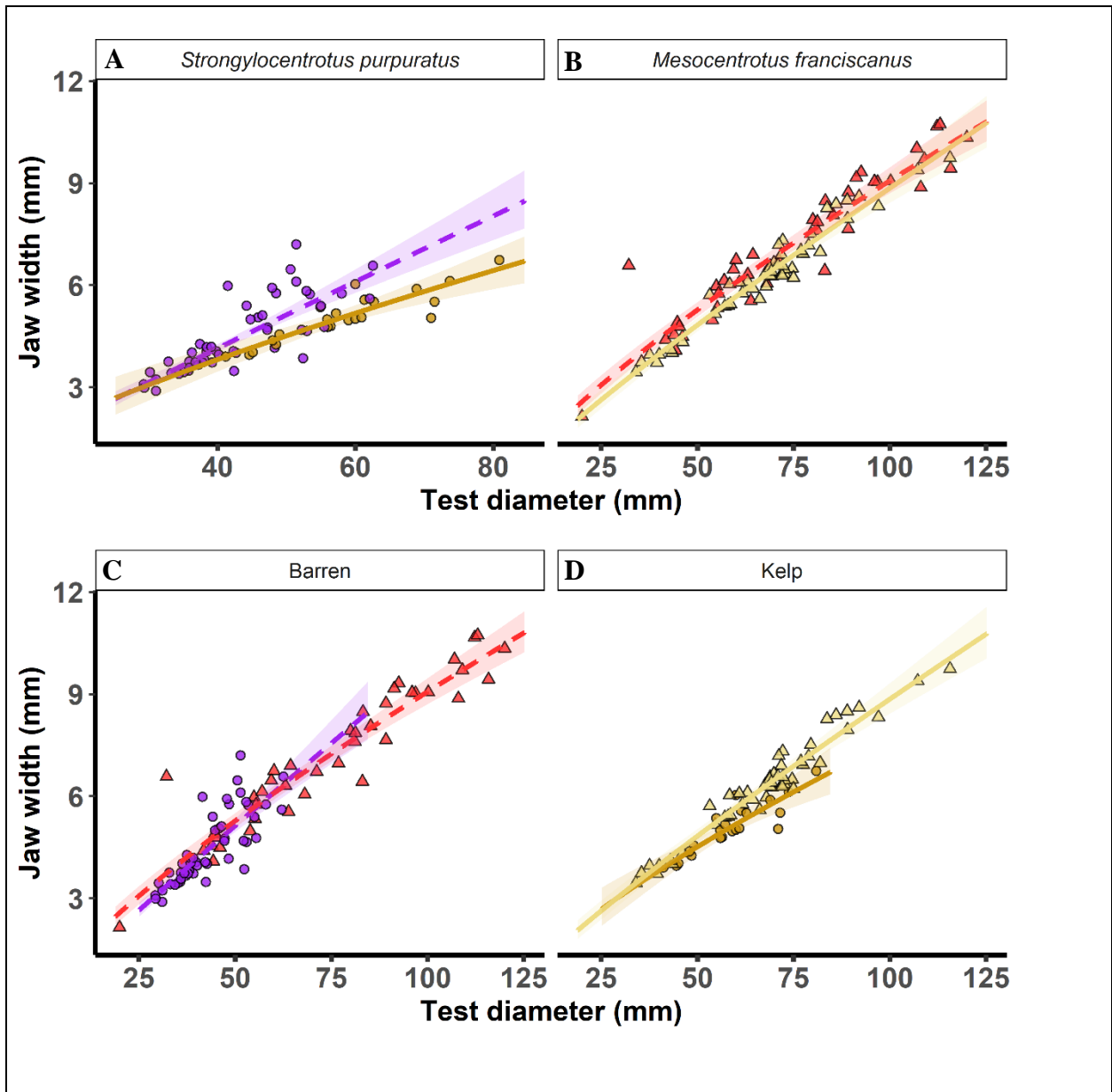


Figure 7. Relationship between urchin jaw width (mm) and test diameter (mm) for A) *Strongylocentrotus purpuratus* and B) *Mesocentrotus franciscanus* individuals collected, and from habitats characterized as C) barren (purple for *S. purpuratus*, red for *M. franciscanus*), and D) kelp habitat (dark yellow for *S. purpuratus*, light yellow for *M. franciscanus*). Points indicate raw data (circles for *S. purpuratus* and triangles for *M. franciscanus*). Lines represent model fit for each habitat type (long dash for barren and solid for kelp) and shading represents the respective standard error.

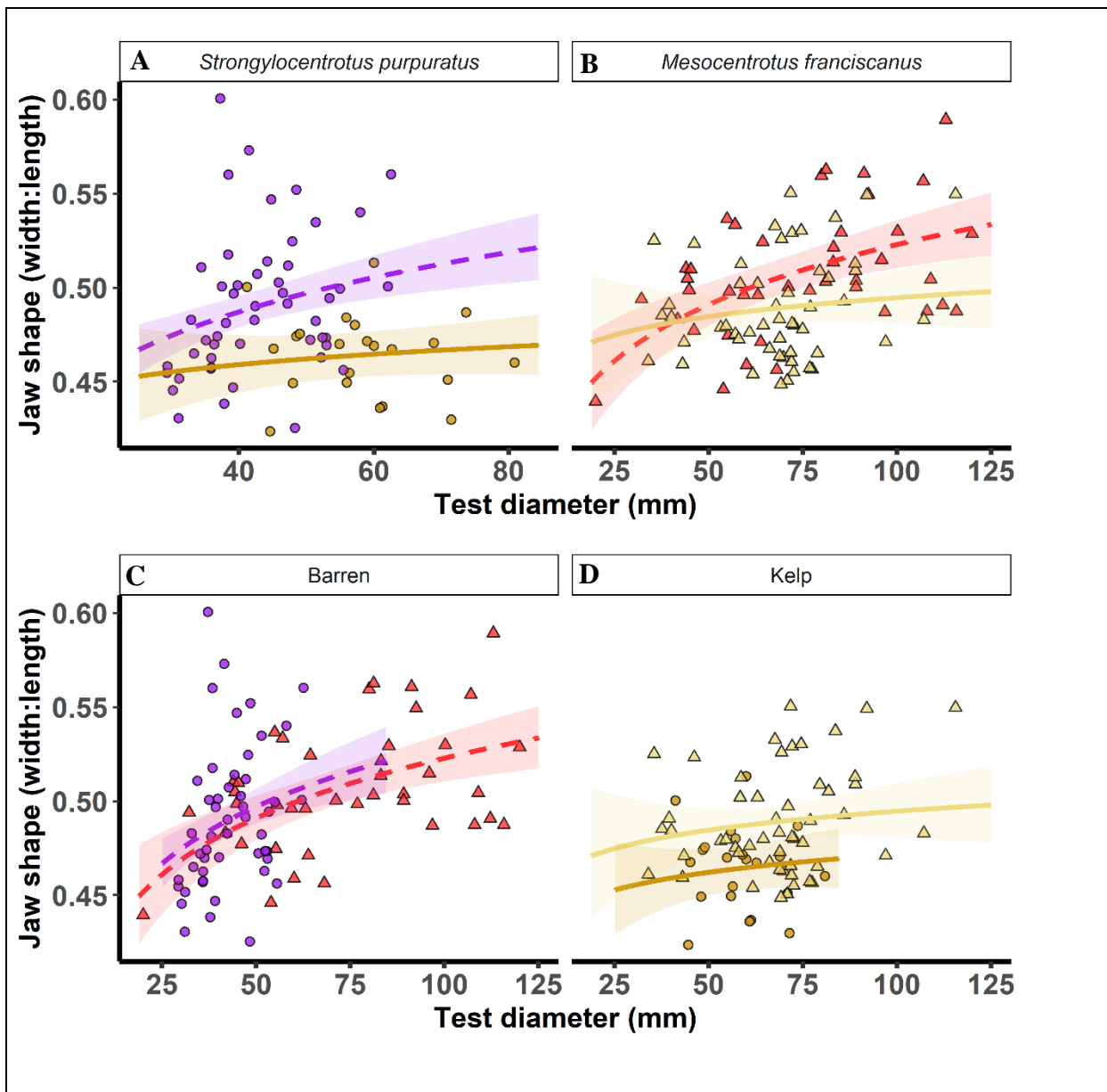


Figure 8. Relationship between urchin jaw shape (width:length) and test diameter (mm) for A) *Strongylocentrotus purpuratus* and B) *Mesocentrotus franciscanus* individuals collected, and from habitats characterized as C) barren (purple for *S. purpuratus*, red for *M. franciscanus*), and D) kelp habitat (dark yellow for *S. purpuratus*, light yellow for *M. franciscanus*). Points indicate raw data (circles for *S. purpuratus* and triangles for *M. franciscanus*). Lines represent model fit for each habitat type (long dash for barren and solid for kelp) and shading represents the respective standard error.

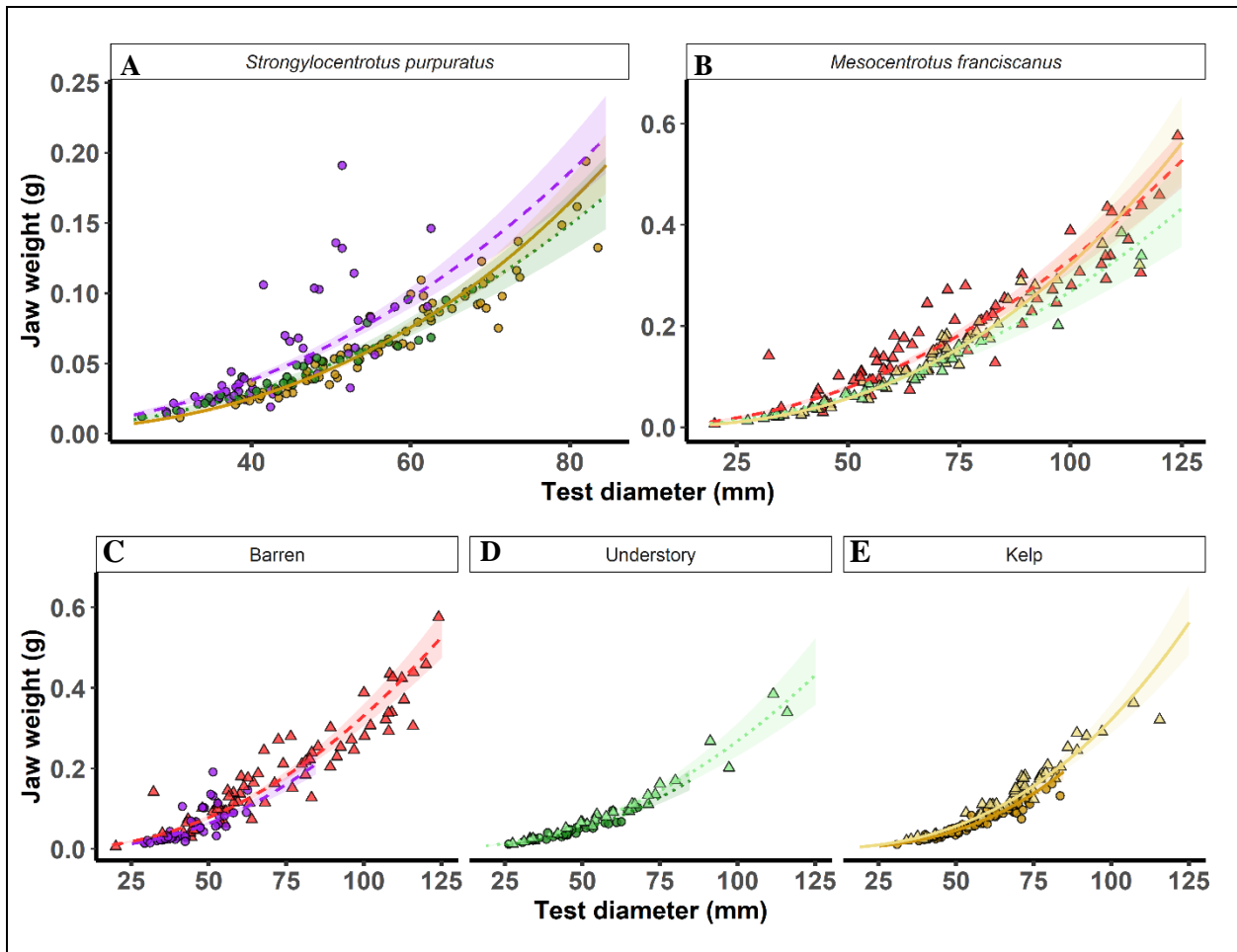


Figure 9. Relationship between urchin jaw weight (g) and test diameter (mm) for all A) *Strongylocentrotus purpuratus* and B) *Mesocentrotus franciscanus* individuals collected; from habitats characterized as C) barren (purple for *S. purpuratus*, red for *M. franciscanus*), D) understory habitat (dark green for *S. purpuratus*, light green for *M. franciscanus*), and E) kelp habitat (dark yellow for *S. purpuratus*, light yellow for *M. franciscanus*). Points indicate raw data (circles for *S. purpuratus* and triangles for *M. franciscanus*). Lines represent model fit for each habitat type (long dash for barren, dotted for understory, and solid for kelp) and shading represents the respective standard error.

**APPENDICES**

Table S1: Akaike’s Information Criterion scores (AIC), their degrees of freedom, and predictors for each model in the backward stepwise model selection process for gonad weight (g). Final models selected are in bold.

Response: Gonad weight (g)			
	<b>Model predictors</b>	<b>df</b>	<b>AIC</b>
<b>1</b>	<b>test diameter*habitat*species</b>	<b>13</b>	<b>751.4108</b>
2	(test diameter + habitat + species) <sup>2</sup>	11	756.2644
3	test diameter*habitat + habitat*species	10	754.3329
4	test diameter*species + habitat*species	9	760.0167
5	test diameter*habitat + test diameter*species	9	758.8378
6	test diameter + habitat + species	6	760.3494

Table S2: Akaike’s Information Criterion scores (AIC), their degrees of freedom, and predictors for each model in the backward stepwise model selection process for each jaw morphometric response variable (i.e., jaw length, jaw width, jaw shape, jaw weight). Final models selected are in bold.

Response: Jaw length (mm)			
	<b>Model Predictors</b>	<b>df</b>	<b>AIC</b>
1	test diameter*habitat*species	9	-291.3536
2	(test diameter + habitat + species) <sup>2</sup>	8	-291.9505
3	test diameter*habitat + habitat*species	7	-292.6161
4	test diameter*species + habitat*species	7	-290.8416
<b>5</b>	<b>test diameter*habitat + test diameter*species</b>	<b>7</b>	<b>-293.9132</b>
6	test diameter + habitat + species	5	-293.6975
Response: Jaw width (mm)			
	<b>Model Predictors</b>	<b>df</b>	<b>AIC</b>
<b>1</b>	<b>test diameter*habitat*species</b>	<b>9</b>	<b>-286.4375</b>
2	(test diameter + habitat + species) <sup>2</sup>	8	-284.7114
3	test diameter*habitat + habitat*species	7	-284.8318
4	test diameter*species + habitat*species	7	-286.2103
5	test diameter*habitat + test diameter*species	7	-283.5567
6	test diameter + habitat + species	5	-285.4509
Response: Jaw shape (width:length)			
	<b>Model Predictors</b>	<b>df</b>	<b>AIC</b>
1	test diameter*habitat*species	9	-445.9322
2	(test diameter + habitat + species) <sup>2</sup>	8	-446.3736
<b>3</b>	<b>test diameter*habitat + habitat*species</b>	<b>7</b>	<b>-448.2171</b>
4	test diameter*species + habitat*species	7	-445.6003
5	test diameter*habitat + test diameter*species	7	-441.7258
6	test diameter + habitat + species	5	-444.9391

Response: Jaw weight (g)			
Model Predictors		df	AIC
1	test diameter*habitat*species	11	25.21072
2	(test diameter + habitat + species) <sup>2</sup>	11	25.21072
3	test diameter*habitat + habitat*species	10	28.56554
4	test diameter*species + habitat*species	9	29.93591
<b>5</b>	<b>test diameter*habitat + test diameter*species</b>	<b>9</b>	<b>24.05250</b>
6	test diameter + habitat + species	6	39.07988

Table S3. Summary results for linear model testing the effect of test diameter, habitat (i.e., Kelp, Barren, Understory), and species (i.e., *S. purpuratus*, *M. franciscanus*) on gonad weight (g) and the Tukey HSD pairwise comparison. Bold values are statistically significant.

Gonad Weight (g)				
Predictor	Estimate	Std. error	t-value	p-value
Multiple R <sup>2</sup> = 0.719; Adjusted R <sup>2</sup> = 0.708				
Intercept (Barren : <i>M. franciscanus</i> )	-8.12	1.14	-7.12	<b>8.31E-12</b>
Kelp	-5.38	2.11	-2.55	<b>1.13E-02</b>
Kelp : <i>S. purpuratus</i>	10.2	3.53	2.89	<b>4.12E-03</b>
Understory	-4.41	1.94	-2.27	<b>2.37E-02</b>
Understory : <i>S. purpuratus</i>	4.31	3.87	1.11	2.66E-01
log(test diameter)	2.29	0.27	8.52	<b>8.87E-16</b>
log(test diameter) : Kelp	1.63	0.5	3.26	<b>1.26E-03</b>
log(test diameter) : Kelp : <i>S. purpuratus</i>	-2.58	0.89	-2.91	<b>3.91E-03</b>
log(test diameter) : Understory	1.22	0.47	2.56	<b>9.98E-03</b>
log(test diameter) : Understory : <i>S. purpuratus</i>	-0.97	1	-0.97	3.33E-01
log(test diameter) : <i>S. purpuratus</i>	1.34	0.64	2.1	<b>3.64E-02</b>
<i>S. purpuratus</i>	-5.65	2.45	-2.31	<b>2.17E-02</b>

Tukey Pairwise Comparison						
Habitat	Contrast	ratio	SE	df	t-ratio	p-value
Barren	<i>M. franciscanus</i> - <i>S. purpuratus</i>	1.191	0.3012	292	0.692	9.83E-01
Understory	<i>M. franciscanus</i> - <i>S. purpuratus</i>	0.835	0.225	292	-0.668	9.85E-01
Kelp	<i>M. franciscanus</i> - <i>S. purpuratus</i>	1.713	0.2704	292	3.412	<b>9.51E-03</b>
Species	Contrast	ratio	SE	df	t-ratio	p-value
<i>M. franciscanus</i>	Barren - Kelp	0.276	0.0441	292	-8.053	<b>1.04E-12</b>
	Barren - Understory	0.55	0.1013	292	-3.243	<b>1.65E-02</b>
	Kelp - Understory	1.995	0.385	292	3.578	<b>5.38E-03</b>

<i>S. purpuratus</i>	Barren - Kelp	0.397	0.0998	292	-3.674	<b>3.83E-03</b>
	Barren - Understory	0.386	0.1236	292	-2.972	<b>3.74E-02</b>
	Kelp - Understory	0.973	0.2386	292	-0.113	1.00E+00
<b>Habitat - Species Contrast</b>		<b>ratio</b>	<b>SE</b>	<b>df</b>	<b>t-ratio</b>	<b>p-value</b>
Barren <i>M. franciscanus</i> - Kelp <i>S. purpuratus</i>		0.473	0.0694	292	-5.101	<b>9.01E-06</b>
Barren <i>M. franciscanus</i> - Understory <i>S. purpuratus</i>		0.46	0.1134	292	-3.149	<b>2.21E-02</b>
Kelp <i>M. franciscanus</i> - Barren <i>S. purpuratus</i>		4.317	1.1197	292	5.639	<b>6.02E-07</b>
Kelp <i>M. franciscanus</i> - Understory <i>S. purpuratus</i>		1.666	0.4222	292	2.016	3.34E-01
Understory <i>M. franciscanus</i> - Barren <i>S. purpuratus</i>		2.164	0.5951	292	2.808	5.90E-02
Understory <i>M. franciscanus</i> - Kelp <i>S. purpuratus</i>		0.859	0.1566	292	-0.834	9.61E-01

Table S4. Summary results for linear model testing the effect of test diameter, habitat (i.e., Kelp, Barren), and species (i.e., *S. purpuratus*, *M. franciscanus*) on jaw length (mm) and the Tukey HSD pairwise comparison. Bold values are statistically significant.

<b>Jaw Length (mm)</b>				
<b>Predictor</b>	<b>Estimate</b>	<b>Std. error</b>	<b>t-value</b>	<b>p-value</b>
Multiple R <sup>2</sup> = 0.890; Adjusted R <sup>2</sup> = 0.887				
Intercept (Barren : <i>M. franciscanus</i> )	-0.42	0.16	-2.67	<b>8.31E-03</b>
Kelp	-0.47	0.23	-2.08	<b>3.87E-02</b>
log(test diameter)	0.71	0.04	19.31	<b>1.54E-43</b>
log(test diameter) : Kelp	0.1	0.05	1.92	5.56E-02
log(test diameter) : <i>S. purpuratus</i>	0.07	0.06	1.14	2.54E-01
<i>S. purpuratus</i>	-0.33	0.25	-1.32	1.90E-01

<b>Tukey Pairwise Comparison</b>						
<b>Habitat</b>	<b>Contrast</b>	<b>ratio</b>	<b>SE</b>	<b>df</b>	<b>t-ratio</b>	<b>p-value</b>
Barren	<i>M. franciscanus</i> - <i>S. purpuratus</i>	1.035	0.021	159	1.68	3.38E-01
Kelp	<i>M. franciscanus</i> - <i>S. purpuratus</i>	1.035	0.021	159	1.68	3.38E-01
<b>Species</b>	<b>Contrast</b>	<b>ratio</b>	<b>SE</b>	<b>df</b>	<b>t-ratio</b>	<b>p-value</b>
<i>M. franciscanus</i>	Barren - Kelp	1.042	0.0178	159	2.433	7.50E-02
<i>S. purpuratus</i>	Barren - Kelp	1.042	0.0178	159	2.433	7.50E-02
<b>Habitat - Species Contrast</b>		<b>ratio</b>	<b>SE</b>	<b>df</b>	<b>t-ratio</b>	<b>p-value</b>

Barren <i>M. franciscanus</i> - Kelp <i>S. purpuratus</i>	1.079	0.028	159	2.91	<b>2.13E-02</b>
Kelp <i>M. franciscanus</i> - Barren <i>S. purpuratus</i>	0.993	0.0268	159	-0.277	9.93E-01

Table S5. Summary results for linear model testing the effect of test diameter, habitat (i.e., Kelp, Barren), and species (i.e., *S. purpuratus*, *M. franciscanus*) on jaw width (mm) and the Tukey HSD pairwise comparison. Bold values are statistically significant.

<b>Jaw Width (mm)</b>				
<b>Predictor</b>	<b>Estimate</b>	<b>Std. error</b>	<b>t-value</b>	<b>p-value</b>
Multiple R <sup>2</sup> = 0.903; Adjusted R <sup>2</sup> = 0.899				
Intercept (Barren : <i>M. franciscanus</i> )	-1.39	0.17	-8.18	<b>8.94E-14</b>
Kelp	-0.45	0.27	-1.64	1.02E-01
Kelp : <i>S. purpuratus</i>	1.11	0.63	1.78	7.76E-02
log(test diameter)	0.78	0.04	19.58	<b>5.62E-44</b>
log(test diameter) : Kelp	0.09	0.06	1.43	1.56E-01
log(test diameter) : Kelp : <i>S. purpuratus</i>	-0.29	0.16	-1.89	6.01E-02
log(test diameter) : <i>S. purpuratus</i>	0.17	0.08	2.14	<b>3.37E-02</b>
<i>S. purpuratus</i>	-0.7	0.31	-2.25	<b>2.59E-02</b>

<b>Tukey Pairwise Comparison</b>						
<b>Habitat</b>	<b>Contrast</b>	<b>ratio</b>	<b>SE</b>	<b>df</b>	<b>t-ratio</b>	<b>p-value</b>
Barren	<i>M. franciscanus</i> - <i>S. purpuratus</i>	0.994	0.0333	157	-0.184	9.98E-01
Kelp	<i>M. franciscanus</i> - <i>S. purpuratus</i>	1.096	0.0288	157	3.472	<b>3.69E-03</b>
<b>Species</b>	<b>Contrast</b>	<b>ratio</b>	<b>SE</b>	<b>df</b>	<b>t-ratio</b>	<b>p-value</b>
<i>M. franciscanus</i>	Barren - Kelp	1.072	0.0233	157	3.222	<b>8.35E-03</b>
<i>S. purpuratus</i>	Barren - Kelp	1.182	0.0433	157	4.57	<b>5.78E-05</b>
<b>Habitat - Species Contrast</b>		<b>ratio</b>	<b>SE</b>	<b>df</b>	<b>t-ratio</b>	<b>p-value</b>
Barren <i>M. franciscanus</i> - Kelp <i>S. purpuratus</i>		1.175	0.0323	157	5.873	<b>1.48E-07</b>
Kelp <i>M. franciscanus</i> - Barren <i>S. purpuratus</i>		0.927	0.0302	157	-2.337	9.41E-02

Table S6. Summary results for linear model testing the effect of test diameter, habitat (i.e., Kelp, Barren), and species (i.e., *S. purpuratus*, *M. franciscanus*) on jaw shape (width:length) and the Tukey HSD pairwise comparison. Bold values are statistically significant.

<b>Jaw Shape (width:length)</b>
---------------------------------

Predictor	Estimate	Std. error	t-value	p-value
Multiple R <sup>2</sup> = 0.233; Adjusted R <sup>2</sup> = 0.209				
Intercept (Barren : <i>M. franciscanus</i> )	-1.07	0.09	-11.7	<b>3.36E-23</b>
Kelp	0.23	0.15	1.48	1.40E-01
Kelp : <i>S. purpuratus</i>	-0.06	0.02	-2.59	<b>1.05E-02</b>
log(test diameter)	0.09	0.02	4.25	<b>3.65E-05</b>
log(test diameter) : Kelp	-0.06	0.04	-1.7	9.20E-02
<i>S. purpuratus</i>	0.01	0.02	0.74	4.60E-01

Tukey Pairwise Comparison						
Habitat	Contrast	ratio	SE	df	t-ratio	p-value
Barren	<i>M. franciscanus</i> - <i>S. purpuratus</i>	0.988	0.0136	159	1.899	2.33E-01
Kelp	<i>M. franciscanus</i> - <i>S. purpuratus</i>	1.049	0.0167	159	2.971	<b>1.78E-02</b>
Species	Contrast	ratio	SE	df	t-ratio	p-value
<i>M. franciscanus</i>	Barren - Kelp	1.025	0.0136	159	1.899	2.33E-01
<i>S. purpuratus</i>	Barren - Kelp	1.089	0.019	159	4.857	<b>1.67E-05</b>
Habitat - Species Contrast		ratio	SE	df	t-ratio	p-value
Barren <i>M. franciscanus</i> - Kelp <i>S. purpuratus</i>		1.075	0.0176	159	4.425	<b>1.04E-04</b>
Kelp <i>M. franciscanus</i> - Barren <i>S. purpuratus</i>		0.963	0.014	159	-2.576	5.27E-02

Table S7. Summary results for linear model testing the effect of test diameter, habitat (i.e., Kelp, Barren, Understory), and species (i.e., *S. purpuratus*, *M. franciscanus*) on jaw shape (width:length) and the Tukey HSD pairwise comparison. Bold values are statistically significant.

Jaw Weight (g)				
Predictor	Estimate	Std. error	t-value	p-value
Multiple R <sup>2</sup> = 0.916; Adjusted R <sup>2</sup> = 0.914				
Intercept (Barren : <i>M. franciscanus</i> )	-10.67	0.29	-36.28	<b>2.15E-110</b>
Kelp	-1.95	0.43	-4.49	<b>1.01E-05</b>
Understory	-0.47	0.46	-1.02	3.07E-01
log(test diameter)	2.08	0.07	29.48	<b>1.17E-89</b>
log(test diameter) : Kelp	0.42	0.11	3.91	<b>1.14E-04</b>
log(test diameter) : Understory	0.06	0.11	0.48	6.30E-01
log(test diameter) : <i>S. purpuratus</i>	0.21	0.11	1.92	5.61E-02

<i>S. purpuratus</i>	-1.02	0.43	-2.38	<b>1.81E-02</b>		
Tukey Pairwise Comparison						
Habitat	Contrast	ratio	SE	df	t-ratio	p-value
Barren	<i>M. franciscanus</i> - <i>S. purpuratus</i>	1.19	0.0419	293	4.926	<b>2.06E-05</b>
Understory	<i>M. franciscanus</i> - <i>S. purpuratus</i>	1.19	0.0419	293	4.926	<b>2.06E-05</b>
Kelp	<i>M. franciscanus</i> - <i>S. purpuratus</i>	1.19	0.0419	293	4.926	<b>2.06E-05</b>
Species	Contrast				t-ratio	p-value
<i>M. franciscanus</i>	Barren - Kelp	1.278	0.0442	293	7.09	<b>1.52E-10</b>
	Barren - Understory	1.271	0.0546	293	5.577	<b>8.30E-07</b>
	Kelp - Understory	0.994	0.0424	293	-0.132	1.00E+00
<i>S. purpuratus</i>	Barren - Kelp	1.278	0.0442	293	7.09	<b>1.52E-10</b>
	Barren - Understory	1.271	0.0546	293	5.577	<b>8.30E-07</b>
	Kelp - Understory	0.994	0.0424	293	-0.132	1.00E+00
Habitat - Species Contrast					t-ratio	p-value
Barren <i>M. franciscanus</i> - Kelp <i>S. purpuratus</i>		1.52	0.0628	293	10.146	<b>8.06E-13</b>
Barren <i>M. franciscanus</i> - Understory <i>S. purpuratus</i>		1.512	0.0799	293	7.817	<b>2.27E-12</b>
Kelp <i>M. franciscanus</i> - Barren <i>S. purpuratus</i>		0.931	0.0524	293	-1.271	8.01E-01
Kelp <i>M. franciscanus</i> - Understory <i>S. purpuratus</i>		1.183	0.07	293	2.839	5.42E-02
Understory <i>M. franciscanus</i> - Barren <i>S. purpuratus</i>		0.936	0.0544	293	-1.134	8.67E-01
Understory <i>M. franciscanus</i> - Kelp <i>S. purpuratus</i>		1.196	0.0612	293	3.502	<b>7.00E-03</b>